Lukas Peicha, BSc

Movement Decoding from EEG: Target or Direction?

MASTER'S THESIS

to achieve the university degree of

Diplom-Ingenieur

Master's degree programme: Biomedical Engineering

submitted to

Graz University of Technology

Supervisor

Univ.-Prof. Dipl.-Ing. Dr.techn. Gernot Müller-Putz

Institute of Neural Engineering

Laboratory of Brain-Computer Interfaces

Graz, September 2017

AFFIDAVIT

I declare that I have authored this thesis independently, that I have not used other than the declared sources/resources, and that I have explicitly indicated all material which has been quoted either literally or by content from the sources used. The text document uploaded to TUGRAZonline is identical to the present master‘s thesis.

Date

Signature

Acknowledgements

At this point, I would like to express my gratitude to all those, who supported me and, most important, tried to keep me motivated while working on my master's thesis.

First of all, I would like to thank my supervisor Univ.-Prof. Dipl.-Ing. Dr.techn. Gernot Müller-Putz for giving me the support I asked for with all his expertise and helpful tips and above all for making it possible to write my thesis at his institute. Speaking of which, special thanks also to the whole team of the Institute of Neural Engineering and in particular to Andi and Patrick for helping me a lot in the early state with basic questions and Maria for assisting me with the experimental setup and electrode-montage.
Special thanks also to my support overseas, Rahman Davoodi, PhD, developer of the MSMS software, who was so kind and answered hundreds of questions concerning the software I was working with.

I really appreciate also the help of my subjects for taking some time for the testing and Johanna for not only giving me scientific inputs and advices but also for joking around quite often.

I would like to thank a lot my closest friends for always having my back during some though times and my better half Steffi for just being there when I needed her to be there and also dealing with my bad moods a lot.

Last but not least thanks to my parents for giving me all their support and opportunities to study at an university. Even more important, thank you for always trusting in me and my decissions even if it all took a little longer. Always remember: Rome was not built in a day either!

Abstract

State-of-the-art brain-computer interface (BCI) systems are not yet capable of continous decoding movement trajectories for neuroprosthesis control. One approach for natural neuroprosthesis control could be a BCI that decodes the intended target and a prosthesis that plans the trajectory afterwards to get there. This study investigated whether a BCI decoder is based on the movement direction or the movement target.

Subjects were asked to perform arm movements with their arms being fixed to an ARMEO Spring rehabilitation device. They received a visual feedback via a computer screen that displayed a virtual arm model in first person view mirroring their real arm movements. Subjects tried to reach one out of two targets on the computer screen with the virtual arm according to specific commands. By inverting the visual feedback (virtual arm moved to the opposite direction of the real arm movement) in a second condition it was tried to learn about the decoder behaviour.

ERD/ERS maps showed a typical event-related desynchronization (ERD) after movement onset in the alpha band (8 Hz - 10 Hz) for both conditions and also a power decrease during the inverted condition in the beta range (15 Hz - 25 Hz) due to the more challenging task.
Time-frequency plots were displaying the course of a motor-related cortical potential (MRCP). A characteristic voltage negativation before the actual movement onset with a negative peak around the onset and an increase in voltage following could be observed over the whole cortex.
Classification accuracies for both conditions peaked during movement execution before reaching the demanded target.

By training the classifier with the normal condition data and subsequently testing with the inverted condition data it was investigated that the decoder was not only based on movement targets but also on movement direction. This finding could be crucial for developing any kind of new neuroprosthesis control.

However, further investigations with expanded and adjusted design of the experimental paradigm need to be done in order to get more distinct results.

key words: electrencephalography (EEG), brain-computer interface (BCI), neuroprosthesis control, target decoding, movement direction decoding

Kurzfassung

Brain-Computer Interface (BCI) Systeme, die dem aktuellen Stand der Technik ensprechen, sind noch nicht in der Lage, Bewegungstrajektorien kontinuierlich zu dekotieren. Ein Ansatz um eine natürliche Steuerung einer Prothese zu erlangen wäre der Einsatz eines BCIs, das nur das angestrebte Ziel der Bewegung dekodiert und die eigentliche Bewegung zum Ziel anschließend von der Neuroprothese selbst ausgeführt wird. In dieser Arbeit wurde untersucht, ob ein BCI Dekoder auf Bewegungsrichtungen basiert oder auf dem Ziel einer Bewegung.

Probanden wurden in einem ARMEO Spring Rehabilitationsgerät mit ihrem Arm befestigt und beauftragt, Armbewegungen durchzuführen. Sie bekamen visuelles Feedback über einen Computerbildschirm, welcher das Modell eines virtuellen Armes in der Ich-Perspektive zeigte. Der virtuelle Arm führte exakt die Bewegung aus, die auch der Proband mit seinem Arm ausführte. Die Probanden versuchten dann, entsprechend den Anweisungen, mit dem virtuellen Arm eines von zwei Zielen am Computerbildschirm zu erreichen. Durch das Invertieren des visuellen Feedbacks (der virtuelle Arm führt genau die gegengleichen Bewegungen aus wie der Proband mit seinem Arm) in einer zweiten Bedingung wurde versucht, etwas über das Verhalten des Dekoders zu erfahren.

Die ERD/ERS Abbildungen zeigten neben typischen ereignisbezogenen Desynchronisationen (ERD) im Alpha-Band (8 Hz - 10 Hz) nach dem Bewegungs-Onset für beide Bedingungen, wegen der komplizierteren Aufgabe auch einen Leistungsabfall im Beta Bereich (15 Hz - 25 Hz) während der invertierten Bedingung. Die Zeit-Frequenz Graphen zeigten den charakteristischen Verlauf von motor-related cortical potentials (MRCPs) über dem ganzen Cortex. Vor dem eigentlichen Bewegungs-Onset entsteht ein Spannungsabfall mit einem negativen Maximum im Bereich des Onsets und einem darauf folgenden Spannungsanstieg. Die Klassifizierungsgenauigkeiten für beide Konditionen erreichten ihr Maximum während der Bewegungsausführung, noch bevor das Ziel erreicht wurde.

Durch das Trainieren des Klassifikators mit den Daten der normalen Bedingung und anschließendem Testen mit den Daten der invertierten Bedingung wurde herausgefunden, dass der Dekoder sowohl auf der Bewegungsrichtung als auch auf dem Ziel der Bewegung basiert. Diese Tatsache könnte entscheidend bei der Entwicklung neuer Steuerungen für Neuroprothesen sein. Allerdings müssen trotz der gewonnenen Erkenntnisse noch weitere Untersuchungen, mit erweitertem und adaptiertem experimentellen Aufbau, gemacht werden, um eindeutigere Ergebnisse zu erzielen.

Schlüsselwörter: Elektroenzephalographie (EEG), Brain-Computer Interface (BCI), Neuroprothesen-Steuerung, target decoding, movement direction decoding

Contents

List of Figures

List of Tables

Abbreviations

BCI ... brain-computer interface
CAR ... common average reference
CP ... cerebral palsy
ECoG ... electrocorticography
EEG ... electroencephalography
EOG ... electrooculography
EPSP ... excitatory post synaptical potential
ERD ... even-related desynchronization
ERS ... event-related synchronization
FES ... functional electrical stimulation
fMRI ... functional magnetic resonance imaging
ISPS ... inhibitory post synaptical potential
LSL ... Lab Stream Layer
MEG ... magnetoencephalography
MI ... motor imagination
MRCP ... motor-related cortical potential
MSMS ... musculoskeletal modulation software
PCA ... principal component analysis
PSP ... post synaptical potential
SCI ... spinal cord injury
SCP ... slow cortical potential
sLDA ... shrinkage linear discriminant analysis
SMR ... sensorimotor rhythm
SSVEP ... steady-state visual evoked potentials
UDP ... user datagram protocol
VEP ... visual evoked potentials

1 Introduction

1.1 The electroencephalogram

In 1924, the German neurologist and psychiatrist Hans Berger managed to record "brain waves". He discovered that the electroencephalogram was a noninvasive method to measure the electrical brain activity on the scalp. [1]

These measurable electrical brain activity also known as postsynaptic potentials (PSPs) are generated at cortical pyramidal neurons and can be measured as field potentials with an EEG. These neurons' dentritic trunks are alligned parallel to each other and perpendicularly to the cortical surface. There are two types of PSPs, the excitatory postsynaptic potentials (EPSPs) causing a depolarisation (increase of the likelihood that the neuron will be firing an action potential) of the postsynaptic neuromembrane and the inhibitory postsynaptic potentials (IPSPs) causing a hyperpolarisation (decrease of the likelihood that the neuron will be firing an action potential). For EPSPs, action potentials that reach the presynaptic ending of the excitatory neuron cause cations at the synaptic cleft to flow into the cell. The resulting depolarisation inside the cell and outside along the neuromembrane results in a extracellular cation flow towards the synaptic cleft and in a intracellular flow away from the cleft. Hence, the depolarisation can spread throughout the cell. For IPSPs, as already mentioned, an inversly directed cation flow causes a hyperpolarisation through the cell [2, 3]. Figure 1 shows a schematic representation of the process of post synaptic potentials.

The activation of particular neurons results in an electrical activity that is very small, so in order to be measured, a collective and synchrone activation (or inhibitation) of tens of thousands of pyramidal cells is prerequisite. EEG oscillations that can be recorded on the scalp are the outcome of the summation of EPSPs and IPSPs [4]. Another requirement for an EEG oscillation to emerge is the specific orientation of the electric fields resulting from the activation of neurons.

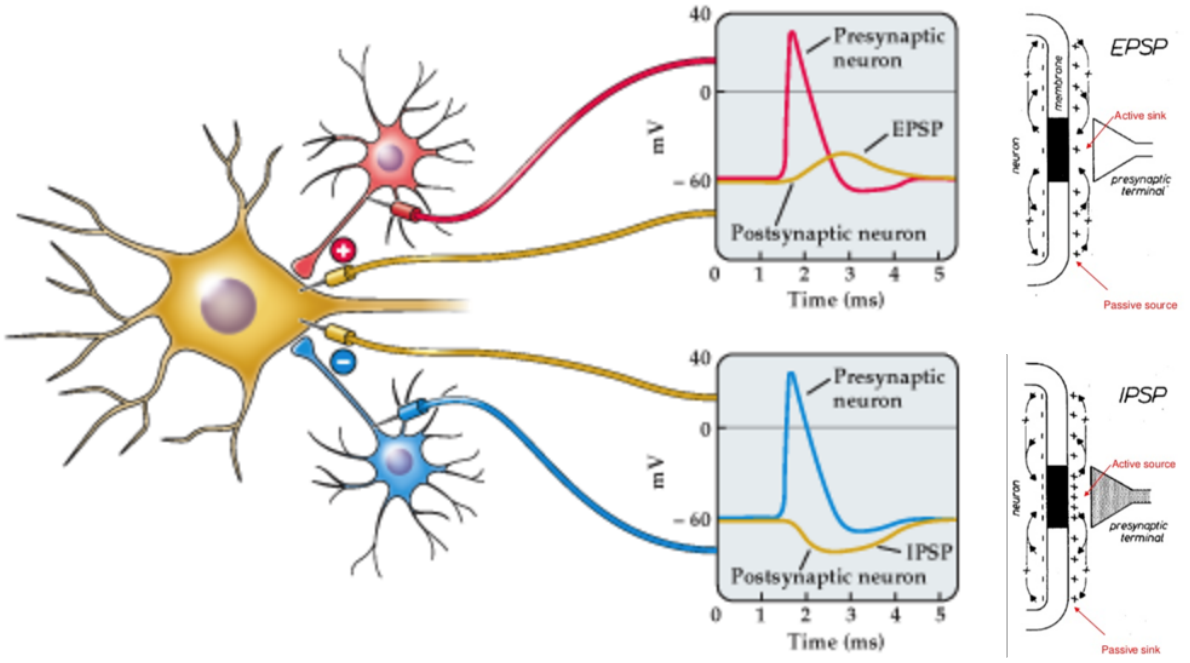

Figure 1: Schematic representation of postsynaptic potentials and iconic current flows along the neuromembranes indicated by arrows and +/- signs. (modified from `http://7e.biopsychology.com/vs03.html`)

Lorente de Nò (1947) was the first to differentiate between closed fields and open fields concerning neural fields' orientation. The state of open-field orientation is constituted by neurons that are alligned so that all their dentritic trees are oriented on one side and their axons on the other side. Thus, electric fields are oriented into the same direction and summate. Measurable EEG oscillations are generated only by structures with some degree of open-field organization. Primarily the outermost layered structure in the human brain's neural tissue, the cerebral cortex, is responsible for that. Since many parallel neurons synchronously receive input from post synaptic potentials, these cells form an electric dipole from an electrical viewpoint. The height of the EEG's potential deflections is proportional to the number of cells. Closed-field oriented structures however, where the electric fields of the neurons are oriented in different directions typically, are cancelling each other out and so they do not generate large summated dipoles. Activities in subcortical structures (e.g. amygdala) can not be measured at the scalp [5, 6].

EEG oscillations only represent a little part of the brain's electrical activity at a particular time. For recording the signals, electrodes are attached to the subject's surface of the head. These electrodes (about 1 cm in diameter) cover an area of about 250,000 neurons that need to be active at the same time [7]. The number of electrodes used can vary up to 256 and the electrode locations are based on standards.

1.2 Brain-computer interface

A brain-computer interface (BCI), which is sketched in Figure 2 is a device, which has the purpose to detect and transform thought-modulated changes in the electrophysiological brain activity, into commands for driving a machine like a prosthesis, a roboter, a computer, a cursor etc. [8, 9]. Hence, it is possible for users to interact with their enviroment only by thought after e.g. spinal cord injuries (SCI) [10].

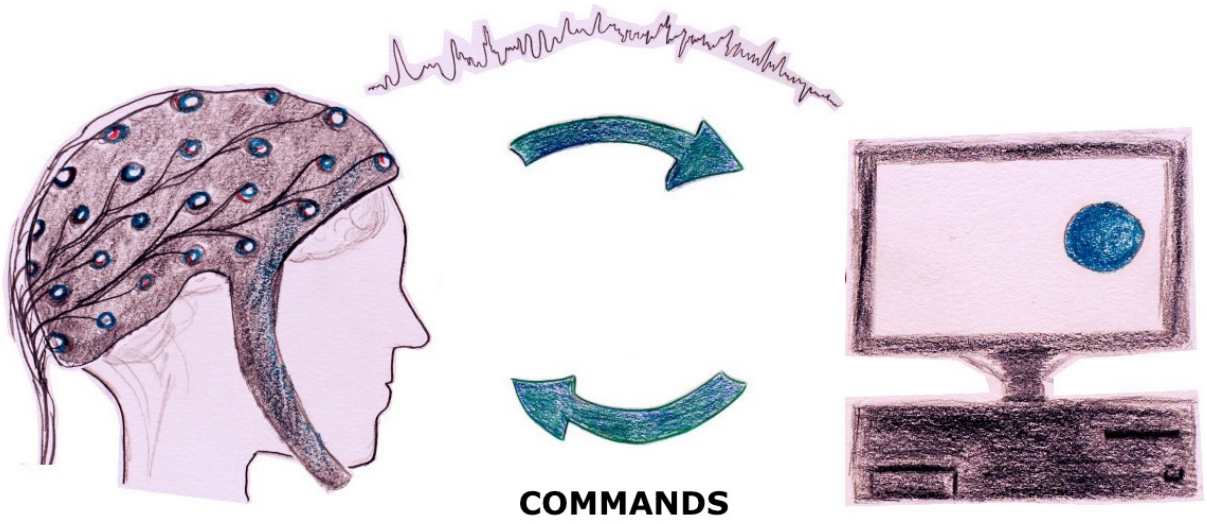

Figure 2: Sketch of a brain-computer interface. Signals are recorded from the subjects's brain and translated into commands for driving a device or issue a command (modified from `https://team.inria.fr/potioc/bci-courses/`).

BCI control is typically achieved by using brain signals, such as components of the EEG, sensorimotor rhythm (SMR), slow cortical potentials (SCP) or event-related potentials (with the P300 component as the most popular representative) for the classification of motor intention or mental states. As can be seen in Figure 3, it is a closed-loop system. Data is acquired from the subject via electrodes and amplifiers before it is preprocessed to remove artifacts. For decision making, features are extracted and classified to feed the results of the classification to an application. Subsequently, the system provides feedback (visual, auditory or haptic) to the user through the specific device (e.g. movement of the neuroprosthesis or special cues on a computer screen) [11].

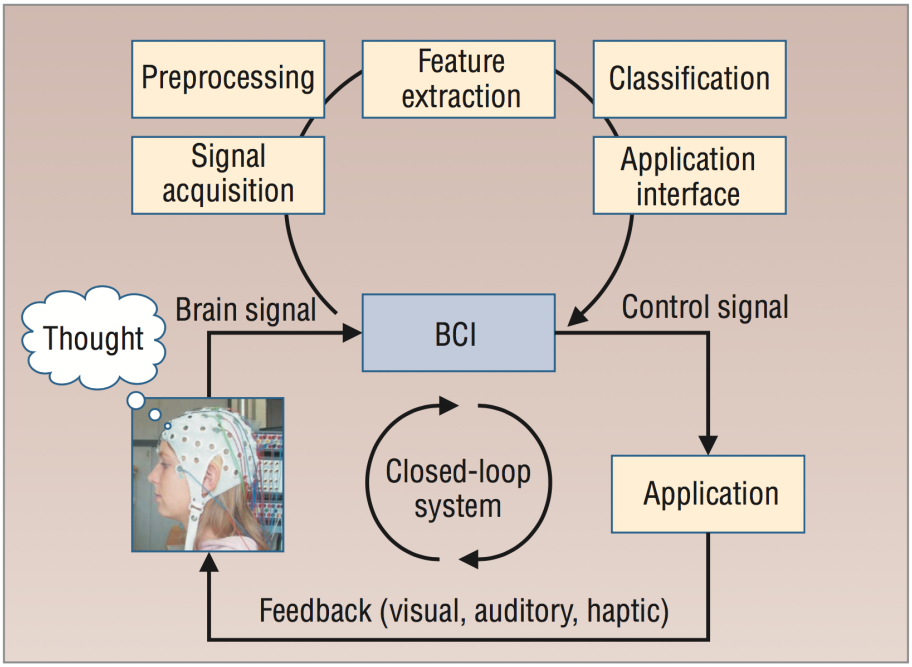

Figure 3: Elements of a non-invasive BCI. Input for the BCI is the user's raw EEG data. The system digitalizes and preprocesses data, extracts and classifies features and feeds the results afterwards to an application interface. The user is controlling the application, hence the system becomes a closed-loop by presenting the user feedback (visual, auditory or haptic) on the accuracy of the focused thought [11].

The key to develop a successful BCI is the flawless communication between the user's brain and the device. There are two main differneces in experimental strategy for BCIs, either they are based on focused attention to an external stimulus or based on particular mental tasks [12]. BCIs that are based on focused attention are used for fast selection like it is necessary for communication purposes [13, 14, 15, 16]. BCIs with special mental strategies however are used for controlling a device like a neuroprosthesis or a wheelchair [17] or for restoring grasping movements [18, 19, 20].

1.2.1 BCI applications

For communication between the brain and a computer several technical approaches and physiological phenomena are used. Nowadays, invasive BCI brain signals include action potentials from nerve cells, synaptic or extracellular field potentials and electrocorticogram (ECoG). The noninvasive BCIs include among others: SCP component of the EEG, other EEG or MEG (magnetoencephalography) oscillations, SMR and event-related potentials [9]. SMR-based BCIs are used for controlling neuroprosthesis. Pfurtscheller et al. [21] was able to restore the grasp function of a tetraplegic patient by using a SMR-based BCI and

motor neuroprosthesis that works with functional electrical stimulation (FES). Müller-Putz et al. [22] showed the coupling of a SMR-based BCI with an implanted Freehand system. The combination of a control signal from a SMR-BCI with a shoulder position sensor for controlling elbow movements and grasping motions was demonstrated by Rohm et al. [19]. Kreilinger et al. [18] showed the latest development which is a continuous elbow control only by different duration of one imagined motor task.

Moreover, SMR-based BCIs are also used for different virtual spelling devices as several publication show. For letter selection two to four control signals, which typically are motor imaginations (MIs) of specific movements, can be used. Different control signals and paradigms are used to score a good spelling rate, which is the performance measure of these BCIs. Scherer et al. [23] achieved an average spelling rate of 1.99 letters/minute in three healthy subjects in a self-paced BCI where the alphabet was shown in two separate columns. Foot MI, as well as right hand - and left hand MI were used for scrolling and selecting letters in either the right or left column, respectively. Blankertz et al. [24] was able to achieve a spelling rate of 2.3 to 7.6 letters/minute in two subjects using hexagonal fields and right hand- and foot MI for letter selection. Scherer et al. [25] recently introduced a row-column- based scanning technique, where cerebral palsy (CP) suffering end users can select icons from a matrix solely by right hand MI. Seven out of ten end users scored better than chance.
Nevertheless it is much more common to use spelling devices based on P300 (P300-speller) rather than SMR due to the need of less electrodes and the more robust way of working in terms of false selection [13, 15, 16, 26].

BCIs are also used for medical applications like in neuro rehabilitation. Motor recovery might be facilitated due to restoration of the neurophysiologic activity. One meaningful example is the stroke rehabilitation. The leading cause of permanent physical disability is the motor impairment after a stroke. Patients can use visual feedback BCI systems to improve their condition of disability. The patients sensorimotor network is activated by triggering limb movements (even though the movement is unreal) and by adapting their thoughts to the provided feedback [11, 27]. Patients with high-level SCI however have less ability for activating external controllers and that ability even decreases the higher the cervical vertebrae lesion is located. The solution might be the usage of the recorded EEG signals together with a neuroprosthesis and a BCI system. Thus, a complete, thought-driven restoration of hand and arm functions could be enabled [11, 12, 22].

BCI systems are also used in assistive technology for providing disabled people assistance in daily environments, like prosthesis control or even web browsing. BCI in assistive technology is mainly used in so-called hybrid BCI systems as an additional channel, since BCI devices alone do not provide 100 % reliable decoding of the subject's real intention [28].

BCIs may even be used for different purposes by healthy users, e.g. for gaming applications. The Berlin Brain Computer Interface provides a paradigm showing encouraging results for even people without previous BCI experience - untrained subjects are capable of moving through a pacman labyrinth within only a short time. Some companies (e.g. cyberlink.com or braingames.com) even sell BCIs for healthy subjects to play simple video games [29, 30].

1.2.2 BCI categories

There are different characterictics for categorizing BCI systems:

1. Invasive/Non-invasive BCI

Invasive BCIs are using intracranial techniques for signal acquisition, such as ECoG (electrodes are placed on the cortex' surface) or single/multi-unit derivation where electrodes are placed inside the grey matter. Non-invasive BCIs, on the contrary, use extracranial brain activity recordings, such as EEG, MEG or functional magnetic resonance imaging (fMRI) [31]. Invasive systems comprise all risks associated with any brain surgery, non invasive systems, however, are basically harmless [11]. For practical reasons, non invasive BCIs are more common.

2. Brain signals

Visual evoked potentials (VEPs) occur after a visual stimulus in the visual cortex [32]. One important control signal, the steady-state visual evoked potential (SSVEP) arises after a stimulus of a frequency higher than 6 Hz. BCI systems based on SSVEPs allow a target selection by means of a users' eye-gaze. The BCI identifies a target through SSVEP feature analysis after a user visually fixes attention on a special target [33].

SCPs are slow voltage shifts in the EEG and last up to several seconds. SCPs are low frequency signals (< 1 Hz) and are associated with changes in the cortical activity level. Positive SCPs correlate with decreased neuronal activity and vice versa [34].
Healthy users and paralized patients both are capable of self-regulation of these brain signals in order to control devices by means of a BCI. The selection of targets on a screen or cursor movement can be achieved by the usage of SCP shifts [35].

Positive peaks in the EEG about 300 ms after applying infrequent target cues within a series of cues (oddball paradigm), are called P300 evoked potentials [36, 37].
P300-based BCIs do not require any type of training. As already mentioned in the previous

chapter these BCI systems are used for so called P300-speller that utilize visual P300 evoked potentials for the selection of specific letters.

SMR are specific oscillations in the EEG that arise in the alpha (8 - 12 Hz) and beta (18 - 26 Hz) bands. These signals can be recorded over sensorimotor areas. SMRs' aplitudes typically decrease during motor imagery (MI) or actual movement [38]. SMR modulations can be learned to generate voluntarily by users [39].

3. Extrinsic/Intrinsic stimulation

Extrinsic BCIs make use of the neuron activity caused by external stimuli such as VEPs or auditory evoked potentials. These systems do not require extenive training, because of the quick and easy setup to generate the control signals, SSVEPs and P300 [40].
Intrinsic BCI systems are not caused by external stimuli, they are rather based on the self regulation of brain rhythms and potentials [40]. Specific brain patterns like modulations in the SMR or the SCPs can be practiced to generate via neurofeedback training and can then be decoded by the BCI. Therefore it is possible for a user to operate a BCI at free will [35, 41].

4. Synchronous/Asynchronous BCI

Synchronous/Asynchronous BCI classification follows according to the input data processing modality. Synchronous BCIs only analyze brain signals during specific predefined time windows. Users are only allowed to send commands during these periods. The Graz BCI represents this type of BCI system [42]. One big advantage of synchronous BCI is that the mental activity onset is known in advance sinceit is associated with a special cue. Asynchronous BCIs analyze brain signals continously no matter when the user is sending commands. These types of BCI offer a more natural human-machine interaction but also require a more complex computation [31, 43].

1.3 Decoding motor execution

As already mentioned in the previous section, one main application of BCI is the restoration of arm movements (i.e. elbow and wrist movements and grasping action) via controlling a motor neuroprosthesis by thoughts only. In this way, paralized persons (e.g. patients with tetraplegia or other SCIs) that have an interruption in the spinal cord but an intact brain can enjoy rehabilitation by bypassing the lack in neural pathway between muscles and brain so that basic movement functions can be restored or replaced [44].

Basically, a BCI should be able to recognize the user's intention of an arm movement and the exact movement is performed by the neuroprosthesis afterwards. One very important objective is the naturalness of the neuroprosthesis control by the patient. I.e., on the one hand the control should be an easy and familiar direct control, so that it is comfortable for the user. On the other hand, the user would not have to learn any complicated control strategies, so the patient's training time could be shortened for convenience reasons.

However, there are two main problems to enable natural prosthesis control: First there is the need of a highly sophisticated neuroprosthesis, that has as many degrees of freedom as a human arm does. Moreover, imagined movements have to be decoded by the BCI as close as possible to guarantee natural feeling of the motion[10].

In the studies of Leigh et al. and Collinger et al. [45, 46], an invasive BCI was used to successfully control a robotic arm. Moreover some other studies also used ECoG signals for movement information decoding. In Pistohl et al.'s study [47], 2D hand positions were decoded during arm movements from low-frequency time-domain signals and broad band gamma power modulations. Schalk et al. [48] was able to decode movement trajectories during two-dimensional joystick control and Milekovic et al. [49] classified one-dimensional joystick movement directions online using low-frequency ECoG signals. Ball et al. [50] used the movement-related potential (low frequency time domain signal) for decoding movement direction during a center-out-reaching task to four and eight different targets.

Research shows that SCI suffering persons could also be helped to restore the ability to move via non-invasive BCIs. Grasp function [21, 22] or elbow function [18, 19] with a SMR-based BCI were already restored. These BCIs are capable of detecting MI and use this as a control signal afterwards. Bradberry et al. [51] worked with a center-out-reaching for decoding hand movement velocities. Kim et al. [52] asked subjects to move their hand according to a predefined trajectory to decode those trajectories and [53] used a drawing task to decode hand movement velocities.

1.4 Decoding movement direction and movement targets

The continous decoding of movements would allow the user maximum control over the prosthesis. This, however, requires to extract a huge amount of data from the brain. This process could eventually cause many problems, because decoded signals tend to contain artifacts like noise or they even lack of movement information.

One solution for this problem could be the usage of an intelligent neuroprosthesis control. This BCI control could only be informed about the intended target and then plans and calculates the movement trajectory on its own. Hence, the BCI has to decode the intended

target only, which requires much less information to extract from the patient's brain than to continously decode movement trajectories. SMR-based BCIs may detect the process of MI but not the actual movement itself. I.e., those BCIs can detect the imagination of an arm movement but not the actual trajectory of the movement [54].

This actually is even more natural than planning a trajectory, since we rather identify the actual target than planning how to get there. The movement is then performed by lower level motor systems [10].

There are already some reports in literature available that tell about success regarding target or movement direction decoding corresponding to a target from EEG. Hammon et al. [55] reported classification of a target location during a reaching movement. In the study of Waldert et al. [8] it is written about classifying self-chosen center-out movements with a joystick. The suitability of EEG signals for decoding movement targets was analyzed in [54] and [56].

Information about a movement is carried by low- and also high-frequency EEG signals (delta band and gamma band to a lesser extend [57]). This information can be used to decode movement direction or targets [51, 58, 56] or movement trajectories [55, 59, 60, 44].

1.5 Motivation

Since the accuracy of a decoder for non-invasive movement trajectories for real-time control is not sufficient yet and neither is the decoding of imagined trajectories, there is the need of a more promising approach like the combination of a decoder for target or movement direction and a special system to generate the movement trajectory.

1.5.1 Goal

One general problem of all studies about the decoding of movent targets is that movements of the human arm or any other device like a cursor towards a target also always requires a specific movement direction, i.e. obviously movement targets and movement directions are correponding to each other. This of course makes it very hard to interpret the results of any study, since it can not clearly be told whether movement directions or targets are being decoded. For training a decoder, however, this information would be of huge importance, since it could decide for example about if targets should be displayed in training paradigms or not. Moreover, there is a variable and large number of potential targets in real life applications to choose from. Hence, a decoder that is based on the

movement target would be dependend on the number of targets in the application. To be independent on that number, a decoder based on the imagined movement direction is needed.

1.5.2 Hypothesis

The hypothesis is the following: when training with normal condition data and testing with inverted condition data the classification accuracies would be above chance level in case of target decoding. When classifification accuracies are below chance level it is assumed that the movement direction is decoded. Therefore a study was conducted where subjects were asked to move their arm to one out of two targets. The subjects received live feedback via a computer screen. Subsequently, the feedback was inverted and the same number of trials was repeated to find out whether the decoder is based on the movement target or the movement direction. The decoder was then trained with data of the normal condition and tested on the inverted condition data.

2 Methods

In the following chapter all used methods for performing the required experiments are described. In addition to the experimental setup including the subjects, the experimental paradigm and the electrode positions, also the part of signal processing which includes the artifact rejection and statistic methods will be explained in detail.

2.1 Master's Internship

The starting point for this study was a master's internship with the title „MSMS arm model". It was about building an anatomical correct arm model including bones and muscles by using the software MSMS (MDDF, University of Southern California, Los Angeles, California), that can be controlled by a user. The user should be able to control movements in the shoulder joint, the elbow joint and the wrist and grasping moves.

2.1.1 MSMS software

MSMS (musculoskeletal modulation software) is a software application that can be used to model and simulate human and prosthetic limbs and the task environment they operate in. The simulations can, without limitation, be executed in a standalone computer via Simulink (MathWorks, Massachusetts, USA). The software was developed by the Medical Device Development Facility which is part of the USC Viterbi Department of Biomedical Engineering at the University of South California, Los Angeles, CA [61] [62].

The most important MSMS features that were useful for the assigned task are:

- building anatomically correct models
- modeling muscle and ligament paths
- offline and real-time dynamic animation and simulation

A full list of features and applications can be found on the MSMS website.

2.1.2 Arm model

For building the specific arm model a simplification of a human arm was created. It consisted only of bones, muscles and so called wrapping objects. Although provided by MSMS, there was no usage of ligaments. In the following sections the models' components and the modeling itself are described.

2.1.2.1 Bones

For starting to build a new model the user first has to add a segment. After selecting the segments' shape (sphere, cylinder, box, hemisphere, capped cylinder or mesh), its parent segment and some joint properties (see section "Joints") can be scaled, translated and rotated as desired. For convenience, the first segment should be locked to the point of origin in the coordinate system, i.e. ground. There is always the option to place a segment anywhere else in the three dimensional space. The MSMS software package provides single bone images which can be used in order to replace the standard shapes of a segment. Therefore someone simply has to change a segments' 3D shape to „mesh“ and browse the local network for the specific bone image the user wants to use. After importing an image the user is still able to scale or rotate it. Also, there are several other segments' properties that a user can adjust, e.g. every segment can be given a specific name, a mass, a center of mass and some inertia-parameters. The full bone model is shown in Figure 4.

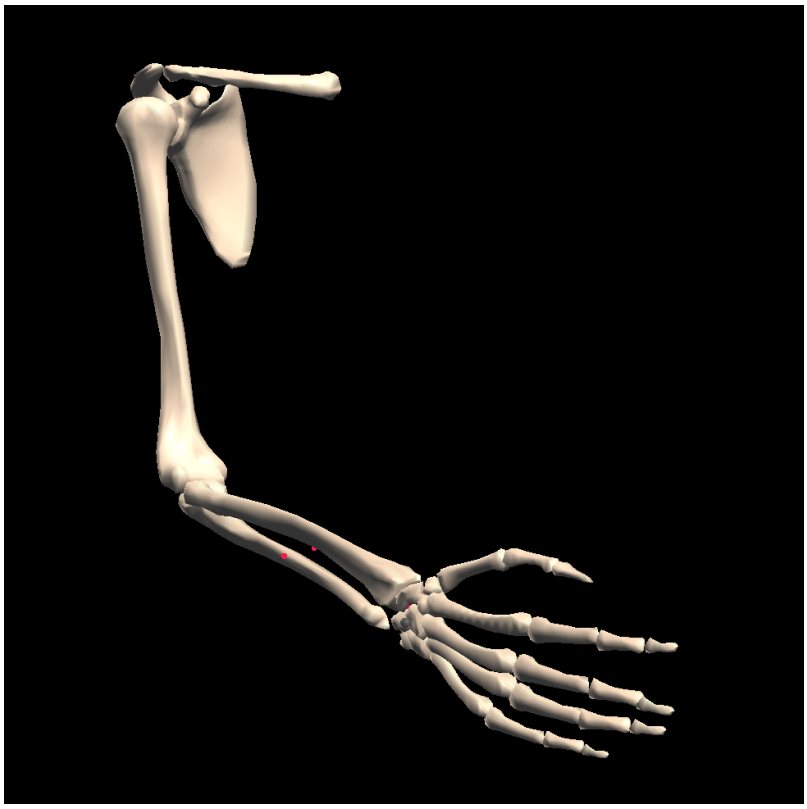

Figure 4: MSMS bone model

2.1.2.2 Joints

To create a joint there is the need of two joint-partners. In the special case of an arm model these two partners are, of course, bones. Every single joint needs to be specified, i.e. there are a lot of different properties to configure. The basic information is the joints' name, its proximal and distal segment and the joint center offset in relation to its parent segment (either the proximal segment or ground). Subsequently, the user needs to set up the joint type and resulting the movement axis and joint limits (see Figure 5). There are several different joint types to choose from as to be seen within Table 1. Each joint type has its specific translational - and rotational degrees of freedom. These specific properties need to be configured precisely in order to guarantee a realistic model.

Table 1: Different joint type options and specific properties.

Type	Properties	No. of trans. degrees of freedom	No. of rot. degrees of freedom
Bearing	one prismatic and three revolute primitives	1	3
Bushing	three prismatic and three revolute primitives	3	3
Cylindrical	one prismatic and one revolute primitives with parallel motion axes	1	1
Gimbal	three revolute primitives	0	3
In-Plane	two coplanar prismatic joint primitives	2	0
Pin/Revolte	one prismatic and one revolute primitives with orthogonal motion axes	1	1
Planar	one revolute and two prismatic primitives	2	1
Slider/Prismatic	one prismatic primitive	1	0
TRANS3	three prismatic primitives	3	0
Universal/Hooke's	two revolute joint primitives	0	2
Weld	zero primitives	0	0

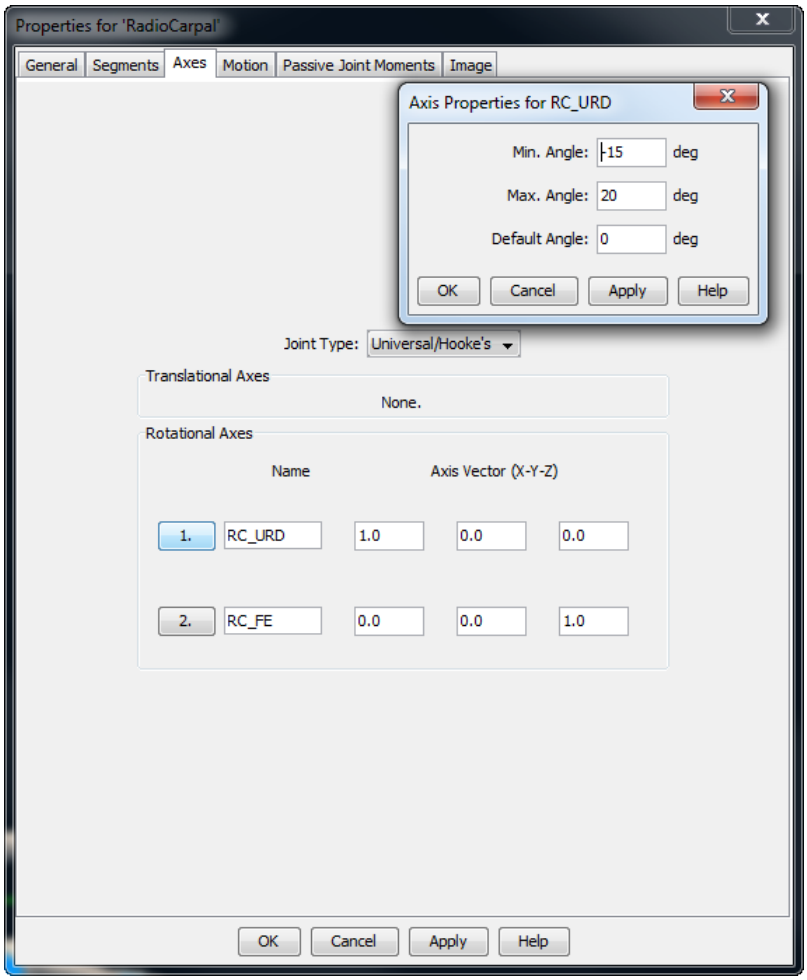

Figure 5: Menu for adjusting joint parameters

2.1.2.3 Wrapping objects

Wrapping objects are abstract objects that can be added to a model in order to design a proper muscle path (see section "Muscles"). A wrapping object can be named by the user and there is also the option of adjusting its shape (cylinder, sphere or ring), position and orientation. These objects are typically placed within joint-areas or along bones to either keep a muscle close to a bone/joint or for making sure that muscles go around specific bone/joint parts (shown in Figure 6). E.g., it can help that muscles do not go through bones.

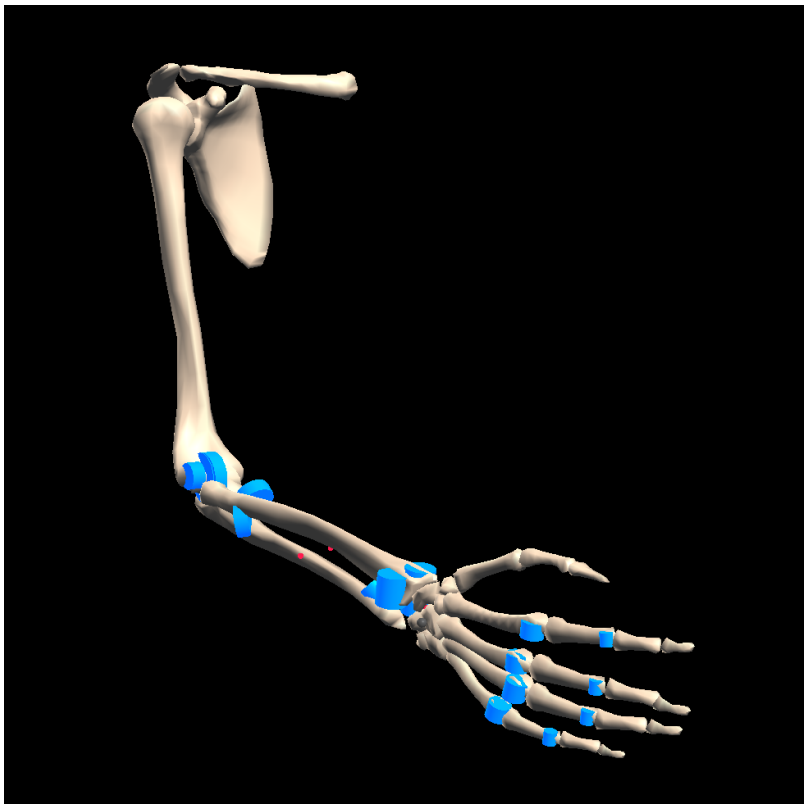

Figure 6: MSMS model including wrapping objects

2.1.2.4 Muscles

Muscles are shown as red strings in MSMS software, i.e. they are only shown abstractly (see Figure 7b). Like configuring bones, joints and wrapping objects, also muscle properties need to be specified. After naming the muscle the user can adjust the muscle path step by step. Every path object (fixed point, moving point or wrapping object) can be edited individually as to be seen in Figure 7a. Additionally, there is the option of configuring a muscles' morphometry and fiber types. This specific model is controlled via kinematic drivers (see section "Controlling"), hence it was not necessary to adjust these special properties. If the user's goal was to calculate or build muscle force-, muscle energetics- or muscle proprioception models, all properties concerning morphometry and fiber types would have to be specified accurately. Detailed information are provided within the MSMS user's manual.

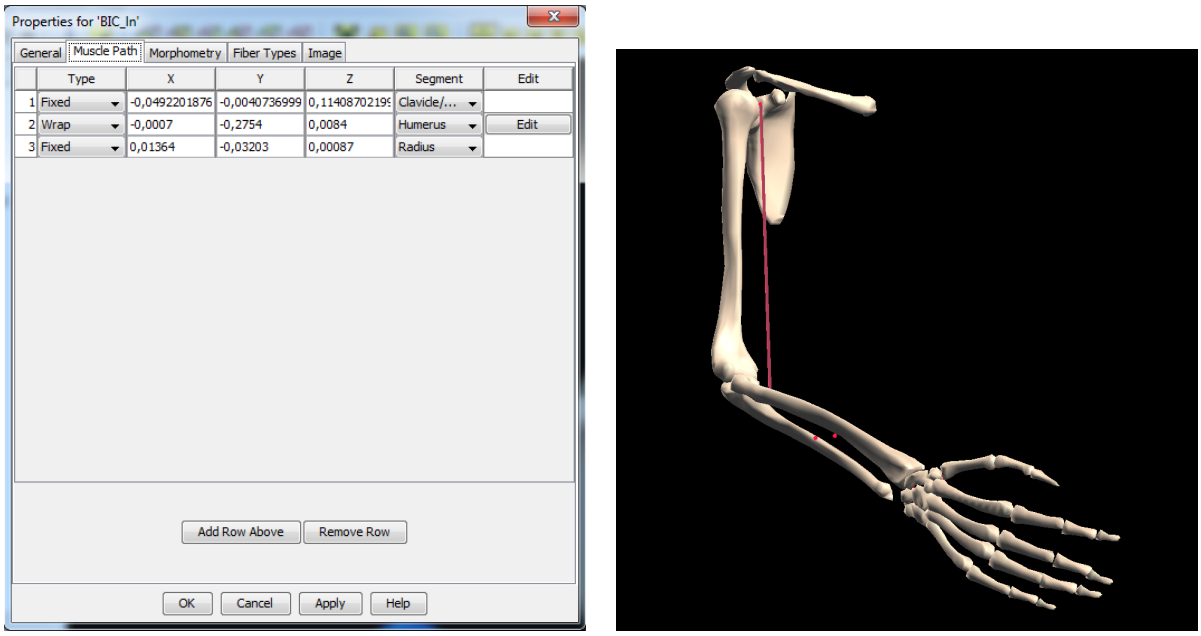

(a) (b)

Figure 7: Figure (a) shows the menu for muscle path cofiguration, Figure (b) shows the long head of biceps brachii within the MSMS model

2.1.2.5 Building the model

This section is a guideline about how the model was constructed step-by-step. Joint Center Offsets, exact points of muscle origins and -insertions and other fine tuning adjustments are not mentioned here. All preferences were chosen after consultation with Rahman Davoodi, head-developer of the MSMS software. For building the arm model the starting point was a segment that consisted of the two separate bones Scapula and Clavicle merged together. Next the Humerus needed to be connected to the first segment. Therefore the Scapula-Clavicle-segment needed to be selected as the parent segment. This action created a joint, the properties of which could be adjusted at that point. For the resulting shoulder joint the joint type chosen was „Gimbal“. This type of joint allows a rotation around three axes. Next, the Ulna was taken as distal part of the Humeroulnar joint, which was adjusted to be a „Pin/Revolte“ type of joint which allows a rotation around only one single axis. To finish the forearm, the Radius was inserted next. The Ulna, as the parent segment, and the Radius created the Radioulnar joint. The Radioulnar joint was also set to be a „Pin/Revolte“-joint. Subsequently the hand was modeled. Therefore all carpal- and metacarpal bones were merged together to reduce the models' complexity. The two forearm-bones and the carpal-metacarpal-segment form the wrist joint. The wrist joint was chosen to be a „Universal/Hooke's“ type of joint for giving the joint two rotational degrees of freedom. To finish the bone part of the model all phalanges

(proximal, middle, distal and proximal, distal for fingers and thumb respectively) were attached to the metacarpal bones. All proximal joints were set to be „Universal/Hooke's"-joints, all the other finger joints „Pin/Revolte"-joints.

After finishing the bone model, the next step was to insert wrapping objects to provide an anatomically correct muscle path. Therefore cylindric-shaped wrapping objects different in height and diameter were placed within joint areas of the elbow, wrist and fingers.

Subsequently, all essential muscles for movements in the joints mentioned (shoulder joint excluded) were fixed into the bone model. For this step the muscle origins and -insertions had to be looked up in an anatomical atlas and then those specific points had to be transferred onto the model. Moreover, for anatomically correct muscle paths, wrapping objects needed to be used. The completed MSMS arm model can be seen in Figure 8.

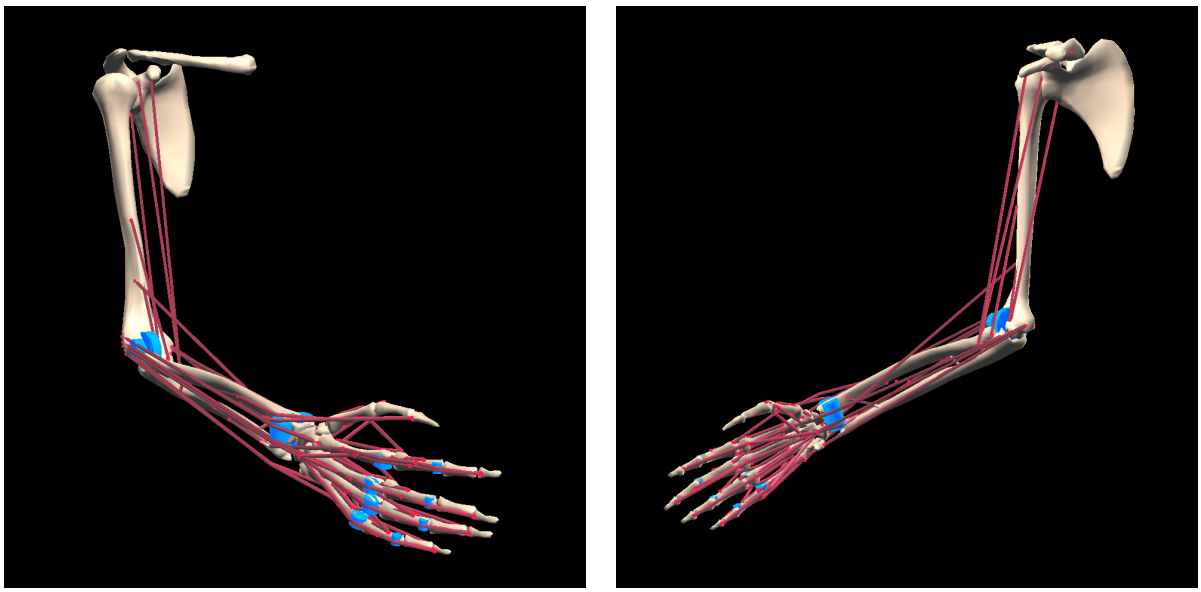

(a) Dorsal view (b) Palmar view

Figure 8: Full MSMS arm model in dorsal (a) and palmar (b) view. The model includes bones, wrapping objects and all muscles that are needed for movements in the elbow-, wrist-, finger- and thumb joints.

2.1.3 Simulation via Simulink

One huge advantage about the MSMS software is the option of a one-klick creation of a Simulink Model to simulate the physics-based movements of the MSMS model. Before exporting the model to Simulink, the simulation can be configured with the simulation setup. In this setup several adjustments can be made. For physics-based simulations a gravity vector can be set. All initial conditions for each degree of freedom in the model

could be entered here as well, e.g., the initial joint angles could be adapted. Moreover it was important to setup the solver, i.e., the simulation time, the type of numerical integration (Fixed-step or Variable-step), also the type of the numerical integration algorithm and the numerical integration step sizes and tolerances could be selected. These parameters could also be changed later in the Simulink model. For exporting the arm model the fixed-step size solver ode3 (Bogacki-Shampine) and a fixed-step size of 1/512 (adjusted according the sampling rate) were chosen as settings.

Also, the user can select the sampling time, the output data filename, and for the live animation which data streaming model and data type should be used. As sampling time, data streaming model and data type 1/512 s, the MSMS UDP Block and Feature Commands were selected respectively.

After adjusting all parameters as desired, the user can simply click the „Convert to Simulink“ command to save a Simulink simulation model (.mdl) in the model's Matlab folder. The generated model can be opened in Matlab's Simulink program (shown in Figure 9). The simulation model will generate motion data when executed, which are sent to MSMS via UDP (user datagram protocol) for online animation. In order to view the simulation motion in MSMS while the simulation is running in Simulink, the animation needs to be setup and run from the animation menu.

In the animation menu „From Live Source“ must be selected as source of animation data. After the animation is setup, the start command is active and the MSMS model will be receiving data from the Simulink model via UDP.

2.1.4 Controlling the model

In order to control the MSMS model via the Simulink model, new components were added to the arm model in MSMS. These so called kinematic drivers can be used to create movements within the joints. It was then able to rotate and/or translate joints according to their degrees of freedom. For every movement a separate kinematic driver needed to be installed, i.e., for flexion/extension, abduction/adduction and internal/external rotation in the shoulder joint three kinematic drivers had to be integrated. The kinematic drivers could then be actuated in Simulink with simple slider blocks so it was possible to animate the MSMS model in real time.

The following sliders got installed: three sliders for controlling the shoulder joint (flexion/extension, abduction/adduction, internal/external rotation), two for controlling the elbow joint (flexion/extension in the Humeroulnar joint, pronation/supination in the Radioulnar joint), two for controlling the wrist joint (pronation supination, radial-/ulnar

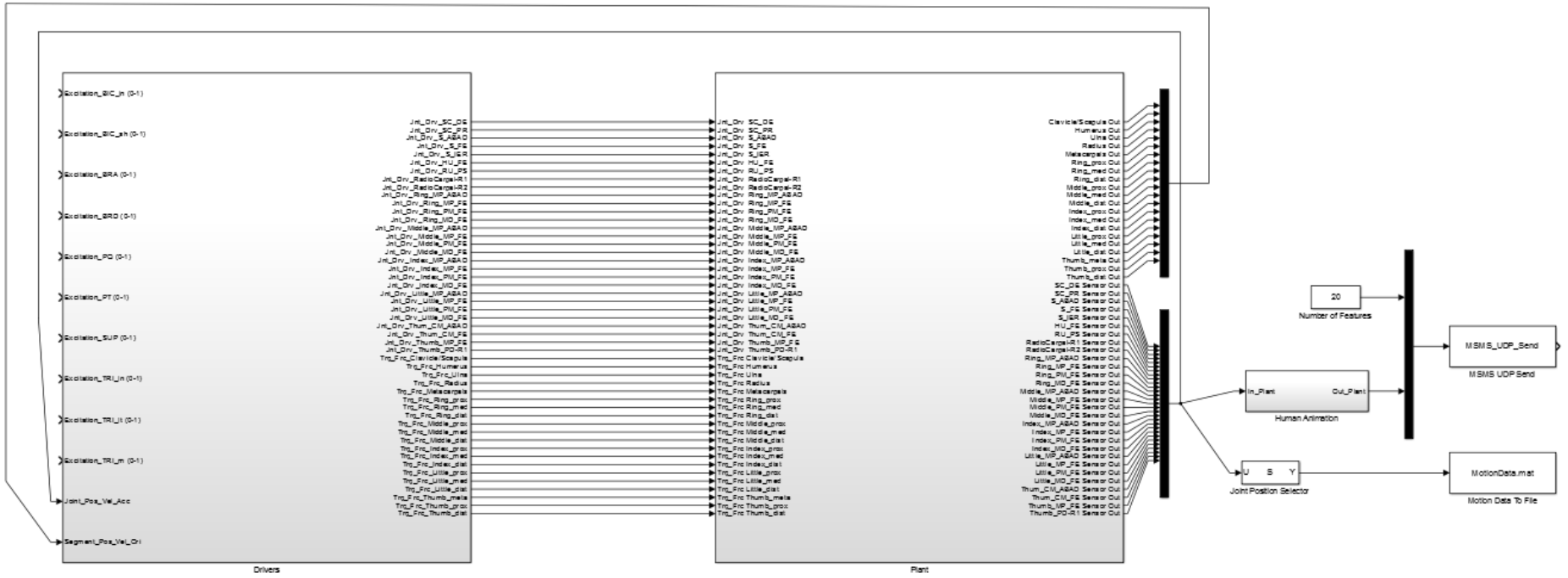

Figure 9: Exported MSMS Simulink model, that was created after using the ”Convert to Simulink” command.

deviation) and finally two for controlling a palmar grasping motion. For the palmar grasp all kinematic drivers actuating the finger joints got linked together and could be controlled by just one single slider. Also, the thumb joints were controlled by one single slider. All joint slider blocks can be seen in Figure 10.

Furthermore, it is also possible to control movement by the muscles. Therefore the user has to apply input muscle activations in the Simulink model, e.g., a constant or time-varying activation. However, this is a very complex topic and it is necessary to ensure that all muscle parameters are correct and within range. Otherwise it is almost impossible for Simulink to numerically integrate the equations of motion.

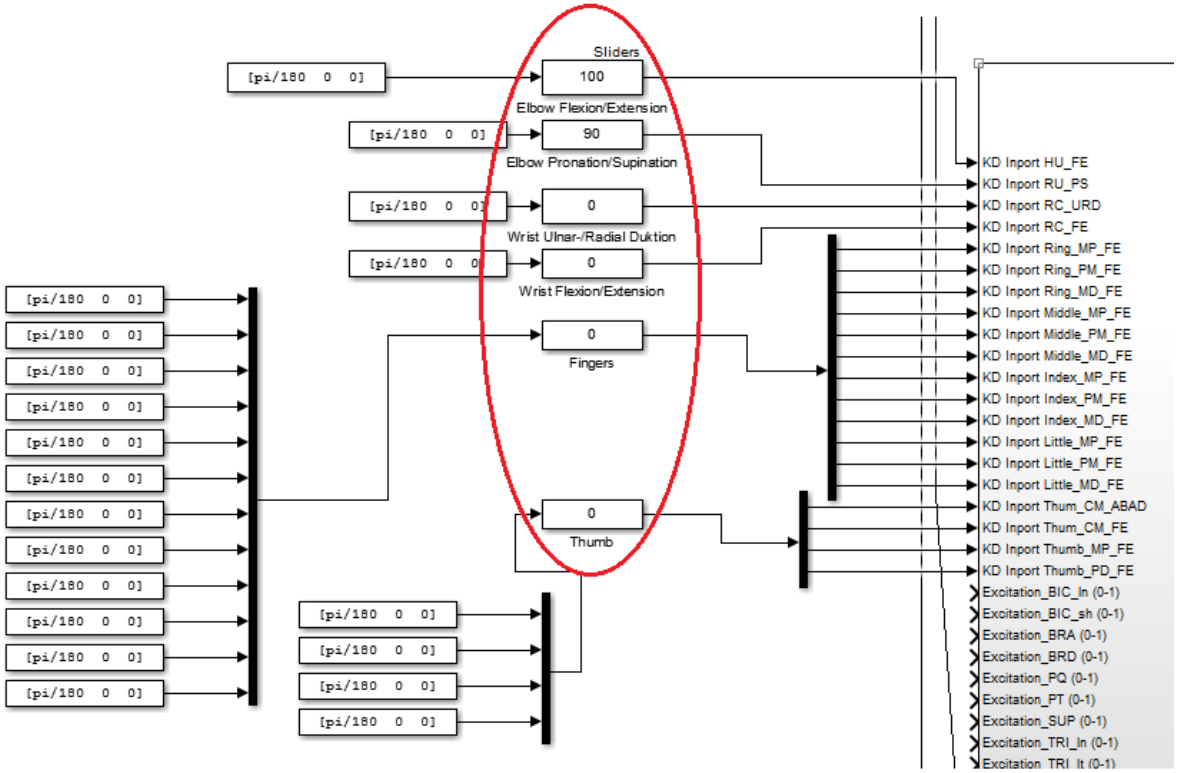

Figure 10: Joint slider blocks that are added in order to control the MSMS model

2.2 Implementation and detailed design decisions

2.2.1 ARMEO Spring device

The ARMEO Spring (Hocoma, Switzerland), which is shown in Figure 11, is a rehabilitation device designed for people with lost or restricted function in their upper extremities. This disability could be caused by either central or peripheral damage of the nervous system (e.g., spinal cord injuries (SCI) or CP), muscular disorders (e.g., upper limb ataxia)

or bone-related disorders (e.g., humerus fracture). Basically it is an ergonomic and adjustable exoskeleton that allows the training of specific exercises in order to increase muscle strength and range of motion by supporting the subjects' arm from gravity. This should help to improve motor function. By providing arm weight support it is possible to use any remaining motor function of the patients and of course to prevent muscle fatigue during exercises or, in case of this experiment, during long testing. Moreover and even more important, through intensive, highly repetitive, task-orientated movements, brain pasticity can be regained after neurological injury and new neural connections can be made [63] [64].

With the built-in sensors of the ARMEO Spring it is possible to keep track of the hand-, elbow- and shoulder position and joint angles during sessions. The data was send directly from the rehabilitative device via Lab Stream Layer (LSL) to a computer where it was processed and then presented to the participants to inform them about their actual hand-/arm position and their actual joint angles in real time.

Figure 11: ARMEO Spring rehabilitative device [64].

2.2.2 Simulink model

Starting point of the specific Simulink model, that was needed for not only recording data (EEG, EOG and movement data) but also for simulating and controlling the MSMS feedback model, was the institute's Moregrasp Simulink model. This Simulink model basically consists of three seperate blocks: The first block is the interface with the customized TOBI signal server (TiA/TiD Client), where all the data is received and saved in the „General Data Format“ („.gdf“) [65]. This storage happens in a separate block. The third block is responsible for generating and displaying the experimental paradigm (described in a later section) and for saving the occurring events.

In order to receive all the specific data, handle the paradigm and also control the MSMS model, the Morgrasp Simulink model needed to be adapted at some points. Therefore two extensions were implemented. First there was the need of a connection between the MSMS Simulink model and the Moregrasp Simulink model. That was achieved by simply paste the MSMS Simulink model into the Moregrasp Simulink model into a subsystem („MSMS Control“) that was constantly receiving data from the TiA/TiD Client before the data was saved.
The second adjustment was needed to be done for the paradigm-block. Since the paradigm was depending on the ARMEO Spring data, the ARMEO Spring's actual hand position needed to be checked constantly. In the „Hand-Target-Check“-block a simple Matlab code compared the actual hand position with the coordinates of the specific target the subject was asked to reach. More detailed information about the experimental paradigm can be found in the designated section. The extensions are shown in Figure 12.

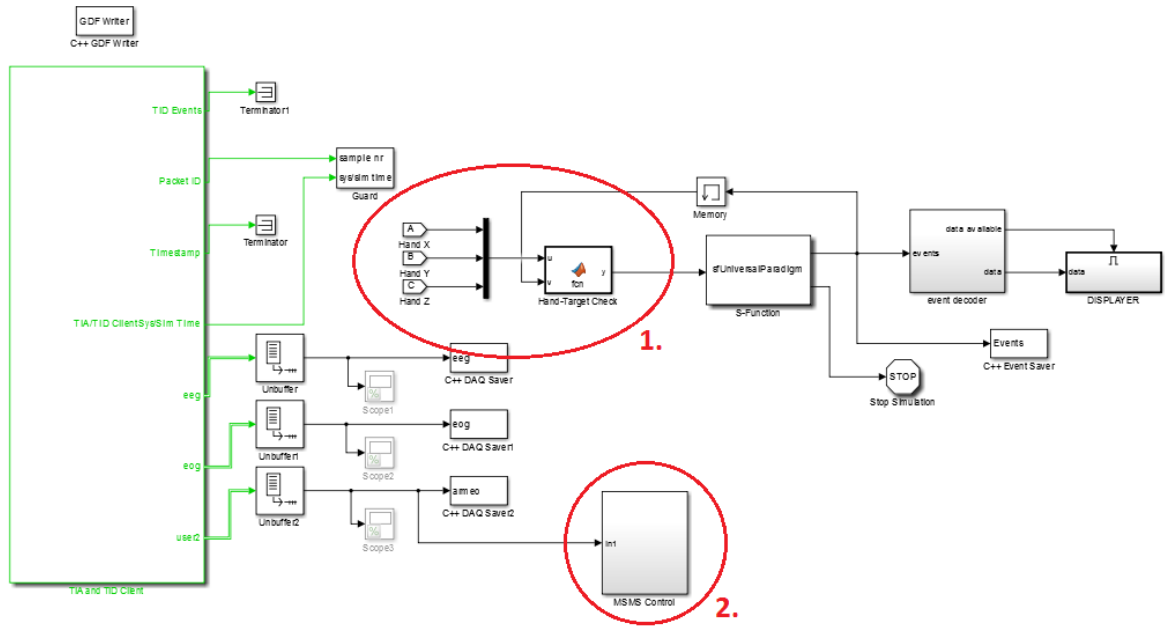

Figure 12: Simulink model. 1. Handling of the experimental paradigm based on the actual ARMEO Spring's hand position. 2. Inclusion of the MSMS model

As already mentioned in a previous section, the use of muscles as controllers for the MSMS arm model requires expertise. Points of origin and insertion need to be found exactly and all muscle parameters need to be adjusted precisely. Since there was no real need of controlling the arm model via muscles, this task was undertaken by kinematic drivers. Hence, all muscles in the MSMS Simulink model were deleted in order for the simulation to run stable. So the only inputs that remained were the kinematic driver inputs, which were supplied by the actual ARMEO Spring movement data constantly gained with the TiA/TiD client.

2.3 Experimental design

2.3.1 Subjects

In the experiment 10 healthy subjects (nine male, one female) were included. All of them were right-handed and had normal or corrected-to-normal vision. None of them had participated in any BCI experiments before. They were aged between 25 and 32 years with a mean value of 27.7 and a standard deviation of 2. All of them signed an informed consent.

2.3.2 Experimental paradigm

For the experiment two conditions were created: (i) During the normal condition subjects moved their arm to the demanded target and were presented a feedback showing the virtual arm on the computer screen moving exactly like the subjects' arm. (ii) During the inverted condition the computer screen presented an inverted feedback to the subjects. I.e., in order to reach the actual target, subjects had to move their arm to the opposite target.

A trial was started by an audio cue that either commanded "Red" or "Blue". The instruction for the subject was to immediately look at the specific target, so eye movements happened in a controlled way before the actual movement onset and will not affect the classification to a later point in time. Otherwise, eye dipole movements would heavily influence the recorded EEG. A second audio cue, "go cue", which was presented as a beep, followed three to five seconds after the trial start. One to three seconds after the go cue participants started to reach towards the specific target. As soon as the subjects controlled the virtual arm to the target asked for, another beep tone (success cue) sounded to confirm that the task was completed successfully. The comparison of the actual arm position and the target coordinates was performed within the Matlab block in the Simulink model mentioned in a previous section. Whenever a specific target was reached, subjects were instructed to move their arm back to the starting position. A trial ended two seconds after reaching a target. The last part of a trial was a break with a randomized length between one and three seconds. The paradigm is skeched in Figure 13.

A run was built up by 15 trials for each target, randomly distributed, resulting in 30 trials for every single run. Overall, 12 runs were recorded - six for normal condition and six for inverted condition, always changing the condition after two runs (see Table 2). In total 360 trials (180 trials per condition; 90 trials per class for every condition) were recorded. Additionally, a resting state run and a run with deliberate eye movements were recorded twice (in the beginning and in the middle of the experiment). However, the recorded signals of theses runs were not used in this work.

The paradigm's sequence (i.e., positioning and presentation of the cues, duration of the single phases or number and order of trials) was controlled by .xml files, that were started by the user via Matlab.

Table 2: Experimental paradigm - run sequence. "Rest run" describes the resting state runs and "EOG run" describes the runs with deliberate eye movements.

Run No.	Type
1	Rest run
2	EOG run
3	Normal condition
4	Normal condition
5	Inverted condition
6	Inverted condition
7	Normal condition
8	Normal condition
9	Rest run
10	EOG run
11	Inverted condition
12	Inverted condition
13	Normal condition
14	Normal condition
15	Inverted condition
16	Inverted condition

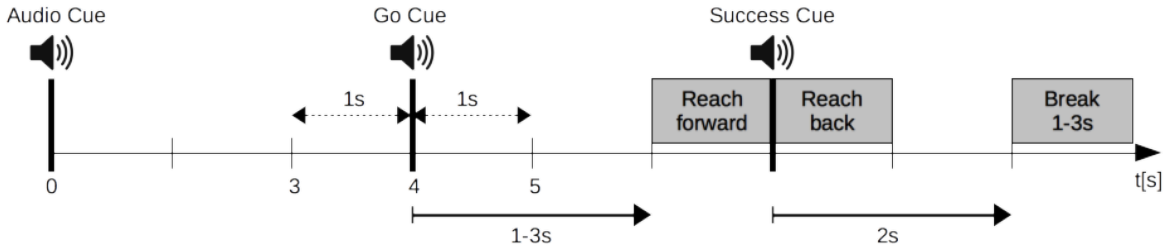

Figure 13: Paradigm and timing of a single trial. Audio cue started the trial, go cue followed after 3 s to 5 s. Subject started self paced movement 1 s to 3 s after go cue. When virtual arm reached specific target, success cue sounded. After success cue, subject moved its arm back to starting position and a 1 s to 3 s break followed.

2.3.3 Setup

In the experimental setup subjects were seated on a chair that was placed in an electrical shielded measurement box, and their right arm was fixed in an ARMEO Spring rehabilitation device. Sound was presented via speakers that were present in the measurement

box as well. Each of the subjects was told to sit as still as possible and to avoid additional muscle activity (e.g. blinking or clenching the teeth) or movement accept the ones being told during the experiment.

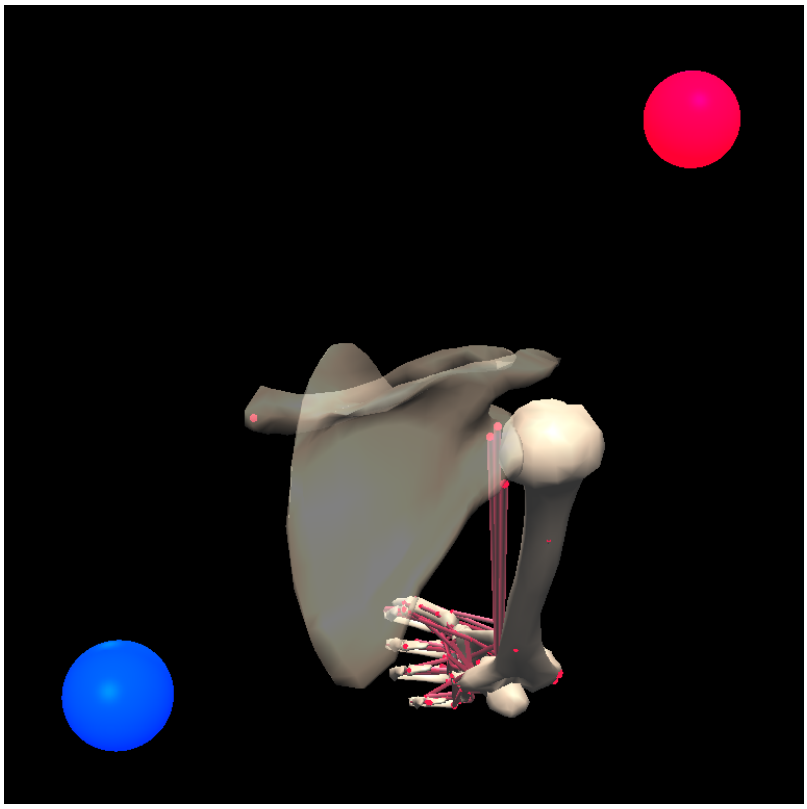

Figure 14: MSMS arm model in experimental setup, i.e. first person view, transparent scapula, joints in starting position and including red and blue target.

Subjects were placed in front of a computer screen that showed a red and a blue target. The targets were positioned in the right upper corner and in the left lower corner, respectively. Moreover, the MSMS arm model (as described in previous sections) was shown on the computer screen as a visual feedback (as depicted in Figure 15). Participants were able to control the model with the ARMEO Spring as mentioned before. For the experiment a self paced center-out reaching task was developed. Therefore subjects had to move their right hand from a starting position (about 150 degrees elbow flexion, 60 degrees shoulder flexion and 0 degree abduction in the shoulder joint) to an end position, that corresponded to touching a specific target with the virtual hand on the computer screen. Subjects were instructed to perform natural, round (not jaggy) and in speed varying arm movements. The final position for reaching the red target required a 100 degree flexion and 20 degree abduction in the shoulder joint and a 150 degree elbow flexion. For reaching the blue target it was a 60 degree flexion, 20 degree adduction and 30 degree internal rotation in

the shoulder joint and a 150 degree elbow flexion.

Figure 15: Experimental setup. A subject sitting in front of a screen which presented feedback. EEG electrodes mounted and connected to 5 USBamps.

2.3.4 EEG measurment and data acquisition

For recording EEG signals from the scalp 68 passive Ag/AgCl electrodes covering frontal, central, parietal and temporal areas were used. Therefore an electrode cap with equidistant electrode positions was taken with a mean horizontal and vertical distance of 2.5 cm (see Figure 16). Three electrooculography (EOG) electrodes, positioned above the nasion and below the outer canthi of both eyes were also used. The reference electrode was placed on the left mastoid, ground on the right mastoid. All electrode impedances were tried to keep below 5 kΩ before starting the testing.

For acquiring raw EEG signals these were band-pass filtered from 0.01 Hz to 200 Hz with an 8^{th}-order Chebyshev filter. Also, a Notch filter at 50 Hz was applied. The sampling rate for the experiment was chosen to be 512 Hz using five biosignal amplifiers (g.tec medical engineering GmbH, Austria). For subsequent source imaging (not performed in this study), electrode positions were measured with ELPOS (Zebris Medical GmbH, Germany).

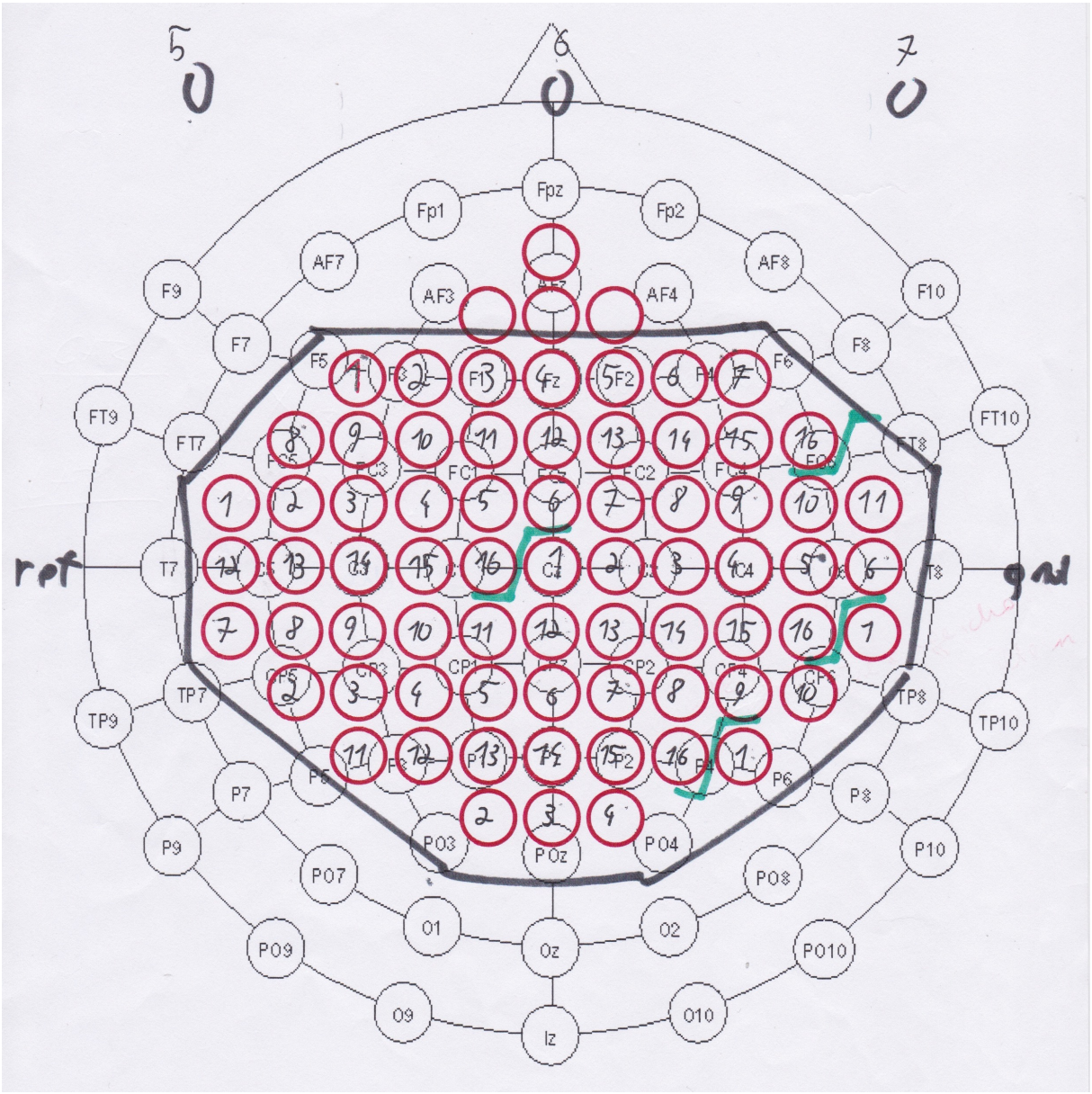

Figure 16: Electrode positions. All numbered red positions within the black frame were used. Green markers indicate a new amplifier. ref and gnd represent reference and ground, respectively. Electrode positions 5, 6 and 7 mark the EOG electrodes.

2.3.5 Software

A customized TOBI Signal Server [66], Matlab and Simulink (MathWorks, Massachusetts, USA) were used to record EEG-, EOG- and movement data (i.e., 3D positions and joint angles of the right arm). Data processing was done with Matlab and Simulink as well. For recording the movement data a custom made plugin, that was developed in the BCI lab, for the ARMEO Spring software was used. For presenting the paradigm Ruby (Yukihiro

Matsumoto et al., `http://rubygame.org/`) was chosen.

2.4 Data processing

2.4.1 Artifact rejection

Before the actual artifact rejection was applied, a possible linear trend was removed from the raw EEG data using the Matlab function loadAndPreprocessSignals() from the BCI lab. Next, trials which were suspected to contain muscle, technical or movement artifacts were marked. Therefore a 4^{th}-order zero-phase Butterworth filter was used to bandpass filter the data from 0.3 Hz to 70 Hz. All trials that exceeded a threshold of three times the standard deviation of the absolute value, Kurtosis or joint probability were deleted and excluded from any further processing steps. For the implementation special Matlab functions (eegthresh(), rejkurt() and jointprob()) provided within the BCILab toolbox (open-source Matlab application), were used.

2.4.2 Determination of the movement onset

All results refer to the movement onset. Hence, it was of prime importance to find the specific moments in time of the movement onsets as close as possible. For determination the recorded x-, y-, and z-datasets of the ARMEO Spring's hand position was used to perform a principal component analysis (PCA). For further calculations only the differentiated first principal component was used. A movement onset was detected every time a certain threshold was crossed after the go cue. The threshold was found empirically. Trials with bad onsets (e.g. subjects started to move and reach for a target before the actual go-cue) were removed.

2.4.3 Motor-related cortical potentials (MRCPs)

Before calculating the MRCPs the preprocessed EEG data was bandpass filtered from 0.3 Hz to 35 Hz with a 4^{th}-order zero-phase Butterworth filter. The MRCPs were calculated for every subject, for both conditions and for each single electrode position with respect to the time intervall of -2 s to 2 s relative to the movement onset. For displaying, also the confidence intervals were determined with a bootstrap test (alpha = 0.05).

2.4.4 ERD/ERS maps

The decrease and increase of relative band power due to an event or cue is called event-related desynchronization or ERD and event-related synchronization or ERS. Changes in brain oscillations are not phase-locked but time-locked to an event or cue. These relative power changes can be visualized in time-frequency plots. [38] [67]

Before the ERD/ERS maps were calculated, a common average reference (CAR) spatial filter was applied on the preprocessed EEG datasets. Then, ERD/ERS analysis was performed for frequency bands between 5 Hz and 40 Hz with respect to a specific reference interval (-1.5 s to -0.5 s relative to movement onset). ERD/ERS analysis was performed in overlapping 2 Hz frequency bands. The statistical significance of the ERD/ERS values was determined by applying a t-percentile bootstrap algorithm with a significance level of $\alpha = 0.05$ [67]. ERD/ERS maps were created using the Matlab functions calcErdsMap() and plotErdsMap(), which are provided within Biosig toolbox, which is a Matlab open-source application from our lab.

2.4.5 Classification accuracies

Before applying a shrinkage linear discriminant analysis (sLDA) to discriminate between the two red and blue targets [68], the already preprocessed EEG data was bandpass filtered from 0.3 Hz to 3 Hz with a 4^{th}-order zero-phase Butterworth filter. This processing step was done to extract low frequency signals. For computational convenience the data was downsampled to 16 Hz. Subsequently the classification accuracy within a time window -2 s to 2 s relative to the movement onset was computed.

Two different analyses were conducted: In the first analysis, data from all bandpass filtered EEG channels was used to classify a moving time window of 750 ms. Therefore all EEG data within the window of the past 750 ms, which corresponded to 16 sample points, were used for calculation before the window was moved one sample further. This procedure was repeated until the last sample was reached. For the calculation of the classification accuracies, which was separately performed for normal and inverted condition, a 10 x 10 fold cross-validation was used.

In order to find out whether the target or the movement direction was decoded, another analysis was performed. Therefore, the normal data was used as training data and the inverted data was used for testing.

3 Results

The following chapter presents the MRCPs and ERD/ERS maps, as well as the classification accuracies for normal and inverted condition and results for the investigation about the decoding of target or movement direction.

3.1 Movement-related cortical potentials

The following Figures 17 and 18 present the MRCPs for the normal and inverted condition, respectively. The MRCPs were calculated for the electrode positions FC3b, FCzb, FC4b, C5b, C3, Cz, C4, C6b, CP3b, CPzb and CP4b with confidence intervals as determined with a bootstrap test ($\alpha = 0.05$). Second zero represents the movement onset, the red and blue target are represented by the red and blue graph, respectively. Plots show the average MRCPs over all subjects (seperate MRCPs for every single subject can be found in the appendix). It can be observed that differences in the normal condition occur at movement onset and around the target approach. The differences in the inverted condition are more distinct. Amplitude differences can be noticed starting about 0.5 s before movement onset lasting up to 2 s after movement onset.

3.2 ERD/ERS maps

Figures 19 and 20 show ERD/ERS maps of subject DV3 for normal and inverted condition, respectively. The subject was chosen, because it showed the best and most specific results. All the other results can be found in the appendix. The time-frequency plots were calculated for 11 channels (FC3b, FCzb, FC4b, C5b, C3, Cz, C4, C6b, CP3b, CPzb and CP4b) from -2 s to 2 s relative to the movement onset. Hot colors indicate significant power decrease (ERD) and cold colors indicate significant power increase (ERS). Vertical dashed lines represent the reference period, vertical solid line represents the movement onset.
During normal condition a strong ERD in the frequency range from about 8 Hz to 10 Hz can be noticed over C3, Cz, C4 and parietal channels after movement onset. Also after movement onset, a strong ERD over C4 in beta range (about 15 Hz to 20 Hz) is noticeable. During inverted condition the power decrease (ERD) can be detected (after movement onset again) over similar areas, ERD in beta range however is more distinct over C3 and parietal areas.

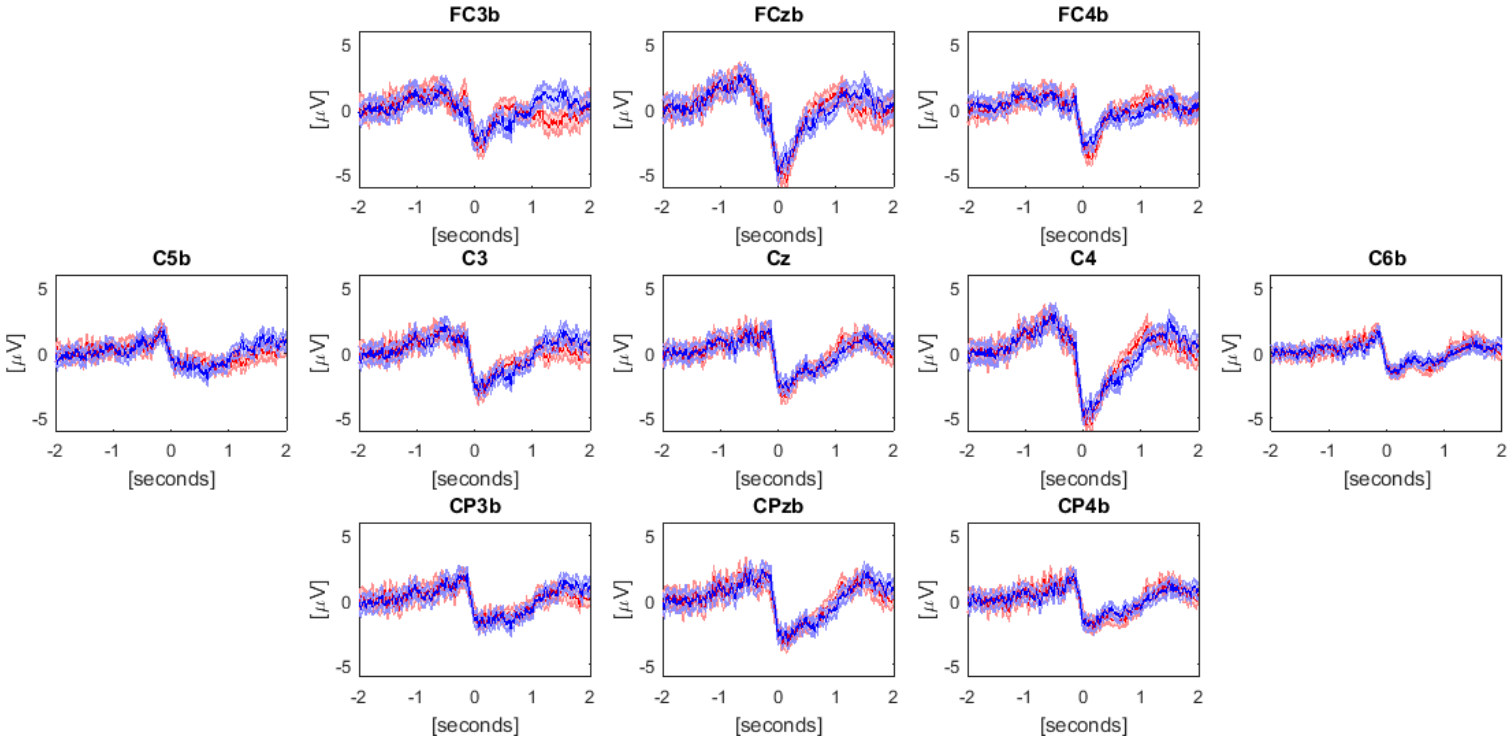

Figure 17: MRCPs evolving for normal condition from -2 s to 2 s relativ to movement onset. The average MRCPs for both, red and blue target including confidence interval as determined with a bootstrap test ($\alpha = 0.05$) are shown.

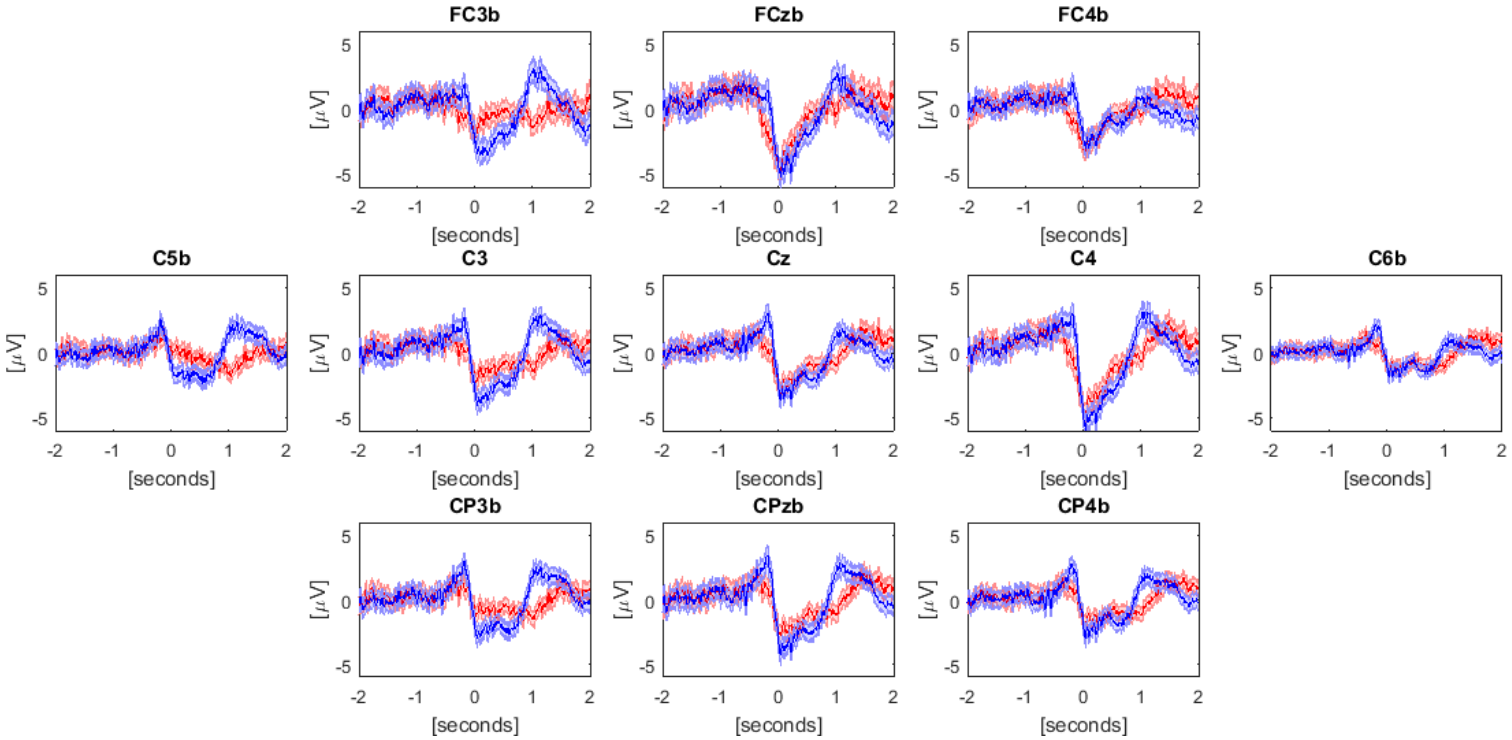

Figure 18: MRCPs evolving for inverted condition from -2 s to 2 s relativ to movement onset. The average MRCPs for both, red and blue target including confidence interval as determined with a bootstrap test ($\alpha = 0.05$) are shown.

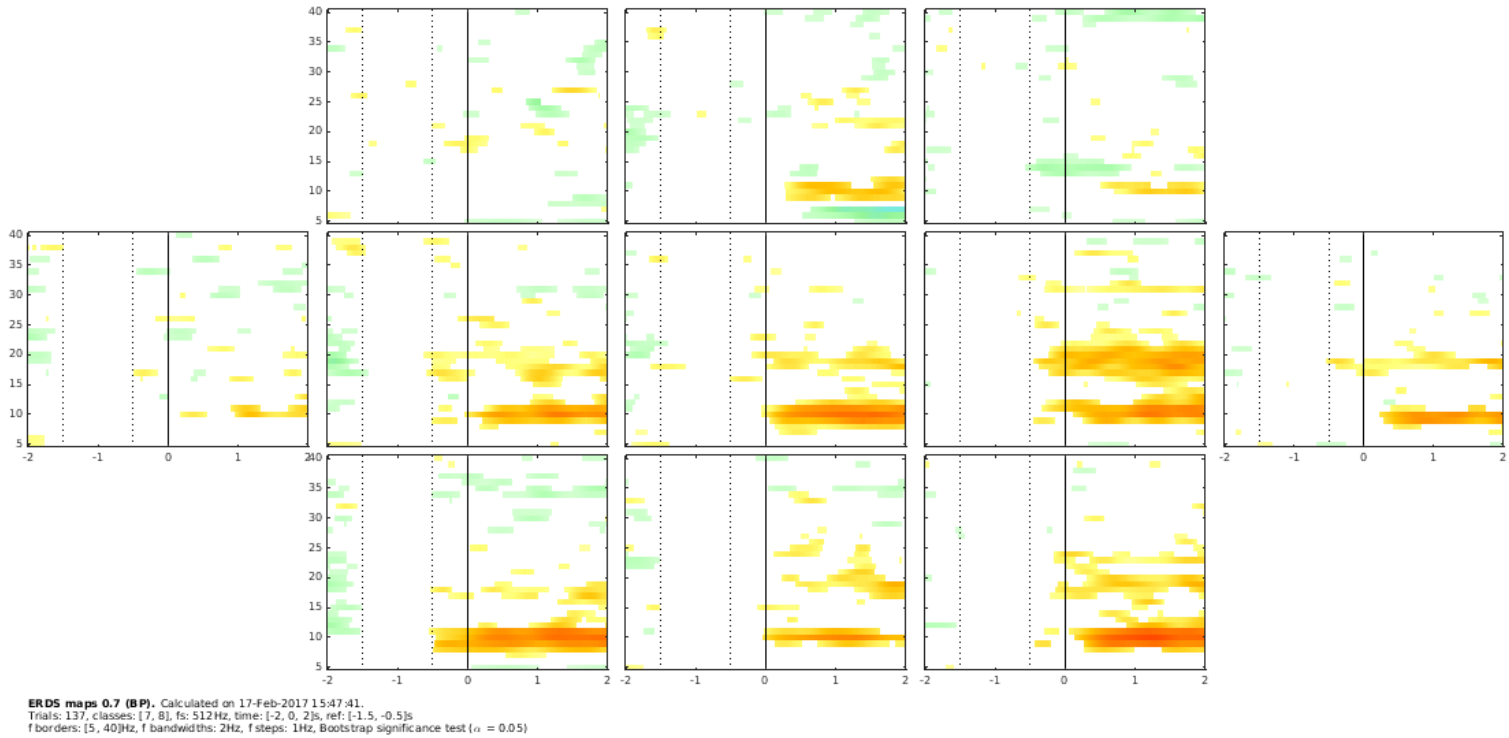

Figure 19: ERD/ERS map for subject DV3 at specific electrode positions during normal condition experiment. Hot colors indicate ERD, cold colors indicate ERS. Vertical dashed lines mark the reference period, vertical solid line marks the movement onset.

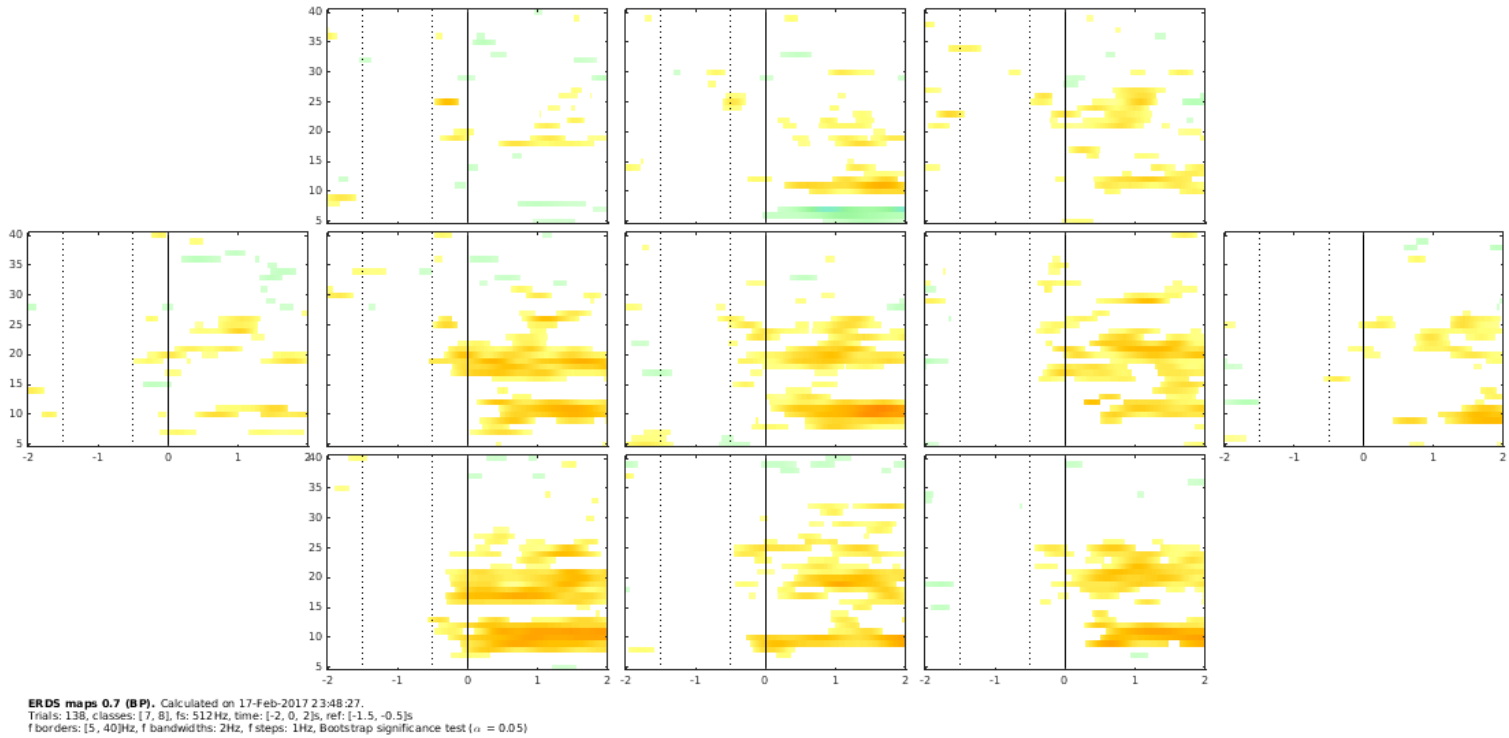

Figure 20: ERD/ERS map for subject DV3 at specific electrode positions during inverted condition experiment. Hot colors indicate ERD, cold colors indicate ERS. Vertical dashed lines mark the reference period, vertical solid line marks the movement onset.

3.3 Classification

Figures 21 and 22 are showing the classification accuracies for the normal condition and inverted condition, respectively. Classification accuracies were calculated in the time interval -1 s to 2 s relative to movement onset (movement onset = 0 s) and are scaled from 0 to 1. For calculation of the significance level (61.35 %) $\alpha = 0.05$ and an adjusted Wald interval was used. That means that α is devided by the number of samples in the time interval. Subsequently, Bonferroni correction for the number of shown sample points was performed [69].
In Table 3 the average movement times and standard deviation for reaching red and blue targets in normal and inverted condition are shown. Seperate plots for every single subject can be found in the appendix. For normal condition the maximum average classification accuracies was 0.78 and for inverted condition it was 0.79. Table 4 shows the maximum classification accuracies for all the subjects and the average.

Table 3: Average times and standard deviation for reaching specific target in normal and inverted condition.

Target	Normal cond. [s]	Inverted cond. [s]
Red	1.20 ± 0.65	1.36 ± 0.76
Blue	1.41 ± 0.74	1.10 ± 0.65

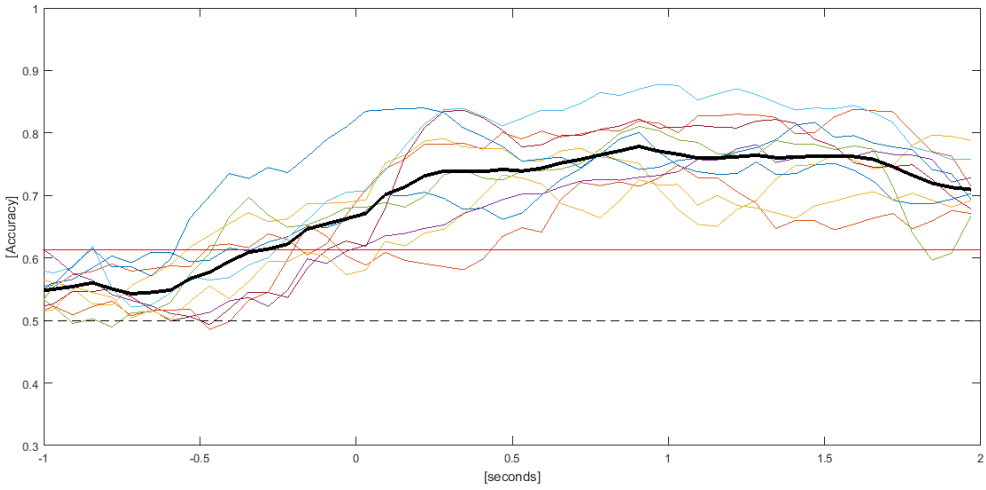

Figure 21: Cross-validated classification accuracies for the normal condition from -1 s to 2 s relativ to movement onset. Plot shows average for every subject and the grand average. Dotted horizontal line marks chance level, red horizontal line marks significance level of 61.35 %

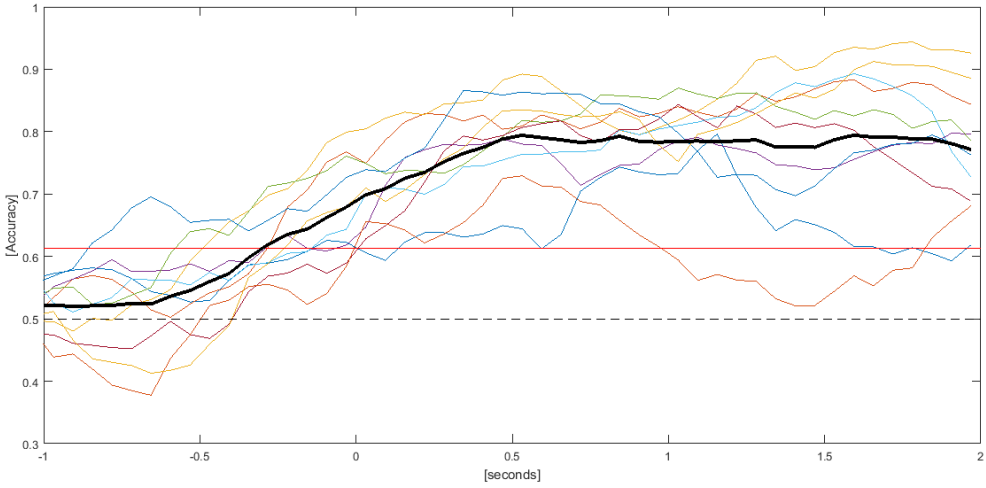

Figure 22: Cross-validated classification accuracies for the inverted condition from -1 s to 2 s relativ to movement onset. Plot shows average for every subject and the grand average. Dotted horizontal line marks chance level, red horizontal line marks significance level of 61.35 %

Table 4: Maximum classification accuracies for all subjects during normal and inverted condition, maximum average classification accuracy and standard deviation (scaled from 0 to 1).

Subject	Class. Acc. Normal cond.	Class. Acc. Inverted cond.
DU4	0.80	0.80
DU5	0.84	0.88
DU6	0.80	0.94
DU7	0.78	0.80
DU8	0.81	0.87
DU9	0.88	0.89
DV1	0.84	0.84
DV2	0.84	0.87
DV3	0.75	0.73
DV4	0.73	0.91
Average	0.78	0.79
SD	0.045	0.062

3.4 Classification (testing with inverted condition)

As mentioned in a previous section the second analysis was about determining whether the target or the movement direction was decoded. Therefore the classifier was trained on the normal condition data and was tested on the inverted condition data. Accuracies below chance level are indicating movement direction decoding, since subjects moved their hand to the opposite direction of the specific target. Target decoding causes accuracies above chance level.

Figures 23 and 24 demonstrate that two groups (I and II), different in results, arose. While group I shows an almost linear increase in classification accuracy after movement onset with a maximum average classification accuracy of 0.71 when reaching the target (Figure 23), group II acts differently. Classification accuracies first decrease until movement onset and then start to increase until it reaches a maximum average of 0.70 shortly after reaching the the target (Figure 24). Classification accuracies again were calculated in the time interval -1 s to 2 s relative to movement onset (movement onset = 0 s) and are scaled from 0 to 1. The significance level was again 61.35 %. Seperate plots for every single subject can be found in the appendix.

Table 5: Maximum classification accuracies for subjects that belong to group I, maximum average classification accuracy and standard deviation (scaled from 0 to 1).

Subject	Class. Acc.
DU4	0.66
DU5	0.80
DU7	0.78
DU8	0.74
DV3	0.68
DV4	0.76
Average	0.71
SD	0.056

Table 6: Maximum classification accuracies for subjects that belong to group II, maximum average classification accuracy and standard deviation (scaled from 0 to 1).

Subject	Class. Acc.
DU6	0.75
DU9	0.82
DV1	0.68
DV2	0.69
Average	0.70
SD	0.065

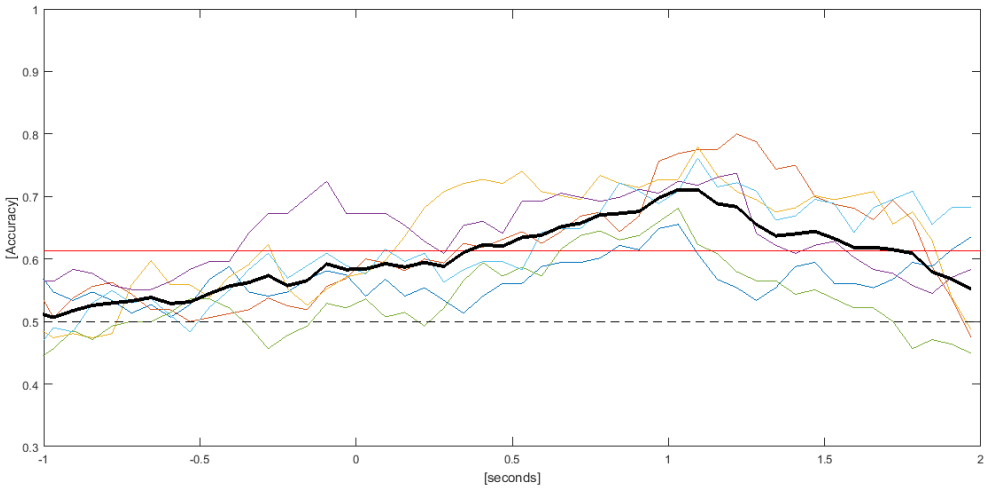

Figure 23: Classification accuracies - training with normal condition data, testing with inverted condition data. Time frame -1 s to 2 s relativ to movement onset. Plot shows average for subjects from group I and the grand average for the group. Dotted horizontal line marks chance level, red horizontal line marks significance level of 61.35 %

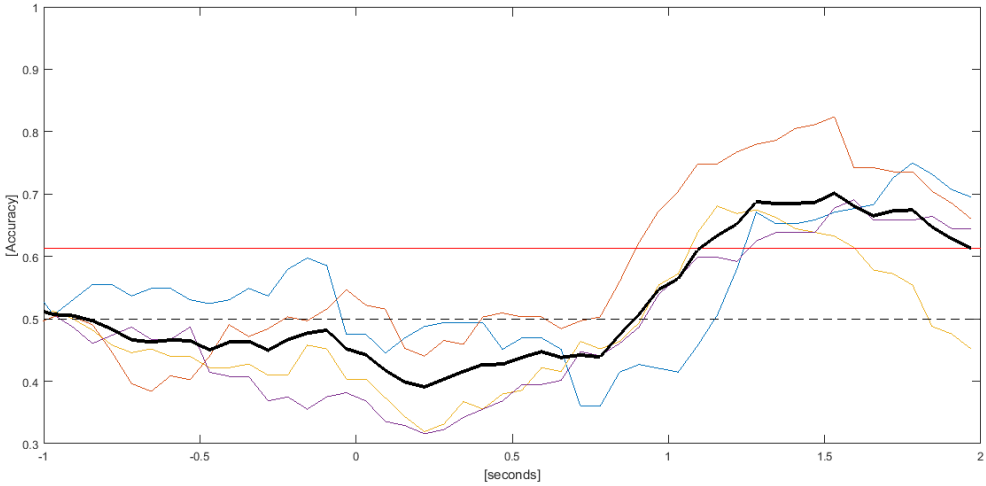

Figure 24: Classification accuracies - training with normal condition data, testing with inverted condition data. Time frame -1 s to 2 s relativ to movement onset. Plot shows average for subjects from group II and the grand average for the group. Dotted horizontal line marks chance level, red horizontal line marks significance level of 61.35 %

4 Discussion

This thesis was about finding out whether a decoder is based on the movement direction or the movement target. Therefore a special study was conducted where subjects were asked to move their arm towards one out of two targets (blue or red) according to specific commands (i.e., audio cues) and received visual feedback in realtime. The provided feedback was either normal (i.e., virtual arm moved to the same directions as the subject's arm) or inverted (i.e., virtual arm moved to the opposite directions as the subject's arm). Movements were decoded by using low-frequency time-domain EEG signal data.

Classification accuracies:

It has been shown that movement decoding (for normal and inverted condition) was possible before the actual movement onset. This phase is also known as the motor planning phase. Also, the maximum classification accuracy for both conditions during movement execution before the actual targets were reached. The lag that is to be seen in the Figures results from the classification time window of 750 ms. The results of this study coincide with the results of other EEG studies analyzing time-domain features during the decoding of movement direction or movement target. In the study of Hammon et al. [55], center out reaching tasks (natural and delayed) are performed to demonstrate that reaching targets can be decoded from EEG and that sufficient information for classifying reaching targets can be found within the signals. In the preliminary study of Lew et al. [60], the feasibility of movement direction decoding, from SCP prior to actual movement execution, during self-paced arm reaching was shown. Waldert et al. demonstrated the possibility of distinguishing four brain activity patterns that are related to four specific reaching movements [8].
However, it has been shown that also power modulations in mostly low-frequency bands carry information which is related to movement direction or movement targets. Lew et al. used signals filtered at low frequencies (below 4 Hz) for decoding movement direction significantly above chance level. SCPs were used showing the best accuracy- and detection performance [60]. Robinson et al. [44] found movement direction depending modulations within EEG signals at frequencies below 6 Hz towards the end of a movement. Hand movement directions can also be decoded from the high-gamma band (65 Hz - 85 Hz). This frequency band encodes a lot of discriminant information concerning particular hand movement directions [70].

This study's motivation was to analyze if information about the movement direction or the movement target is carried by low-frequency time-domain EEG signals. This was done by designing the experimental structure in a way that subjects also received inverted feedback when testing the classifier. In case of decoding the movement target, the inversion of

movements would not affect the classifier, consequently the classification accuracies would stay above chance level. When decoding the movement direction, however, inverting the movements would affect the classifier, thus classification accuracies would drop below chance level. Two different groups could be observed: in group I the decoder was obviously mainly based on movement targets - classification accuracies are clearly above chance level with a linear increase and a maximum shortly before reaching the target (again keeping in mind the lag due to the classifiction window length of 750 ms). Group II shows a different trend in the classification accuracy curve - first there is a decrease and then the classification accuracy starts to increase. So obviously first movement directions were decoded and then movement targets.

Generally, one needs to be aware when interpreting classification accuracies around times when reaching a target. Of course, the experimental paradigm was designed in a way to avoid eye movements at movement onset and during movement execution. However, when approaching the demanded target with the virtual arm, subjects may not have suppressed moving their eyes. This is due to the fact, that this visuomotor task requires some level of hand-eye coordination in order to really hit a target. Thus, the classifier may have recognized the change of the eye dipole's electrical field due to eye movements in the end of the reaching phase. For clarification and quantification of this effect further analyses need to be done. Moreover, also systematic differences in the reaching times (i.e., average time for reaching a specific target) of the different targets could be decisive for a successful classification.

MRCPs:

Different reaching times and different movement amplitudes could have also affected the MRCPs. Different MRCPs could have evolved not due to different targets but because of other movement parameters, e.g. movement speed [71]. Anyway, the MRCP's curve show a typical negativation before the actual movement onset with a negative peak at the point of time of the onset with an increase in voltage following. This graph, for the normal condition, is maximal at the midline centro-parietal area [71].

The inverted condition was obviously more challenging for the subjects than the normal condition. Hence, the motor planning and execution of the movement was enforced. The differences between the two classes (red and blue) probably result from higher degree of difficulty. The differences especially evolve before movement onset and during the motor execution phase. The curve's diversity between the two classes before the actual movement onset correspond to a more complex motor planning and thus, is intrinsic. The differences in amplitude after movement onset however, could either be intrinsic and therefore may result from the execution of a more complex motorplan due to the inverted feedback. Or

these differences may also result from an altered movement profile due to correction movements within the motor execution while approaching the target and therefore be extrinsic. If the differences in the motor execution phase are extrinsic by nature, the same differences could also be generated in the normal condition with the same diversified movement profile.

ERD/ERS maps:

The ERD/ERS maps of subject DV3 for normal and inverted condition show time-frequency plots for 11 chosen electrode positions. When generating these maps some important brain feature can be utilized. Which is the ability to switch from a synchronized into a desynchronized state and vice versa, according to the synchrony of neuronal population. Hence, maps illustrate various frequency bands that show different reactivity patterns [72]. Only significant changes of event-related power decrease or power increase, in relation to a specific reference interval, are shown [67].

As already mentioned previously, information related to movement direction or movement targets are mostly carried in low-frequency bands and the gamma band to a lesser extend. This can be confirmed by observing the normal condition results, which shows clearly an ERD in the frequency range of 8 Hz - 10 Hz especially over central and parietal regions after motor onset. During the inverted condition, similar results can be detected. Especially noticeable is the ERD after motor onset in the beta range (15 Hz - 25 Hz) over central and parietal regions. Beta waves are related to special mental states like active concentration or task engagement [73] which is due to the more challenging task to reach a target with inverted feedback.

Limitations of this work:

The fundamental hypothesis can be accepted, in case of target decoding classification accuracy is clearly above chance level, and in case of movement direction decoding it is below chance level. However, it was not possible to clearly determine whether a decoder is based on movement direction or the movement target, since both results were achieved (Group I and II). In order to make a distinct conclusion or at least to recognize a trend, the study needs to be expanded (more subjects should be considered) and somehow adjusted. These adjustments should include an improved design of the experimental paradigm in a way to prevent eye movements while approaching the targets to avoid that these influence the classifier. Moreover target positions and starting position need to be adjusted, to ensure that all distances (distances to red and blue target in both normal and inverted condition) are the same and therefore reaching times are equal.

Outlook:

This study could be used as the base for further investigation concerning the decoder behaviour of a BCI. As already mentioned in the introduction, BCI systems could be used to restore lost ability to move a patient's arm via a neuroprosthesis by thoughts only. The continuous decoding of movement trajectories, which would allow maximum control over the neuroprosthesis, is still a future's dream. Hence, there is the need of an interplay of a working decoder that has the ability to decode the intended target only and the trajectory towards the target is then performed by the neuroprosthesis. By adaption and expansion of the already existing study, this could be a promising approach.

5 Conclusion

Taken together, the decoding of arm movements to one out of two targets from low-frequency time-domain EEG signals was shown. By designing the experimental paradigm in a way, that subjects were receiving realtime feedback in the first condition and realtime inverted feedback in a second condition while moving their arm according to specific commands, evidence was found that the decoding was not only based on movement targets but also on the movement direction. This findings need to be investigated with more attention and need to be considered when developing novel control systems for robotic arms or neuroprosthesis.

References

[1] Hans Berger. Über das Elektrenkephalogramm des Menschen. Arch. für Psychiatrie und Nervenkrankheiten, 87:527–570, 1929.

[2] Ernst Niedermeyer and Fernando Lopes da Silva. Electroencephalography: basic principles, clinical applications and related fields, volume 1. Lippincott Williams & Wilkins, 2004.

[3] Hansen Zschoke. Klinische Elektroenzephalographie. Springer Verlag, 2nd edition, 2009.

[4] Diego A. Pizzagalli. Electroencephalography and high-density electrophysiological source location. In John Cacioppo, Louis G. Tassinary, and Gary G. Berntson, editors, Handbook of psychophysiology, pages 56–84. Cambridge: Cambridge University Press., 3rd edition, 2007.

[5] Monica Fabiani, Gabriele Gratton, and Kara D. Federmeier. Event-related brain potentials: Methods, theory and applications. In John Cacioppo, Louis G. Tassinary, and Gary G. Berntson, editors, Handbook of psychophysiology, pages 85–119. Cambridge: Cambridge University Press., 3rd edition, 2007.

[6] Bruce D. Bartholow and David M. Amodio. Using event-related brain potentials in social psychological research: A brief review and tutorial. In Eddie Harmon-Jones and Jennifer S. Beer, editors, Methods in social neuroscience, pages 198–232. New York: Guilford Press, 2009.

[7] Sylvain Baillet, John C. Mosher, and Richard M. Leahy. Electromagnetic brain mapping. IEEE Signal Processing Magazine, pages 14–30, 2001.

[8] Stephan Waldert, Hubert Preissl, Evariste Demandt, Christoph Braun, Niels Birbaumer, Ad Aertsen, and Carsten Mehring. Hand movement direction decoded from MEG and EEG. The Journal of Neuroscience, 28(4):1000–1008, 2008.

[9] Niels Birbaumer. Breaking the silence: Brain-computer interfaces (BCI) for communication and motor control. Psychophysiology, 43:517–532, 2006.

[10] Gernot R. Müller-Putz, Andreas Schwarz, Joana Pereira, and Patrick Ofner. From classic motor imagery to complex movement intention decoding: The noninvasive graz-BCI approach. Progress in Brain Research, 228:39–70, 2016.

[11] Gert Pfurtscheller, Gernot R. Müller-Putz, Reinhold Scherer, and Christa Neuper. Rehabilitation with brain-computer interface systems. Computer, 41(10):58–65, 2008.

[12] Jonathan R. Wolpaw, Niels Birbaumer, Dennis J. McFarland, Gert Pfurtscheller, and Theresa M. Vaughan. Brain-computer interfaces for communication and control. Clinical Neurophysiology, 113(6):767–791, 2002.

[13] Sebastian Halder, Andreas Pinegger, Ivo Käthner, Selina C. Wriessnegger, Josef Faller, Joao Antunes, Gernot R. Müller-Putz, and Andrea Kübler. Brain-controlled application using dynamic P300 speller matrices. Artificial Intelligence in Medicine, 63(1):7–17, 2015.

[14] Andrea Kübler and Niels Birbaumer. Brain-computer interfaces and communication in paralysis: Extinction of goal directed thinking in completely paralysed patients? Clinical Neurophysiology, 119(11):2658–2666, 2008.

[15] Femke Nijboer, Adrian Furdea, Ingo Gunst, Jürgen Mellinger, Dennis J. McFarland, Niels Birbaumer, and Andrea Kübler. An auditory brain-computer interface (BCI). Journal of Neuroscience Methods, 167:43–50, 2008.

[16] Andreas Pinegger, Selina C. Wriessnegger, and Gernot R. Müller-Putz. Introduction of a universal P300 brain-computer interface communication system. Biomedizinische Technik, 58:1–2, 2013.

[17] Ferran Galán, Marnix Nuttin, Eileen Lew, Pierre W. Ferrez, Gerolf Vanacker, Johan Philips, and Jose del R. Millan. A brain-actuated wheelchair: Asynchronous and non-invasive brain-computer interfaces for continous control of robots. Clinical Neurophysiology, 119(9):2159–2169, 2008.

[18] Alex Kreillinger, Martin Rohm, Vera Kaiser, Robert Leeb, Rüdiger Rupp, and Gernot R. Müller-Putz. Neuroprosthesis control via a noninvasive hybrid brain-computer interface. IEEE Intelligent Systems, 28(5):40–43, 2013.

[19] Martin Rohm, Matthias Schneiders, Constantin Müller, Alex Kreillinger, Vera Kaiser, Gernot R. Müller-Putz, and Rüdiger Rupp. Hybrid brain-computer interfaces and hybrid neuroprostheses for restoration of upper limb functions in individuals with high-level spinal cord injury. Artificial Intelligence in Medicine, 59(2):133–142, 2013.

[20] Rüdiger Rupp, Martin Rohm, Matthias Schneiders, Alex Kreillinger, and Gernot R. Müller-Putz. Functional rehabilitation of the paralyzed upper extremity after spinal cord injury by noninvasive hybrid neuroprostheses. Proceedings of the IEEE, 103(6):954–968, 2015.

[21] Gert Pfurtscheller, Gernot R. Müller, Jörg Pfurtscheller, Hans J. Gerner, and Rüdiger Rupp. 'Thought' - control of functional electrical stimulation to restore hand grasp in a patient with tetraplegia. Neuroscience Letters, 351(1):33–36, 2003.

[22] Gernot R. Müller-Putz, Reinhold Scherer, Gert Pfurtscheller, and Rüdiger Rupp. EEG-based neuroprosthesis control: A step towards clinical practice. Neuroscience Letters, 382(1-2):169–174, 2005.

[23] Reinhold Scherer, Gernot R. Müller-Putz, Christa Neuper, Bernhard Graimann, and Gert Pfurtscheller. An asynchronously controlled EEG-based virtual keyboard: improvement of the spelling rate. IEEE Transactions on Biomedical Engineering, 6(51):979–984, 2004.

[24] Benjamin Blankertz, Guido Dornhege, Matthias Krauledat, Michael Schröder, John Williamson, Roderick Murray-Smith, and Klaus-Robert Müller. The Berlin Brain–Computer Interface presents the novel mental typewriter Hex-O-Spell. In Proceedings of the 3rd International Brain–Computer Interface Workshop and Training Course, pages 108–109. Technischen Universität Graz, 2006.

[25] Reinhold Scherer, Martin Billinger, Johanna Wagner, Andreas Schwarz, Dirk Tassilo Hettich, Elaina Bolinger, Mariano Lloria Garcia, Juan Navarro, and Gernot R. Müller-Putz. Thought-based row-column scanning communication board for individuals with cerebral palsy. Annals of Physical and Rehabilitation Medicine, 58(1):14–22, 2015.

[26] Femke Nijboer, Eric W. Sellers, Jürgen Mellinger, M. A. Jordan, Tamara Matuz, Adrian Furdea, Sebastian Halder, U. Mochty, Dean J. Krusienski, Theresa M. Vaughan, Jonathan R. Wolpaw, Niels Birbaumer, and Andrea Kübler. A P300-based brain–computer interface for people with amyotrophic lateral sclerosis. Clinical Neurophysiology, 119:1909–1916, 2008.

[27] Surjo R. Soekadar, Niels Birbaumer, and Leonardo G. Cohen. Brain-computer-interfaces in the rehabilitation of stroke and neurotrauma. In Kenji Kansaku, editor, Systems-Neuroscience and Rehabilitation. Springer Tokyo, 2011.

[28] José del R. Millán, Rüdiger Rupp, Gernot R. Müller-Putz, Roderick Murray-Smith, Claudio Giugliemma, Michael Tangermann, Carmen Vidaurre, Febo Cincotti, Andrea Kübler, Robert Leeb, Christa Neuper, Klaus R. Müller, and Donatella Mattia. Combining brain-computer interfaces and assistive technologies: State-of-the-art and challenges. Frontiers in Neuroscience, 4(161), 2010.

[29] Brendan Z. Allison, Bernhard Graimann, and Axel Gräser. Why use a BCI if you're healthy? IEEE Intelligent Systems, 23(3):7–11, 2008.

[30] Roman Krepki, Benjamin Blankertz, Gabriel Curio, and Klaus R. Müller. The berlin brain-computer interface (BBCI). IEEE Transactions on Automatic Control, 23(4):538–544, 2003.

[31] Michel Besserve. Analyse de la dynamique neuronale pour les interfaces cerveau-machines: un retour aux sources. PhD thesis, Université Paris-Sud 11, 2007.

[32] David Regan. Human Brain Electrophysiology: Evoked Potentials and Evoked Magnetic Fields in Science and Medicine. Elsevier: New York, NY, USA, 1989.

[33] Bin Guangyu, Gao Xiaorong, Wang Yijun, Hong Bo, and Gao Shangkai. Vep-based brain-computer interfaces: Time, frequency, and code modulations [research frontier]. IEEE Computational Intelligence Magazine, 4(4):22–26, 2009.

[34] Niels Birbaumer, Thomas Elbert, Anthony G. M. Canavan, and Brigitte S. Rockstroh. Slow potentials of the cerebral cortex and behavior. Physiological Reviews, 70(1):1–41, 1990.

[35] Thilo Hinterberger, Stefan Schmidt, Nicola Neumann, Jürgen Mellinger, Benjamin Blankertz, Gabriel Curio, and Niels Birbaumer. Brain-computer communication and slow cortical potentials. IEEE Transactions on Biomedical Engineering, 51:1011–1018, 2004.

[36] Lawrence A. Farwell and Emanuel Donchin. Talking off the top of your head: Toward a mental prosthesis utilizing event-related brain potentials. Electroencephalography and Clinical Neurophysiology, 70(6):510–523, 1988.

[37] Emanuel Donchin and D. B. D. Smith. The contingent negative variation and the late positive wave of the average evoked potential. Electroencephalography and Clinical Neurophysiology, 29(2):201–203, 1970.

[38] Gert Pfurtscheller and Fernando H. Lopes da Silva. Event-related EEG/MEG synchronization and desynchronization: basic principles. Clinical Neurophysiology, 110:1842–1857, 1999.

[39] Gert Pfurtscheller and Christa Neuper. Motor imagery and direct brain-computer communication. Proceedings of the IEEE, 89(7):1123–1134, 2001.

[40] Boris Kleber and Niels Birbaumer. Direct brain communication: neuroelectric and metabolic approaches at tübingen. Cognitive Processing, 6(1):65–74, 2005.

[41] Dean J. Krusienski, Gerwin Schalk, Dennis J. McFarland, and Jonathan R. Wolpaw. mu-rhythm matched filter for continuous control of a brain-computer interface. IEEE Transactions on Biomedical Engineering, 54(2):273–280, 2007.

[42] Gert Pfurtscheller, Christa Neuper, Gernot R. Müller-Putz, Bernhard Obermaier, Gunther Krausz, Alois Schlögl, Reinhold Scherer, Bernhard Graimann, Claudia Keinrath, Michael Woertz, Gabriela M. Supp, and Christoph Schrank. Graz-BCI: State

of the art and clinical applications. IEEE Transactions on Neural Systems and Rehabilitation Engineering, 11:1–4, 2003.

[43] Chun Sing Louis Tsui and John Q. Gan. Asynchronous BCI control of a robot simulator with supervised online training. In Tino P., Corchado E., Byrne W., and Yao X., editors, Intelligent Data Engineering and Automated Learning - IDEAL 2007, volume 4881. Springer, Berlin, Heidelberg, 2007.

[44] Neethu Robinson, Cuntai Guan, A. P. Vinod, Kai Keng Ang, and Keng Peng Tee. Multi-class EEG classification of voluntary hand movement directions. Journal of Neural Engineering, 10(5):056018, 2013.

[45] Leigh R. Hochberg, Daniel Bacher, Beata Jarosiewicz, Nicolas Y. Masse, John D. Simeral, Joern Vogel, Sami Haddadin, Jie Liu, Sydney S. Cash, Patrick van der Smagt, and John P. Donoghue. Reach and grasp by people with tetraplegia using a neurally controlled robotic arm. Nature, 485(7398):372–375, 2012.

[46] Jennifer L. Collinger, Brian Wodlinger, John E. Downey, Wei Wang, Elizabeth C. Tyler-Kabara, Douglas J. Weber, Angus JC. McMorland, and Meel Velliste. 7 degree-of-freedom neuroprosthetic control by an individual with tetraplegia. Lancet, 381(9866):557–564, 2013.

[47] Tobias Pistohl, Tonio Ball, Andreas Schulze-Bonhage, Ad Aertsen, and Carsten Mehring. Prediction of arm movement trajectories from ECoG-recordings in humans. Journal of Neuroscience Methods, 167(1):105–114, 2008.

[48] Gerwin Schalk, Jan Kubanek, Kai J. Miller, N.R. Anderson, Eric C. Leuthardt, Jeffrey G. Ojemann, D. Limbrick, D.W. Moran, Lester A. Gerhardt, and Jonathan R. Wolpaw. Decoding two-dimensional movement trajectories using electrocorticographic signals in humans. Journal of Neural Engineering, 4(3):264–275, 2007.

[49] Tomislav Milekovic, Jörg Fischer, Tobias Pistohl, Johanna Ruescher, Andreas Schulze-Bonhage, Ad Aertsen, Jörn Rickert, Tonio Ball, and Carsten Mehring. An online brain-machine interface using decoding of movement direction from the human electrocorticogram. Journal of Neural Engineering, 9(4):1–14, 2012.

[50] Tonio Ball, Andreas Schulze-Bonhage, Ad Aertsen, and Carsten Mehring. Differential representation of arm movement direction in relation to cortical anatomy and function. Journal of Neural Engineering, 6(1):1–16, 2009.

[51] Trent J. Bradberry, Rodolphe J. Gentili, and José L. Contreras-Vidal. Reconstructing three-dimensional hand movements from noninvasive electroencephalographic signals. The Journal of Neuroscience, 30(9):3432–3437, 2010.

[52] Jeong-Hun Kim, Felix Bießmann, and Seong-Whan Lee. Decoding three-dimensional trajectory of executed and imagined arm movements from electroencephalogram signals. IEEE Transactions on Neural Systems and Rehabilitation Engineering, 23(5):867–876, 2015.

[53] Jun Lv, Yuanqing Li, and Zhenghui Gu. Decoding hand movement velocity from electroencephalogram signals during a drawing task. Biomedical Engineering Online, 9(64):1–21, 2010.

[54] Patrick Ofner and Gernot R. Müller-Putz. Movement target decoding from EEG and the corresponding discriminative sources: a preliminary study. Conf. Proc. IEEE Eng. Med. Biol. Soc., 2015:1468–71, 2015.

[55] Paul S. Hammon, Scott Makeig, Howard Poizner, Emanuel Todorov, and Virginia R. de Sa. Predicting reaching targets from human EEG. IEEE Signal Processing Magazine, 25(1):69–77, 2008.

[56] Patrick Ofner and Gernot R. Müller-Putz. Using a noninvasive decoding method to classify rhythmic movement imaginations of the arm in two planes. IEEE Transactions on Biomedical Engineering, 62(3):972–981, 2015.

[57] Martin Seeber, Reinhold Scherer, and Gernot R. Müller-Putz. EEG oscillations are modulated in different behavior-related networks during rhythmic finger movements. The Journal of Neuroscience, 36(46):11671–11681, 2016.

[58] Patrick Ofner and Gernot R. Müller-Putz. Decoding of velocities and positions of 3D arm movement from EEG. Conf. Proc. IEEE Eng. Med. Biol. Soc., 2012:6406–6409, 2012.

[59] Yijun Wang and Scott Makeig. Decoding intended movement from human EEG in the posterior parietal cortex. Neuroimage, 47:103, 2009.

[60] Eileen Y. L. Lew, Ricardo Chavarriaga, Stefano Silvoni, and José del R. Millán. Single trial prediction of self-paced reaching directions from EEG signals. Frontiers in Neuroscience, 8(222), 2014.

[61] USC Department of Biomedical Engineering. MSMS information on MDDF homepage. `mddf.usc.edu:85/?page_id=94&param_var=98`.

[62] Rahman Davoodi. MSMS User's Guide. Medical Device Development Faculity, University of Southern California, version 2.2 edition, 2012.

[63] Hocoma AG. ARMEO Spring User Manual, version 2 edition.

[64] Hocoma AG. Hocoma webpage. `https://www.hocoma.com/solutions/armeo-spring/`.

[65] Alois Schlögl, Oliver Fritz, Herbert Ramoser, and Gert Pfurtscheller. GDF - A general data format for biosignals version 1.25. http://arxiv.org/pdf/cs/0608052v6, 2005.

[66] Christian Breitwieser, Ian Daly, Christa Neuper, and Gernot R. Müller-Putz. Proposing a standardized protocol for raw biosignal transmission. IEEE Transactions on Biomedical Engineering, 59(3):852–859, 2012.

[67] Bernhard Graimann, Jane E. Huggins, S. P. Levine, and Gert Pfurtscheller. Visualization of significant ERD/ERS patterns in multichannel EEG and ECoG data. Clinical Neurophysiology, 113(1):43–47, 2002.

[68] Roger Peck and John Van Ness. The use of shrinkage estimators in linear discriminant analysis. IEEE Transactions on Pattern Analysis and Machine Intelligence, 4(5):530–537, 1982.

[69] Gernot R. Müller-Putz, Reinhold Scherer, Clemens Brunner, Robert Leeb, and Gert Pfurtscheller. Better than random? A closer look on BCI results. International Journal of Bioelectromagnetism, 10(1):52–55, 2008.

[70] Carlos A. Loza, Gavin R. Philips, Mehrnaz Kh. Hazrati, Janis J. Daly, and Jose C. Principe. Classification of hand movement direction based on EEG high-gamma activity. Conf. Proc. IEEE Eng. Med. Biol. Soc., 2014:6509–6512, 2014.

[71] Hiroshi Shibasaki and Mark Hallett. What is the Bereitschaftspotential? Clinical Neurophysiology, 117(11):2341–2356, 2006.

[72] Fernando Lopes da Silva. Neural mechanisms underlying brain waves: From neural membranes to networks. Electroencephalography and Clinical Neurophysiology, 79(2):81–93, 1991.

[73] Gernot R. Müller-Putz, René Riedl, and Selina C. Wriessnegger. Electroencephalography (EEG) as a research tool in the information systems discipline: Foundations, measurement, and applications. Communications of the Association for Information Systems, 37(46):911–948, 2015.

Appendix

Paper

Proceedings of the
7th Graz Brain-Computer Interface Conference 2017 DOI: 10.3217/978-3-85125-533-1-63

MOVEMENT DECODING FROM EEG: TARGET OR DIRECTION?

G.R. Müller-Putz, L. Peicha, P. Ofner

[1] Institute of Neural Engineering, Graz University of Technology, Graz, Austria

E-mail: gernot.mueller@tugraz.at

ABSTRACT: Arm movements have already been decoded non-invasively from electroencephalography (EEG) signals. In this study we analyzed whether the target or the movement direction of the arm can be decoded from the EEG. Ten healthy subjects executed right arm movements to one out of two targets and simultaneously received feedback on a computer screen. We then inverted the feedback movements to analyze if the EEG carries information about the target or about the movement direction. We found two groups, one encoding the target and one encoding first the movement direction followed by the target. These findings are relevant for the development of future motor neuroprostheses and non-invasive robotic arm control.

INTRODUCTION

Brain-computer interfaces (BCIs) can be used to control neuroprostheses or robotic arms. Together, these technologies allow to restore or replace basic movement function of spinal cord injured (SCI) persons. For example, in [1] a robotic arm was successfully controlled using an invasive BCI. Also non-invasive BCIs based on electroencephalography (EEG) signals can be used to restore movement function in persons with SCI. Our group demonstrated the restoration of grasp function [3], [4] and elbow function [5], [6] with a sensorimotor rhythm (SMR)-based BCI. SMR-based BCIs detect movement imagination (MI) and use it as a control signal. However, the MI itself is often not intuitive (e.g., a foot MI may be used to control the right arm). Furthermore, only the process of imagination can be detected but not the movement itself. For example, imagining squeezing a ball and playing tennis may not be distinguishable with a SMR-based BCI. However, to control a neuroprosthesis in a more natural way or even a robotic arm with its many degrees-of-freedom, more information about the movement needs to be extracted from the EEG. Interestingly, low-frequency EEG signals carry more specific information about the movement and can be used to decode even movement trajectories [7]–[9] or movement directions/targets [10]–[13]. However, the accuracy of a non-invasive movement trajectory decoder is not yet sufficient for real-time control, not to mention the decoding of imagined movement trajectories. The decoding of movement direction or movement target combined with a system which then generates the trajectory may be a more promising approach.

A general issue of studies decoding movement targets is that hand or cursor movements towards a certain target always requires a certain movement direction, i.e. movement targets correspond to movement directions. That blurs the results of such studies because it cannot be determined whether targets or movement directions are being decoded. However, that information is important when training a decoder (e.g., if targets should be shown in the training paradigm). Furthermore, in a real life application there is always a variable number of potential targets. A decoder based on the imagined or attempted movement direction would be independent on the number of targets but not a decoder based on movement targets. To investigate whether a decoder is based on targets or the movement direction, we conducted a study (here with executed movements) where subjects moved their arm to one out of two targets and received feedback on a computer screen. Then, we inverted the feedback and conducted the same number of trials to analyse whether our decoder is based on the movement direction or the movement target. We hypothesize that in case of target decoding, the classification accuracies would be above chance level. Classification accuracies below chance level would indicate the decoding of the movement direction.

MATERIALS AND METHODS

Subjects: For the experiment 10 healthy subjects (one female), all of them right-handed and with normal or corrected-to-normal vision, were recruited. None of them had participated in any prior BCI experiments. They were aged between 25 and 32 (mean 27.7 and SD of 2) years. All of them signed an informed consent.

EEG Measurement: We used 68 passive electrodes covering frontal, central, parietal and temporal areas for recording EEG signals from the scalp. An electrode cap with equidistant electrode positions was used. Also, three electrooculography (EOG) electrodes, positioned above the nasion and below the outer canthi of the eyes were used. Reference was placed on the left mastoid, ground on the right mastoid. All electrode impedances were tried to keep below 5kΩ. An 8-th order Chebyshev band-pass filter from 0.01Hz to 200Hz and a Notch filter at 50Hz was applied. Signals were sampled with

 DOI: 10.3217/978-3-85125-533-1-63

512Hz using biosignal amplifiers (g.tec medical engineering GmbH, Austria). Moreover, we measured electrode positions with ELPOS (Zebris Medical GmbH, Germany). EEG, EOG and movement data (3D positions and joint angles of the right arm) were recorded with a customized TOBI Signal Server [14] and Matlab (MathWorks, Massachusetts, USA). For recording the movement data a custom made plugin for the ARMEO Spring software was used.

Experimental Paradigm: Subjects were seated in a chair and their right arm was fixed in an ARMEO Spring rehabilitation device (Hocoma, Switzerland). The ARMEO Spring is basically an exoskeleton and supports the subjects' arm from gravity to prevent muscle fatigue. With the sensors of the ARMEO Spring it is possible to keep track of the hand- and elbow position and joint angles.
For the experiment a self paced center-out reaching task was employed. Subjects moved their right arm from a starting position (about 150 degrees elbow flexion, 60 degrees shoulder flexion and 0 degree abduction in the shoulder joint (see Figure 1)) to one of two targets (red and blue) presented on a computer screen. The red and blue target were positioned in the right upper corner and in the left lower corner, respectively (see Figure 2). The final position for reaching the red target required a 100 degree flexion and 20 degree abduction in the shoulder joint and a 150 degree elbow flexion. For reaching the blue target it was a 60 degree flexion, 20 degree adduction and 30 degree internal rotation in the shoulder joint and a 150 degree elbow flexion. The computer screen also showed an arm model as a visual feedback (see Figure 2). The arm model was previously built with the software MSMS (MDDF, University of Southern California, Los Angeles, California). The model received its joint angles and coordinates from the ARMEO Spring and showed the participants their actual hand-/arm position in real time.
The experiment consisted of two conditions: (i) *normal condition* where the virtual arm on the computer screen moved exactly like the subjects' arm and (ii) *inverted condition* where the virtual arm movements were inverted to real arm movements (i.e. subjects had to move their arm to the opposite target to reach the actual target with the virtual arm).

Figure 1: Experimental setup. A subject connected with the ARMEO Spring, EEG mounted in the position in front of a screen which presents feedback to the subject.

The paradigm is shown in Figure 3. At second 0 an audio cue started a trial by either saying „Red" or „Blue". The subjects got instructed to immediately look at the specific target to avoid eye movements during the reaching phase which could have affected the classification. Three to 5 s after the trial start a beep sounded representing the go cue. The participants got instructed to start their reaching movements to the specific target 1 to 3 s after the go cue. When the virtual arm on the computer screen touched the specific target, a second beep tone sounded serving as a success cue.

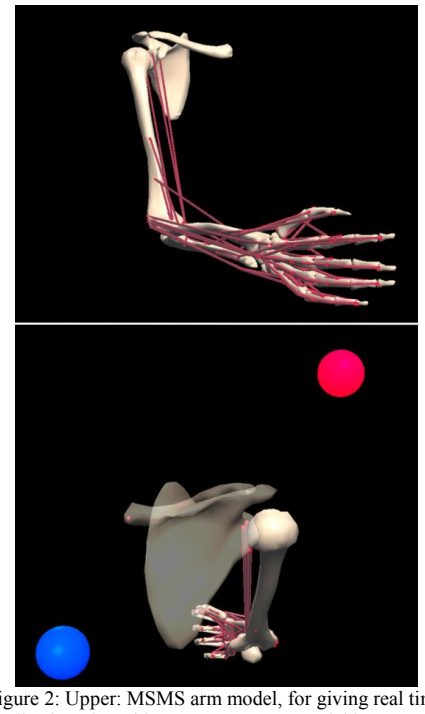

Figure 2: Upper: MSMS arm model, for giving real time feedback to the subjects. Lower: Arm model in experimental setup, i.e. first person view, transparent scapula, all joints in starting position and including both targets

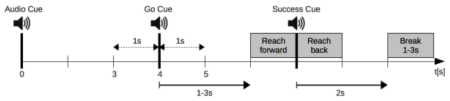

Figure 3: Paradigm and timing of a single trial.

After successfully touching a target subjects moved

 DOI: 10.3217/978-3-85125-533-1-63

their arm back to the starting position. The trial ended 2 s after the success cue. After a trial, a break between 1 and 3 s followed. Each run consisted of 30 trials (15 trials for each target, randomly distributed). 12 runs were recorded - 6 for normal condition and 6 for inverted condition, always changing the condition after 2 runs. Thus, in total we recorded 180 trials - 90 trials for each condition. Additionally, we recorded 2 resting state runs and 2 runs with deliberate eye movements (not used in this work).

Signal Processing: We removed trials which were suspected to contain muscle, technical or movement artifacts. Therefore the data got filtered from 0.3Hz to 70Hz (4-th order zero-phase Butterworth filter) and trials that exceeded a threshold of 3 times the standard deviation of the absolute value, Kurtosis or joint probability were excluded from any further processing steps.
For determining the movement onset a principal component analysis (PCA) was done on the x/y/z hand position data recorded by the ARMEO Spring. We differentiated the first principal component and detected a movement onset whenever a certain threshold was crossed after the go cue. The threshold was found empirically.
For calculating the movement-related cortical potentials (MRCPs) a 0.3 Hz - 35 Hz 4-th order zero-phase Butterworth band-pass filter was applied and data segments averaged. MRCPs were calculated for both conditions and electrode positions FCz, C3, Cz and C4.
In order to discriminate between the two red and blue targets, we applied a shrinkage linear discriminant analysis (sLDA) [15] to calculate classification accuracies. A 0.3Hz - 3Hz 4-th order zero-phase Butterworth band-pass filter was applied on the raw EEG data to extract low frequency signals. Subsequently, we downsampled data to 16Hz for computational convenience. We computed the classification accuracy within the time window -2s to 2s relative to movement onset. In one analysis, we classified a moving time window of 750ms using data from all band-pass filtered EEG channels, i.e., we used all EEG data within a window of the past 750ms (12 sample points) and then moved the window one sample further. Classification accuracies were calculated using a 10x10 fold cross-validation. This analysis was separately performed for the normal and inverted condition.
In another analysis, we used the data of the normal condition as training data and the data of the inverted condition for testing in order to find out whether it was target or movement direction decoding.

RESULTS

Classification of directions: Figure 4 and 5 show the classification accuracies for the normal condition and inverted condition, respectively. Classification accuracies are scaled from 0 to 1 and time is relative to the movement onset (=0s). The significance level was 61.35% ($\alpha = 0.05$, adjusted Wald interval, Bonferroni corrected for the number of shown sample points) [16]. The maximum average classification accuracies were 0.78 (normal) and 0.79 (inverted). Table 1 shows the average movement times to the targets for each condition.

Table 1: average time and standard deviation in seconds to reach red and blue target during normal and inverted condition

Target	Normal cond. [s]	Inverted cond. [s]
Red	1,20 ± 0,65	1,36 ± 0,76
Blue	1,41 ± 0,74	1,10 ± 0,65

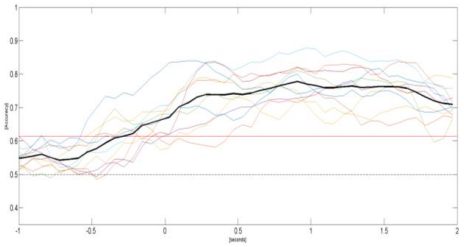

Figure 4: Cross-validated classification accuracies in the normal condition (all subjects and the grand average).

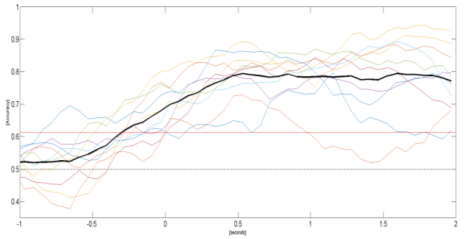

Figure 5: Cross-validated classification accuracies in the normal condition (all subjects and the grand average).

Classification (testing with inverted conditions): We trained the classifier on the normal condition and tested it on the inverted condition. Accuracies below chance level indicate movement direction decoding as hand movements were executed in the opposite direction to the target. Accuracies above chance level indicate target decoding. Two groups arose: group I shows an increasing classification accuracy after the movement onset (Figure 6); group II shows first a decrease of classification accuracy followed by an increase (Figure 7). Time is relative to the movement onset (=0s) and the significance level was 61.35%. The maximum average classification accuracies were 0.71 (group I) and 0.70 (group II).

 DOI: 10.3217/978-3-85125-533-1-63

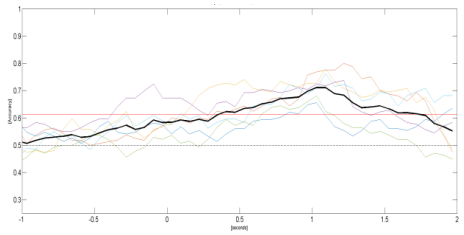

Figure 6: Classification accuracies when training on the normal condition and testing on the inverted condition (group I).

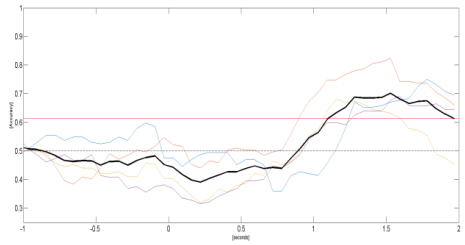

Figure 7: Classification accuracies when training on the normal condition and testing on the inverted condition (group II).

Motor related cortical potentials: Figure 8 and 9 show the MRCPs for the normal and inverted condition, respectively. The figures show the confidence intervals as determined with a bootstrap test ($\alpha = 0.05$) at the electrode positions FCz, C3, Cz and C4. In the normal condition, differences between the two targets are observable at movement onset and around the approach to the target. The inverted condition shows more distinct differences between the targets. These amplitude differences are from ca. 0.5s before movement onset up to 2s after movement onset.

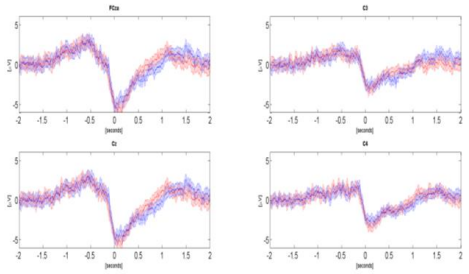

Figure 8: MRCPs evolving in the normal condition. Shown are the MRCPS for both targets (red, blue)

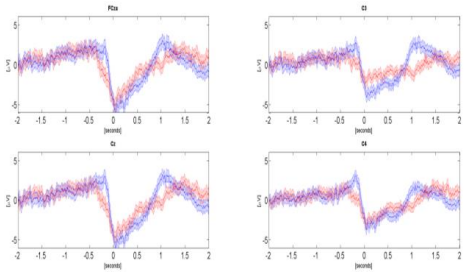

Figure 9: MRCPs evolving in the inverted condition.

DISCUSSION

We demonstrated the decoding of movements to one out of two targets from low-frequency time-domain EEG. Movements were decoded with normal and with inverted feedback. It was possible to decode the movement before movement onset, i.e. in the motor planning phase. Keeping in mind the lag introduced due to the 750ms classification time window, the classification accuracies peaked in the movement execution phase before the targets were reached. Our results are in line with other EEG studies which analyzed time-domain features during movement direction/target decoding [10], [12], [17]. However, also power modulations mostly in low-frequency bands and the high-gamma band have been shown to carry movement direction/target related information [12], [13], [18].

The motivation of our study was to analyze if low-frequency time-domain EEG signals carry information about the movement direction or the target. We did this by inverting the feedback when testing the classifier. In case of target decoding, the classifier would not be affected by the required inversion of movements and classification accuracies would still be above chance level. In case of movement direction decoding, however, the classifier would be affected and classification accuracies would be below chance level, i.e. mirrored around the chance level. Our results can be divided into two groups: in one group the decoder was mainly based on the movement targets, in the other group the decoder first decoded movement directions and then movement targets. This finding has to be considered when novel control systems for future neuroprostheses or robotic arms are developed.

Generally, classification accuracies around the time when the target was reached have to be interpreted with caution. The paradigm was designed to avoid eye movements at movement onset, but subjects may not have suppressed eye movements when approaching a target with the virtual hand as this was a visuomotor task requiring hand-eye coordination. Thus, eye movements may have happened at the end of the reaching movement and the classifier may have picked up the change of the electrical field of the eye dipole.

 DOI: 10.3217/978-3-85125-533-1-63

Further analysis has to quantify this effect. Furthermore, systematic differences between the movement times of the two targets may be responsible for the successful classification. Different MRCPs may have been evolved not because of different targets but because of different movement times or movements amplitudes (MRCPs are influenced by movement parameters, e.g. movement speed [19]).

The MRCPs show a typical negative peak around movement onset [19]. The inverted feedback condition was more difficult to the subjects than the normal condition and therefore challenged more the motor planning and the movement execution. This higher difficulty probably enhanced the differences between the MRCPs in the inverted condition. The differences before movement onset correspond to the motor planning and are intrinsic. However, the amplitude differences after movement onset are either due to the execution of a motor plan which accounts for the inverted feedback (intrinsic) or due to different movement profiles (extrinsic), e.g. more correction movements. If the differences are extrinsic in nature, the same differences may evolve in the normal condition with the same altered movement profile.

We report here a study with healthy subjects. Further studies have to confirm if the same effects can be found in persons with SCI.

CONCLUSION

We show the decoding of movements to one out of two targets from low-frequency time-domain EEG. Furthermore, we found evidence that the decoding is based on movement targets but also on the movement direction.

ACKNOWLEDGEMENTS

This work was supported by the EU ICT Programme Project H2020-643955 MoreGrasp, and the ERC Consolidator Grant ERC-681231, Feel Your Reach.

REFERENCES

[1] Hochberg LR, Bacher D, Jarosiewicz B, Masse NY, Simeral JD, Vogel J, et al. Reach and grasp by people with tetraplegia using a neurally controlled robotic arm. Nature. 2012;485(7398):372–5.

[2] Collinger JL, Wodlinger B, Downey JE, Wang W, Tyler-Kabara EC, Weber DJ, et al. High-performance neuroprosthetic control by an individual with tetraplegia. Lancet. 2013; 381(9866):557–64.

[3] Pfurtscheller G, Müller GR, Pfurtscheller J, Gerner HJ, Rupp R. "Thought" – control of functional electrical stimulation to restore hand grasp in a patient with tetraplegia. Neurosci Lett. 2003; 351(1):33–6.

[4] Müller-Putz GR, Scherer R, Pfurtscheller G, Rupp R. EEG-based neuroprosthesis control: a step towards clinical practice. Neurosci Lett. 2005;382(1-2):169–74.

[5] Kreilinger A, Rohm M, Kaiser V, Leeb R, Rupp R, Mueller-Putz GR. Neuroprosthesis Control via a Noninvasive Hybrid Brain-Computer Interface. IEEE Intell Syst. 2013;28(5):40–3.

[6] Rohm M, Schneiders M, Müller C, Kreilinger A, Kaiser V, Müller-Putz GR, et al. Hybrid brain-computer interfaces and hybrid neuroprostheses for restoration of upper limb functions in individuals with high-level spinal cord injury. Artif Intell Med. 2013;59(2):133–42.

[7] Bradberry TJ, Gentili RJ, Contreras-Vidal JL. Reconstructing three-dimensional hand movements from noninvasive electroencephalographic signals. J Neurosci. 2010;30(9):3432–7.

[8] Ofner P, Müller-Putz GR. Decoding of velocities and positions of 3D arm movement from EEG. in Proc. IEEE EMBC 2012. 2012:6406–9.

[9] Ofner P, Müller-Putz GR. Using a noninvasive decoding method to classify rhythmic movement imaginations of the arm in two planes. IEEE Trans Biomed Eng. 2015;62(3):972–81.

[10] Hammon P, Makeig S, Poizner H, Todorov E, De Sa V. Predicting Reaching Targets from Human EEG. IEEE Signal Process Mag. 2008;25(1):69–77.

[11] Wang Y, Makeig S. Decoding Intended Movement from Human EEG in the Posterior Parietal Cortex. Neuroimage. 2009;47:S103.

[12] Lew EYL, Chavarriaga R, Silvoni S, Millán JDR. Single trial prediction of self-paced reaching directions from EEG signals. Front Neurosci. 2014;8:222.

[13] Robinson N, Guan C, Vinod AP, Ang KK, Tee KP. Multi-class EEG classification of voluntary hand movement directions. J Neural Eng. 2013; 10(5):056018.

[14] Breitwieser C, Daly I, Neuper C, Müller-Putz GR. Proposing a standardized protocol for raw biosignal transmission. IEEE Trans Biomed Eng. 2012; 59(3):852–9.

[15] Peck R, Van Ness J. The use of shrinkage estimators in linear discriminant analysis. IEEE Trans Pattern Anal Mach Intell. 1982;4(5):530–7.

[16] Müller-Putz GR, Scherer R, Brunner C, Leeb R, Pfurtscheller G. Better than random? A closer look on BCI results. Int J Bioelectromagn. 2008; 10(1):52–5.

[17] Waldert S, Preissl H, Demandt E, Braun C, Birbaumer N, Aertsen A, et al. Hand movement direction decoded from MEG and EEG. J Neurosci. 2008;28(4):1000–8.

[18] Loza CA, Philips GR, Hazrati MK, Daly JJ, Principe JC. Classification of hand movement direction based on EEG high-gamma activity. in Proc. IEEE EMBC 2014. 2014:6509–12.

[19] Shibasaki H, Hallett M. What is the Bereitschaftspotential? Clin Neurophysiol. 2006; 117(11):2341–56.

MRCPs

The following Figures 25 - 44 show the MRCPs evolving for normal and inverted condition from -2 s to 2 s relativ to movement onset. MRCPs for 11 different electrode positions for every single subject and for both, red and blue target including confidence interval as determined with a bootstrap test ($\alpha = 0.05$) are depicted.

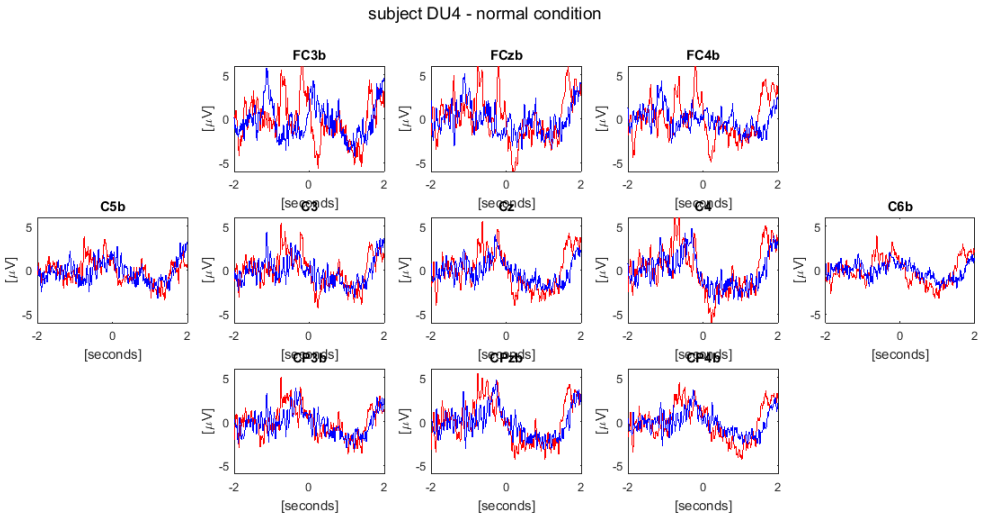

Figure 25

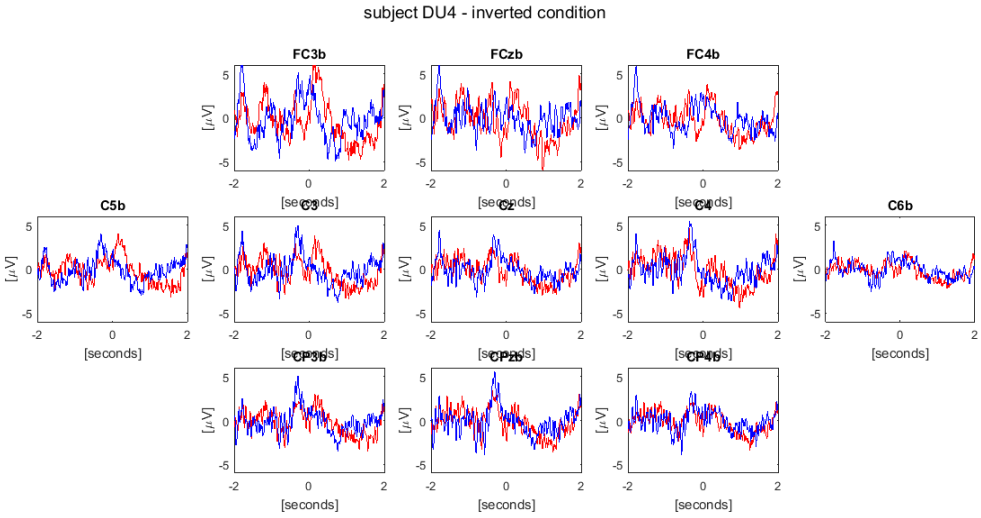

Figure 26

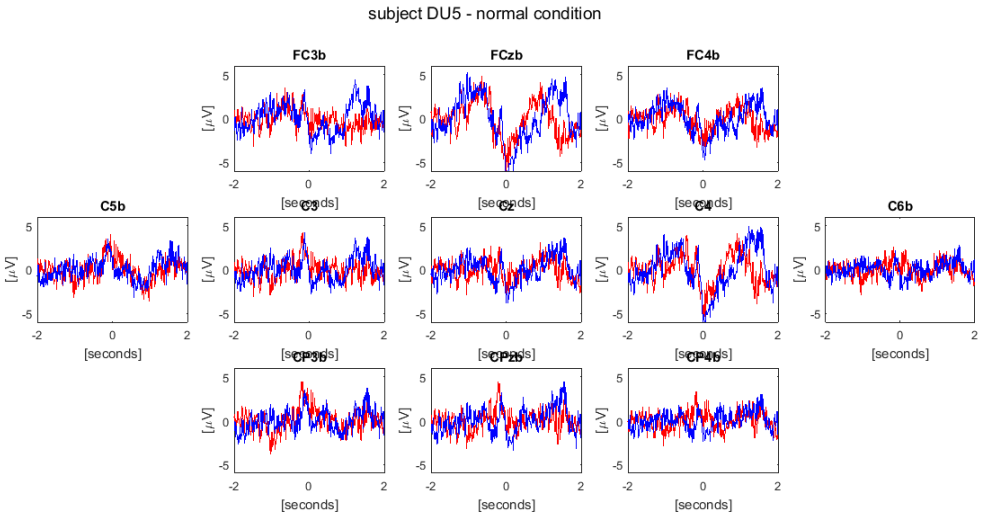

Figure 27

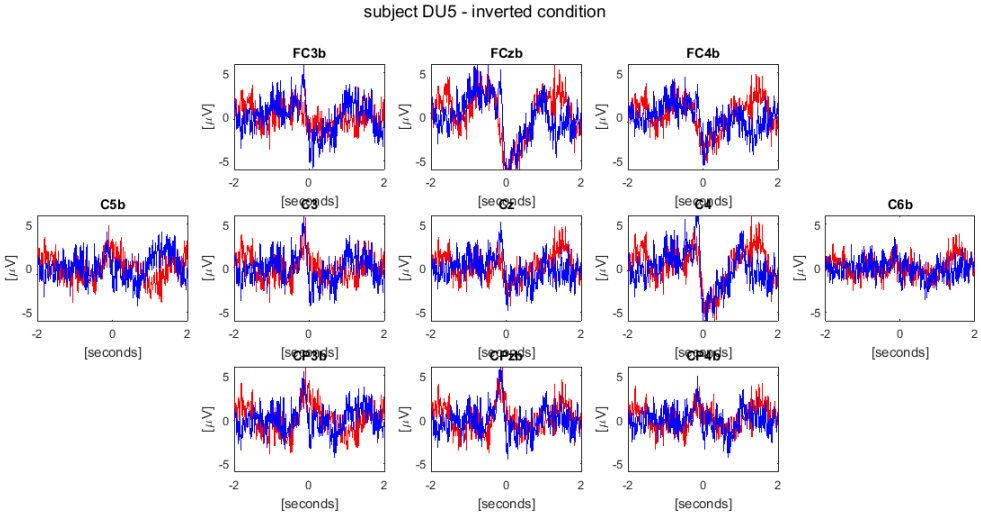

Figure 28

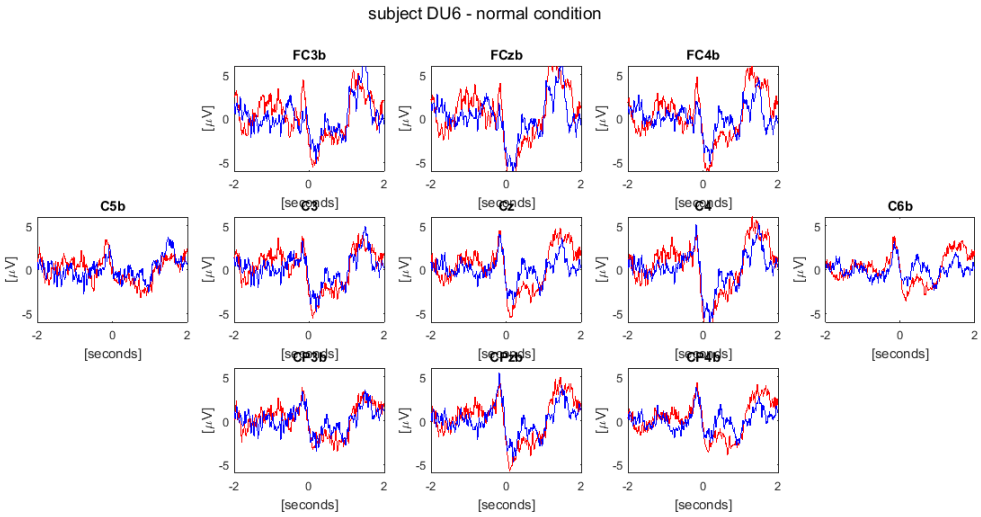

Figure 29

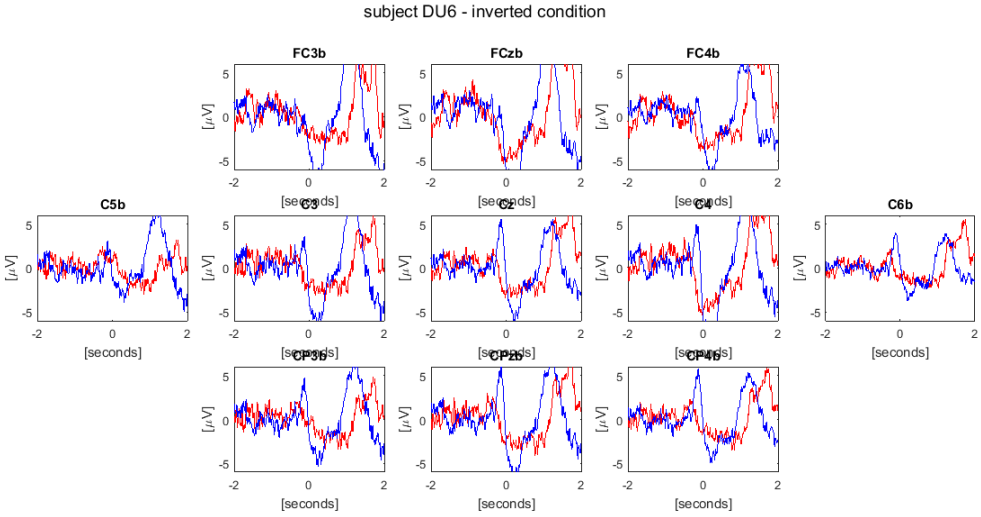

Figure 30

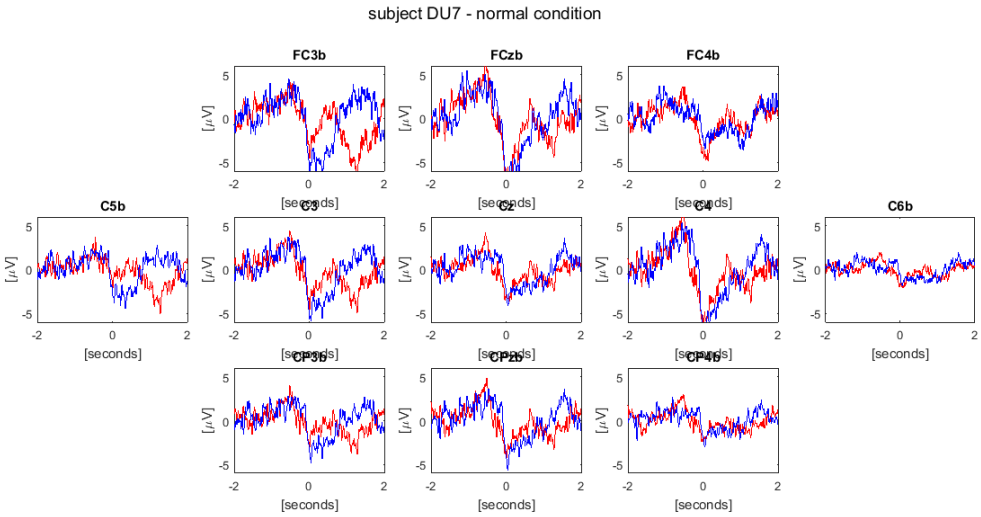

Figure 31

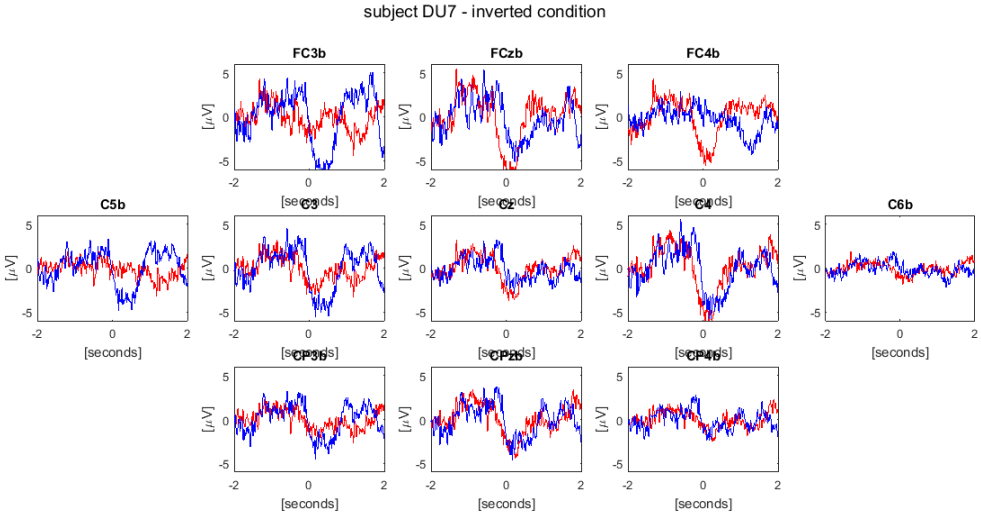

Figure 32

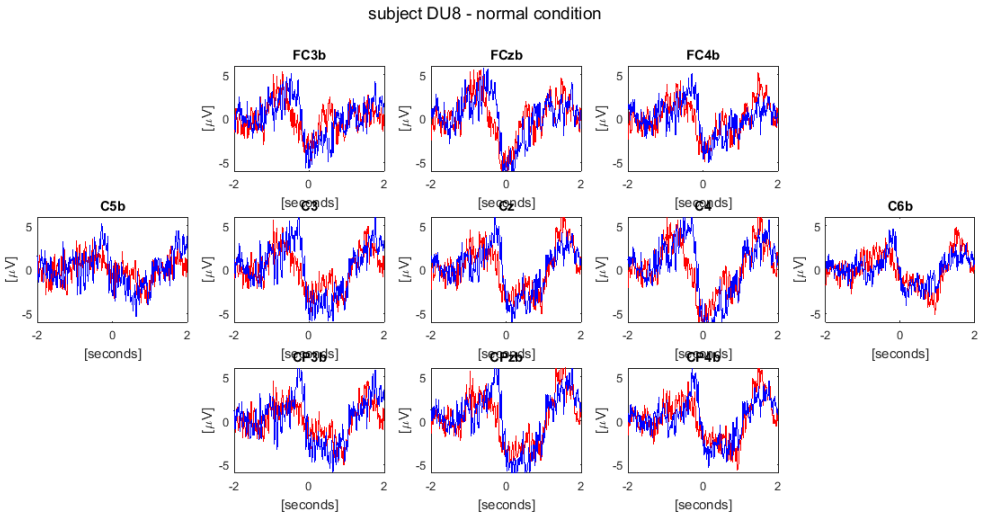

Figure 33

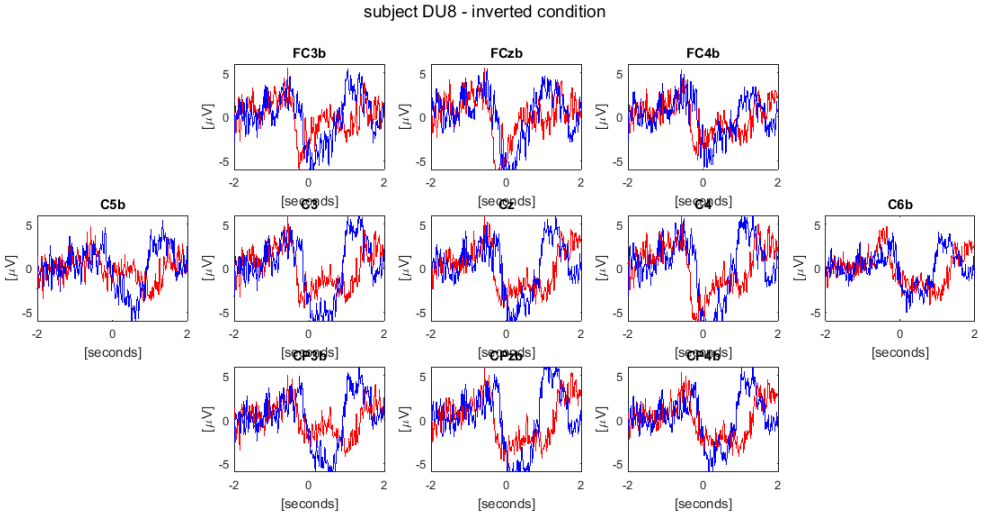

Figure 34

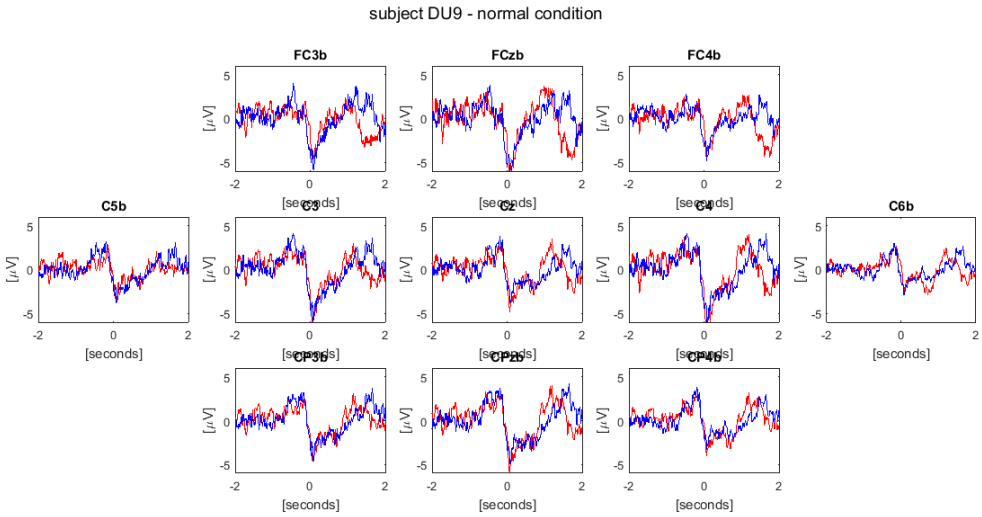

Figure 35

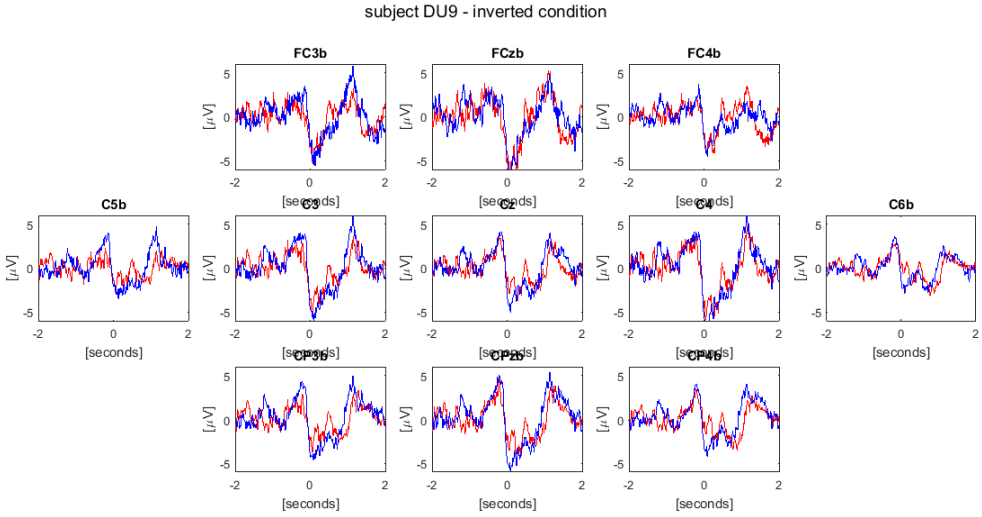

Figure 36

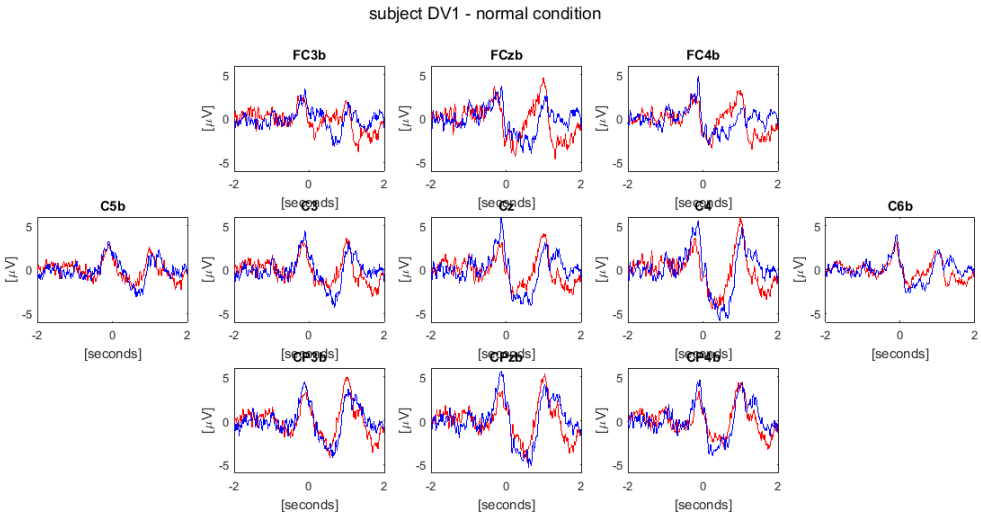

Figure 37

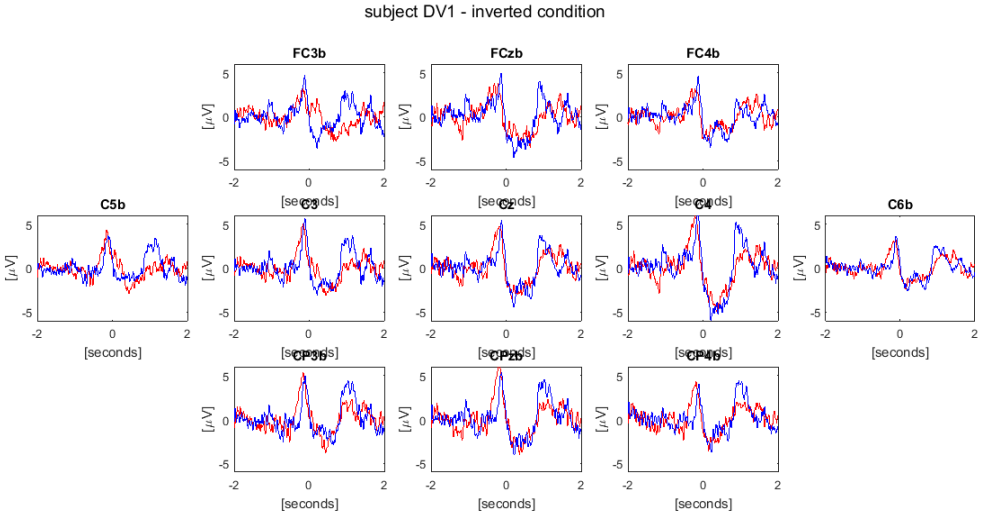

Figure 38

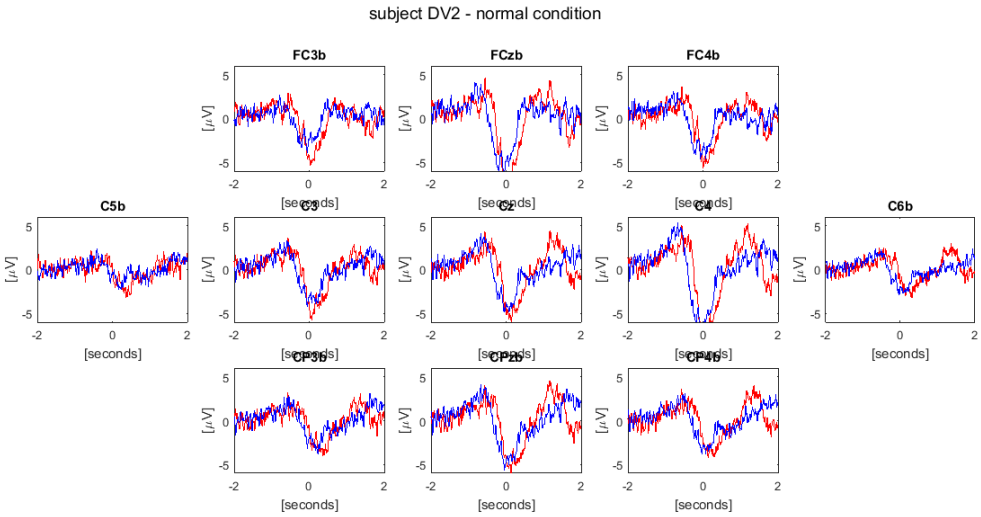

Figure 39

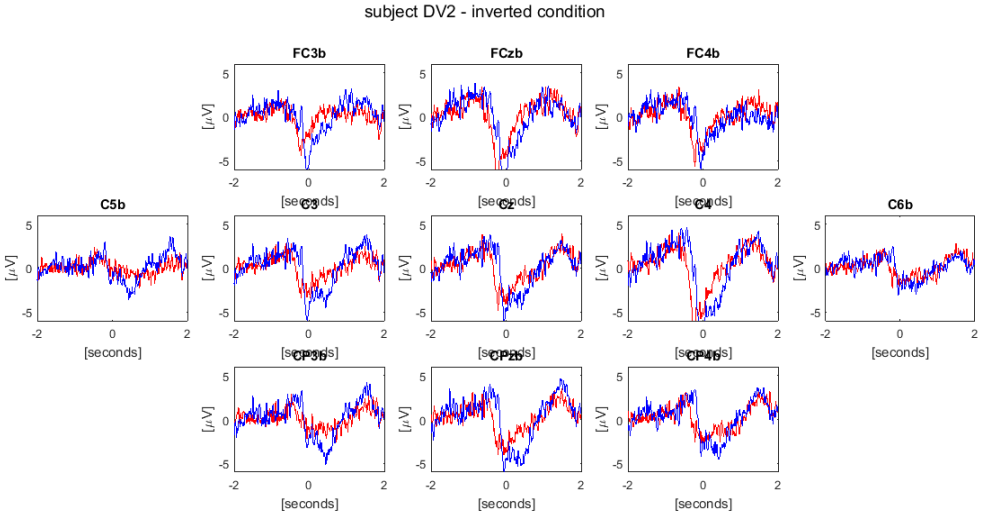

Figure 40

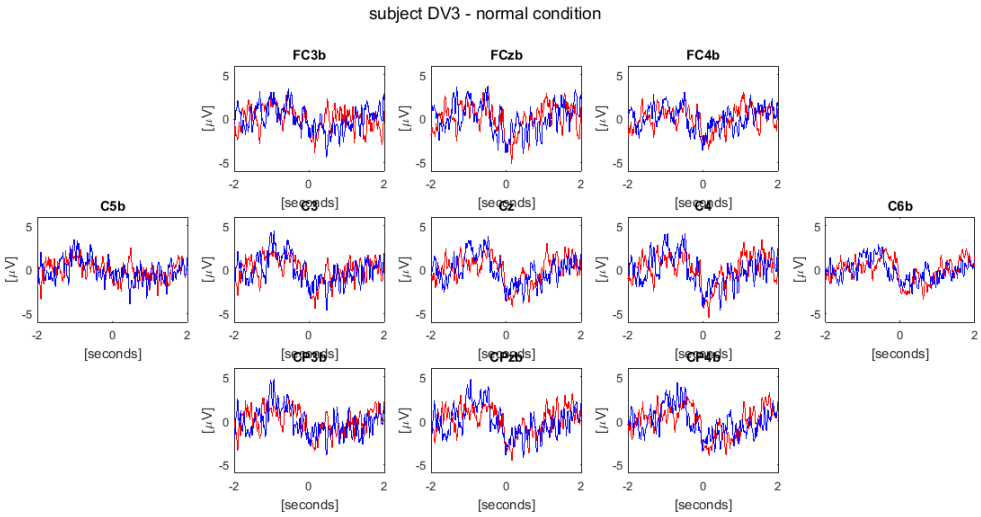

Figure 41

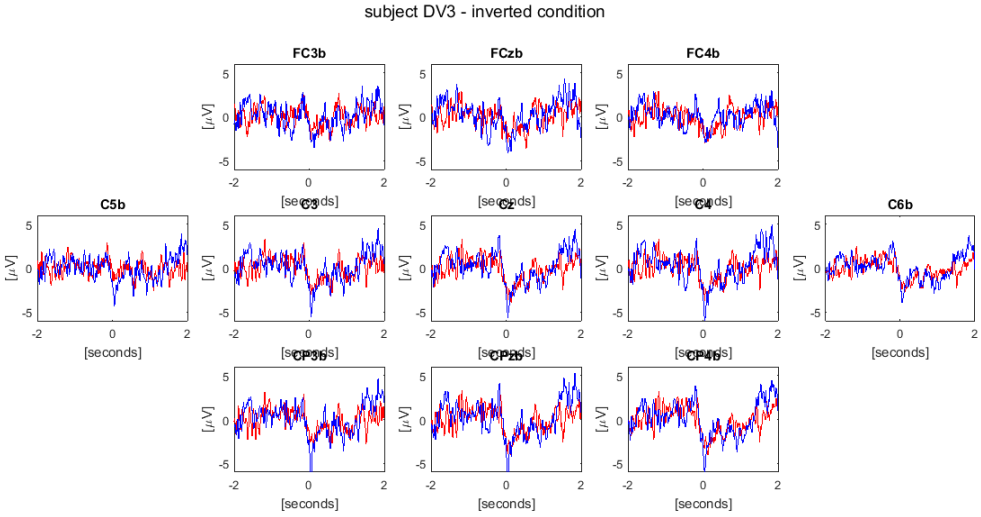

Figure 42

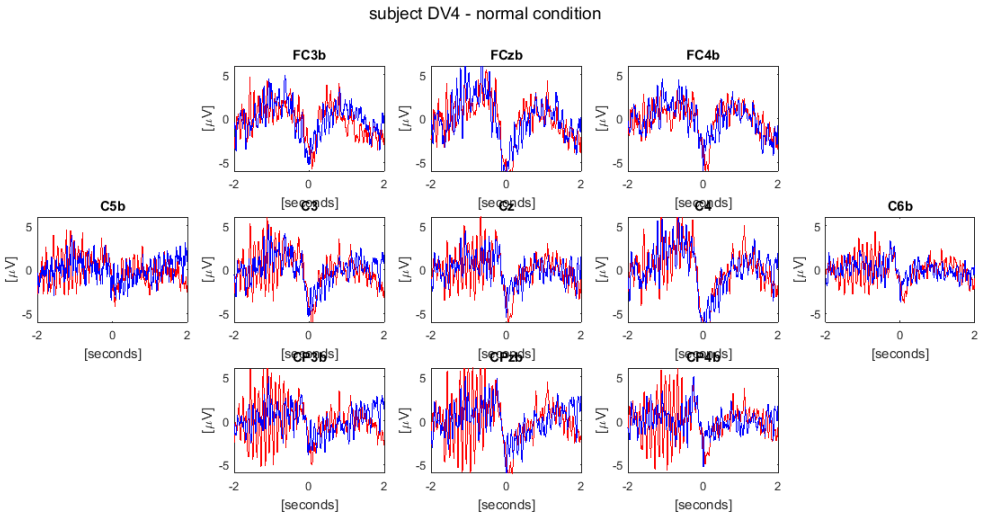

Figure 43

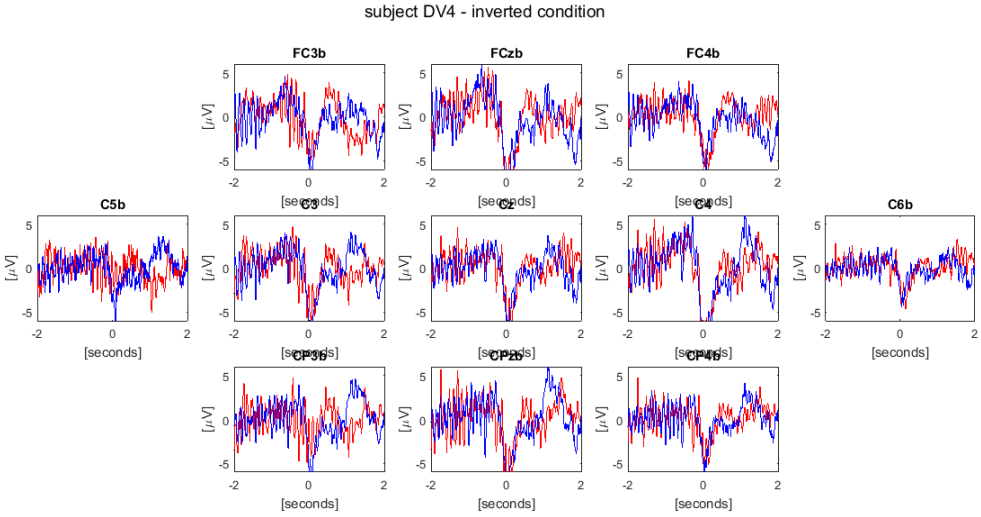

Figure 44

ERD/ERS maps

The following Figures 45 - 62 depict the ERD/ERS maps for every single subject (excluding subject DV3, as those were already shown in the main part of the thesis) for both conditions, normal and inverted. Hot colors indicate ERD, cold colors indicate ERS. Vertical dashed lines mark the reference period, vertical solid line marks the movement onset.

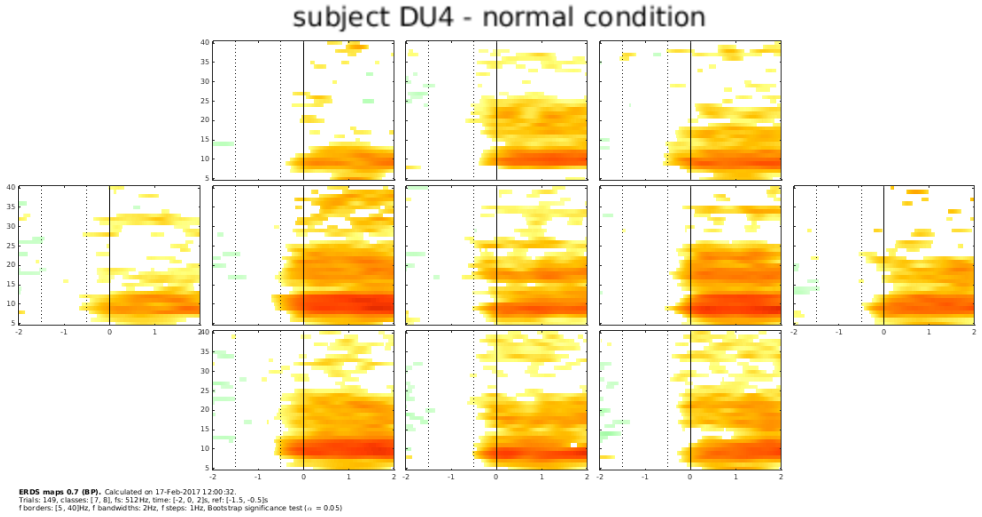

Figure 45

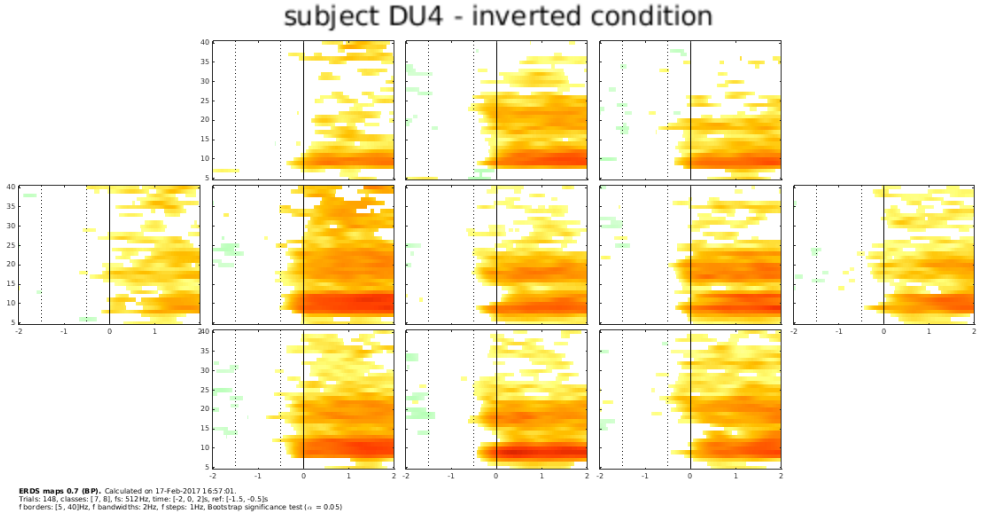

Figure 46

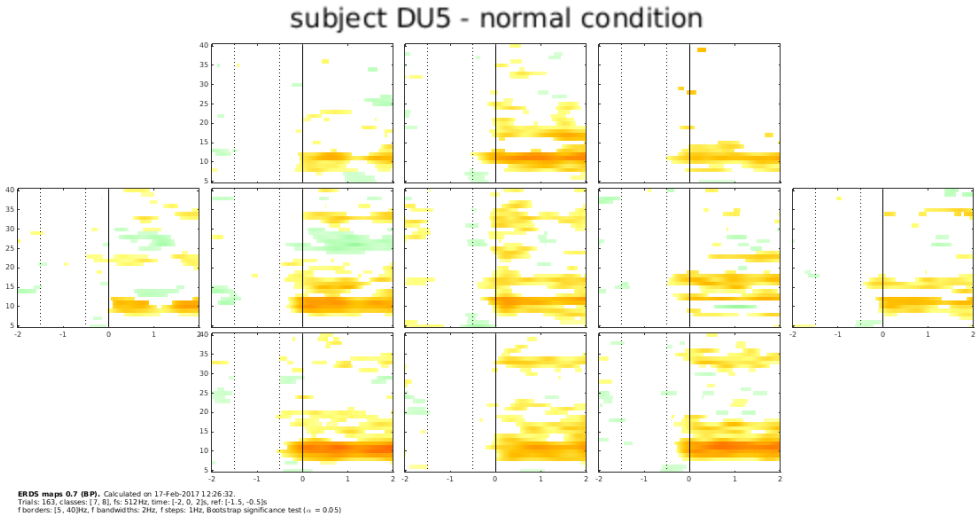

Figure 47

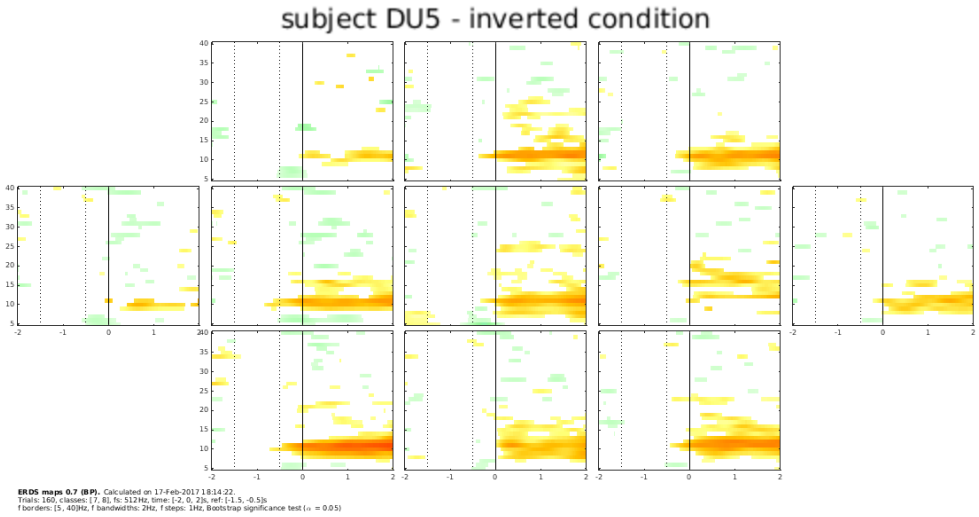

Figure 48

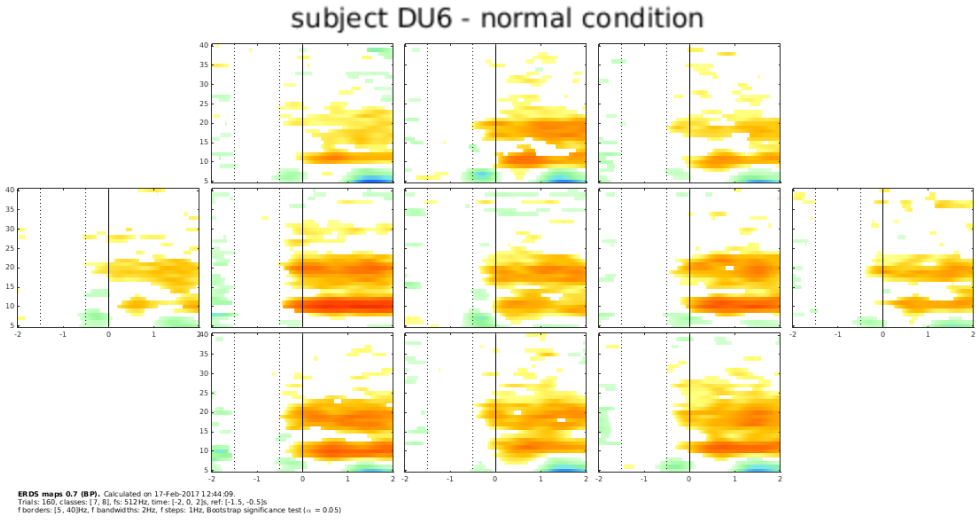

Figure 49

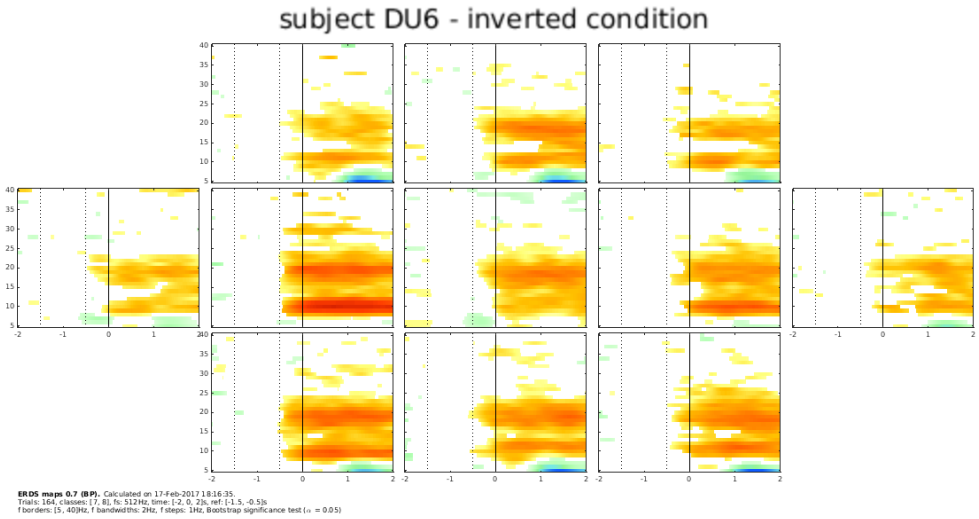

Figure 50

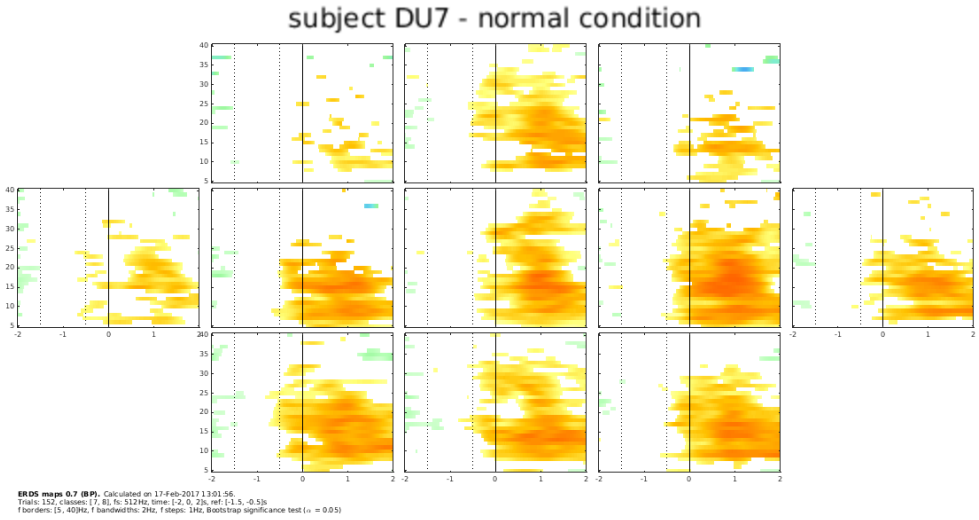

Figure 51

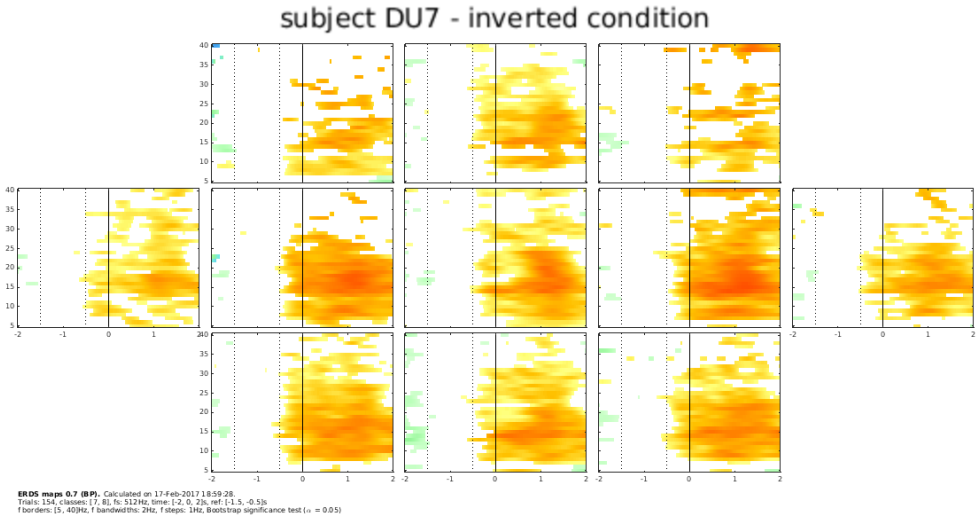

Figure 52

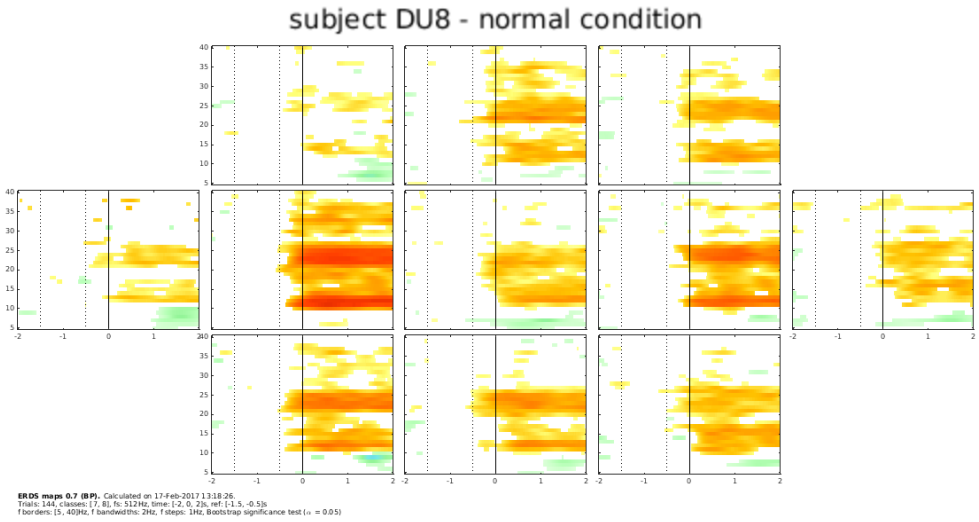

Figure 53

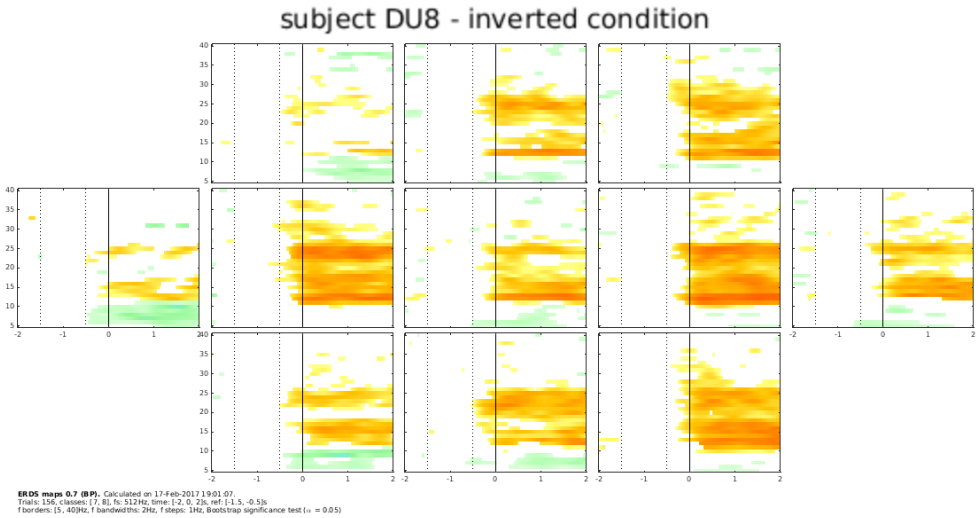

Figure 54

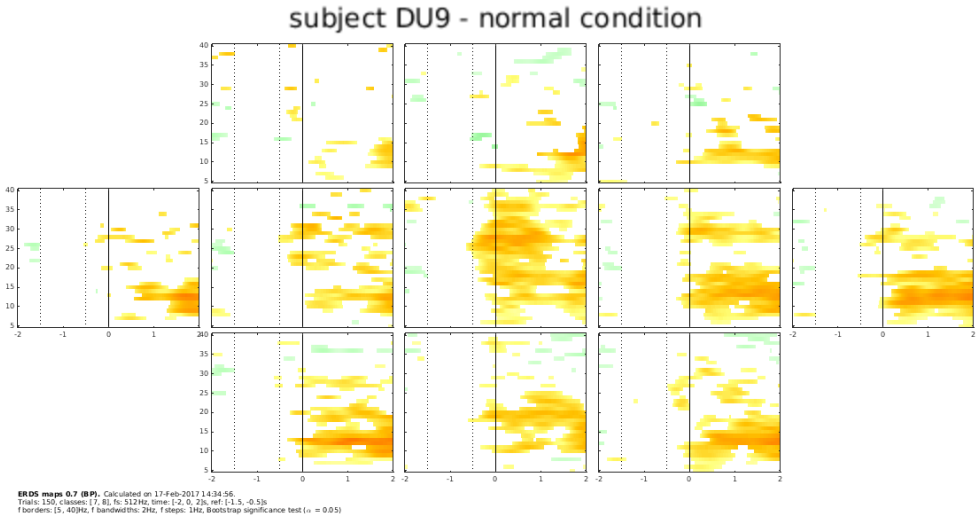

Figure 55

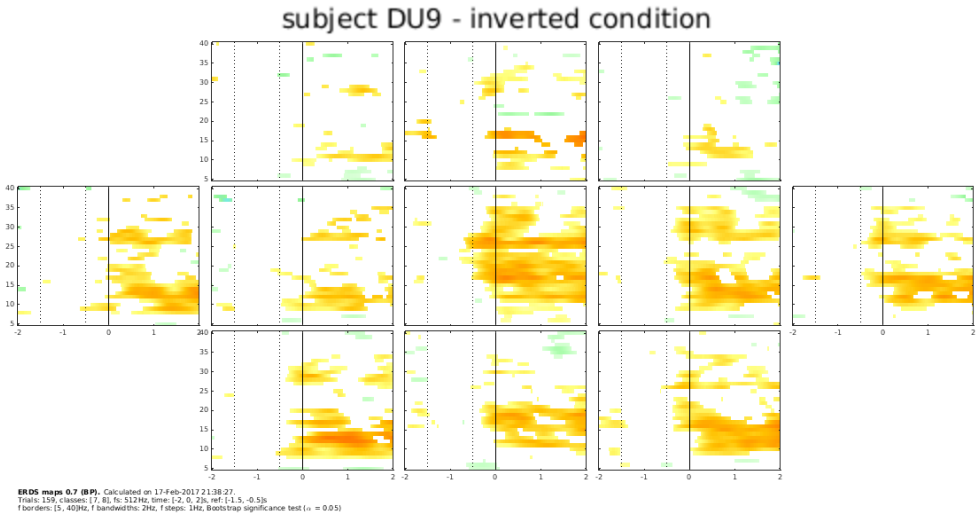

Figure 56

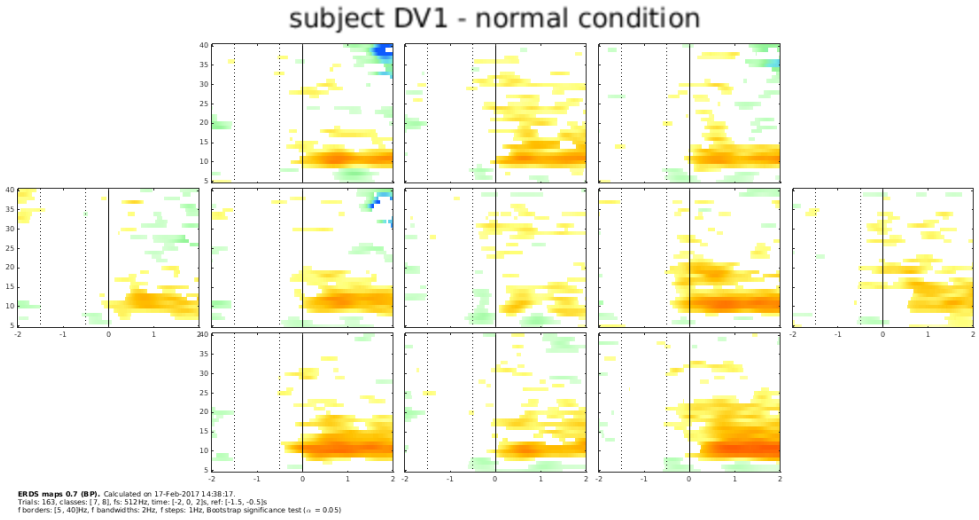

Figure 57

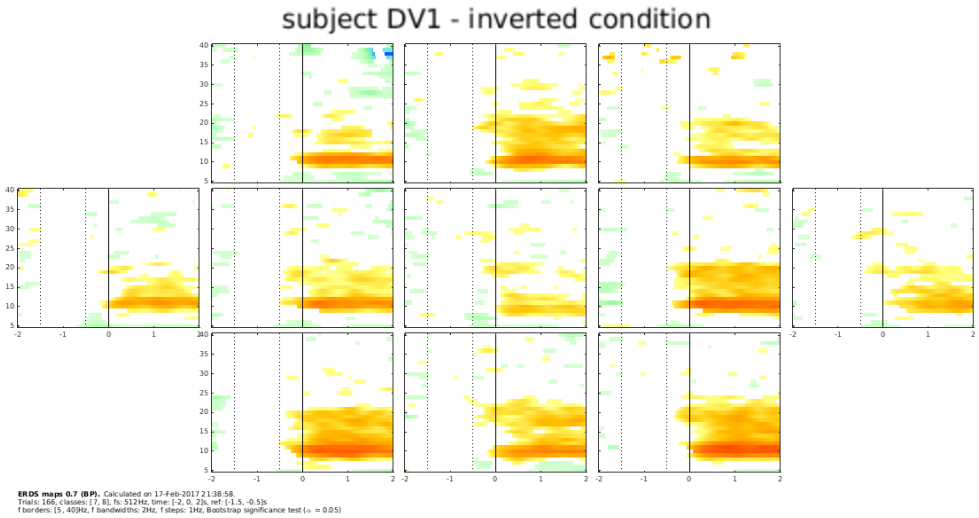

Figure 58

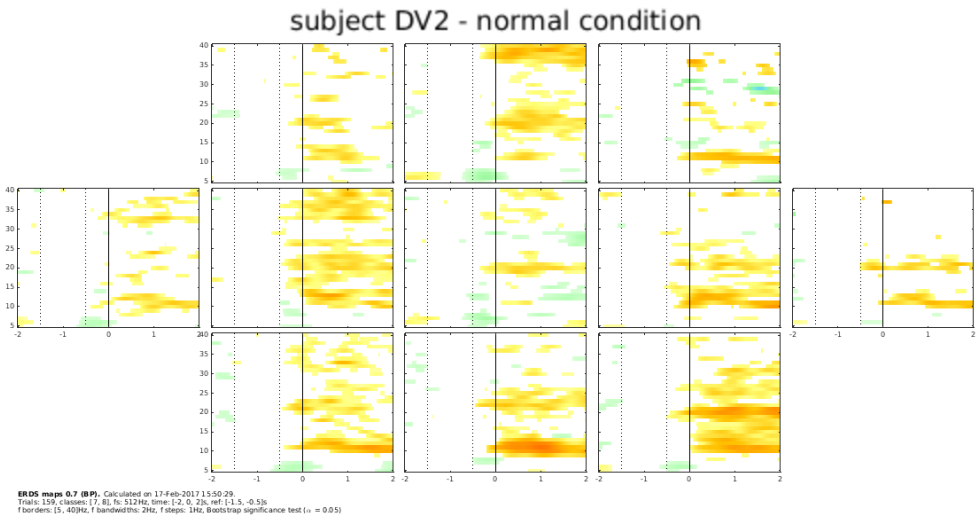

Figure 59

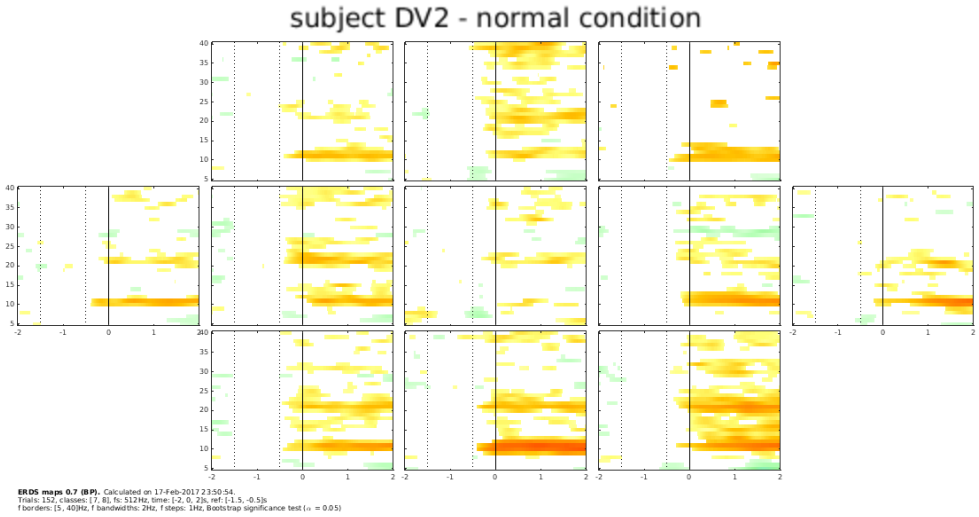

Figure 60

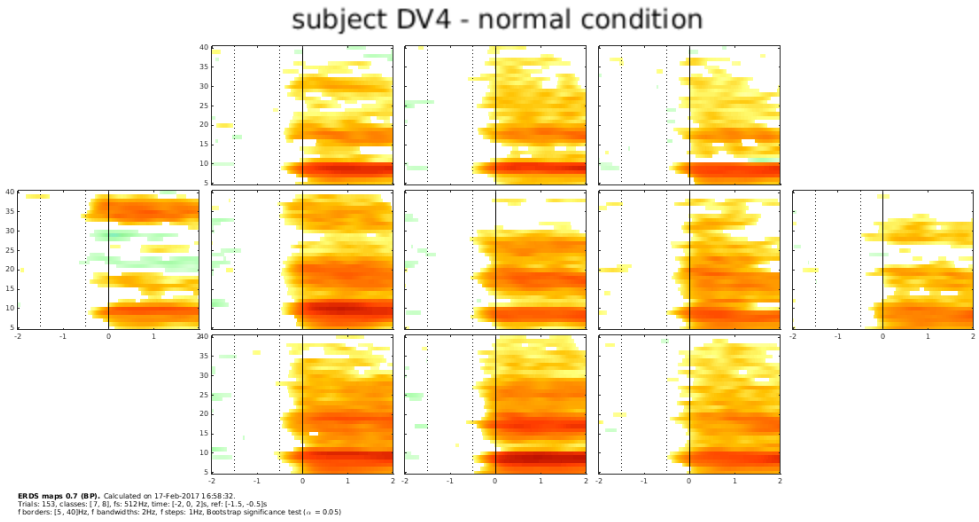

Figure 61

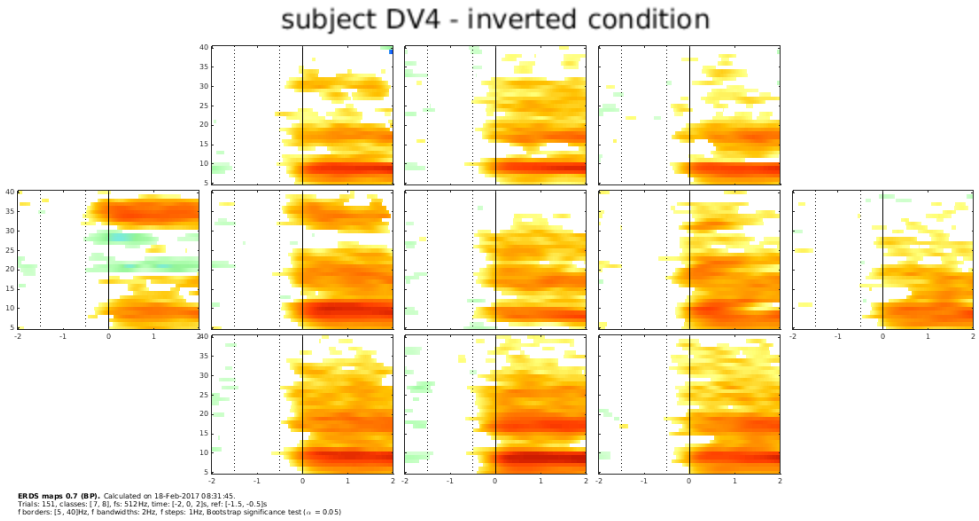

Figure 62

Classification

Figures 63 - 82 display the cross-validated classification accuracies for normal and inverted condition from -1 s to 2 s relativ to movement onset for every single subject. Dotted horizontal line marks chance level, red horizontal line marks significance level of 61.35 %

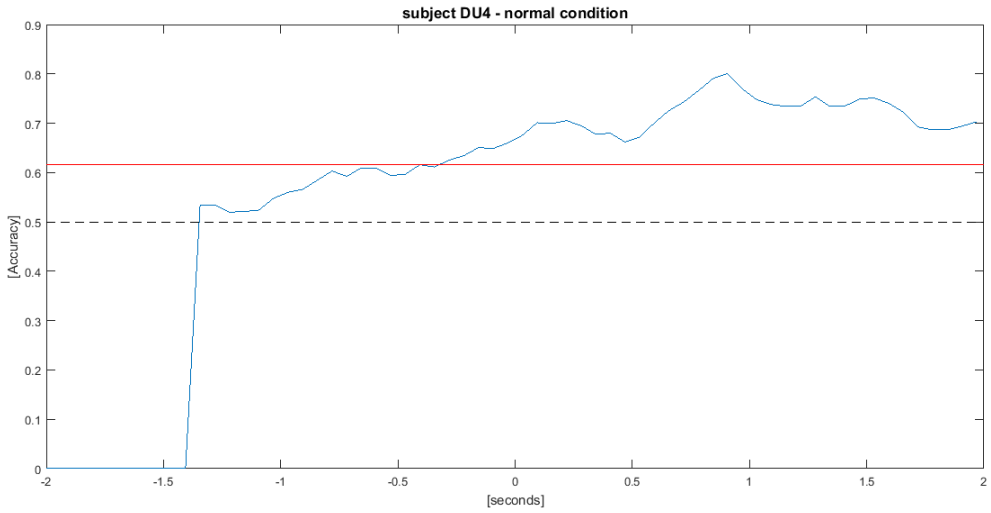

Figure 63

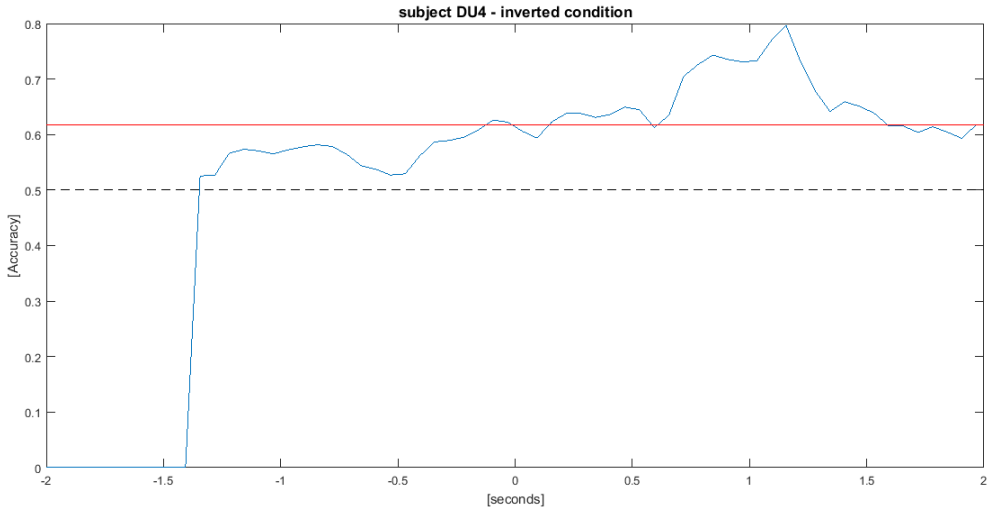

Figure 64

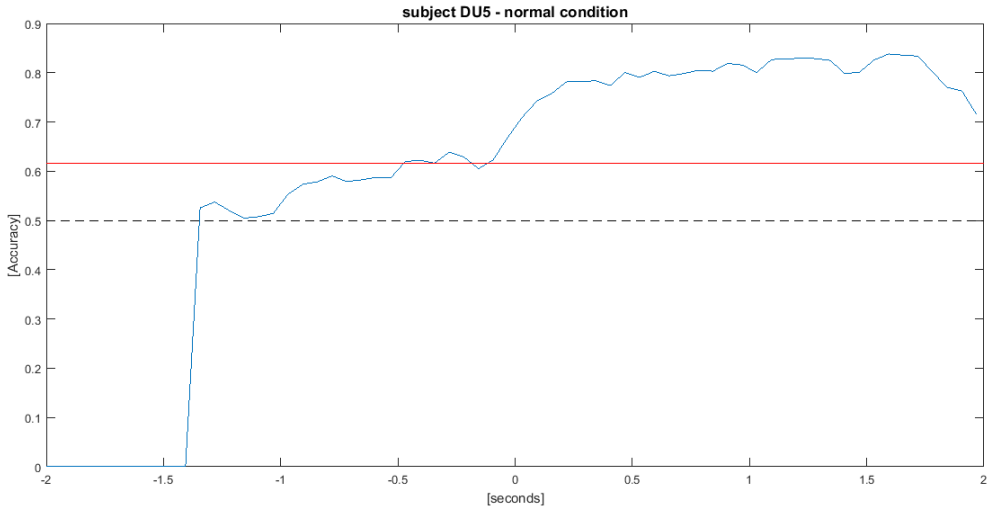

Figure 65

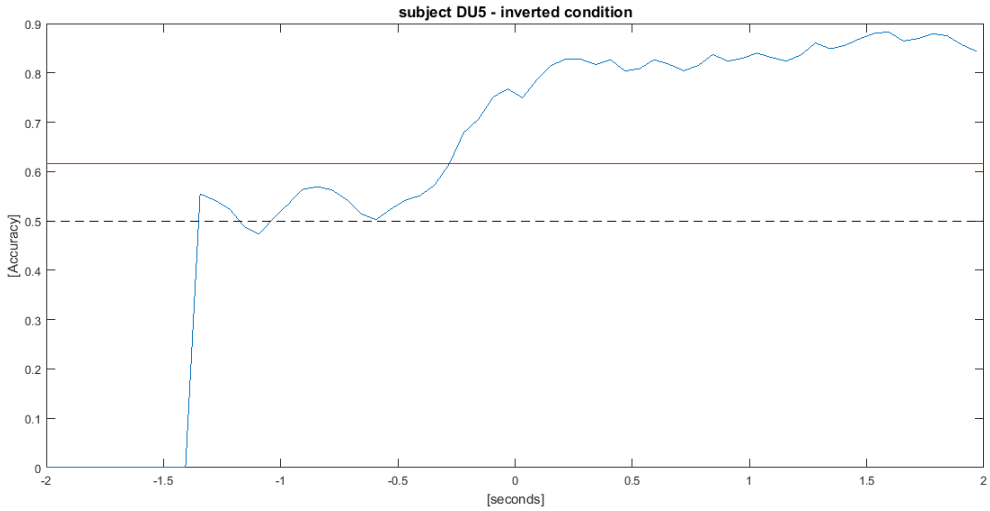

Figure 66

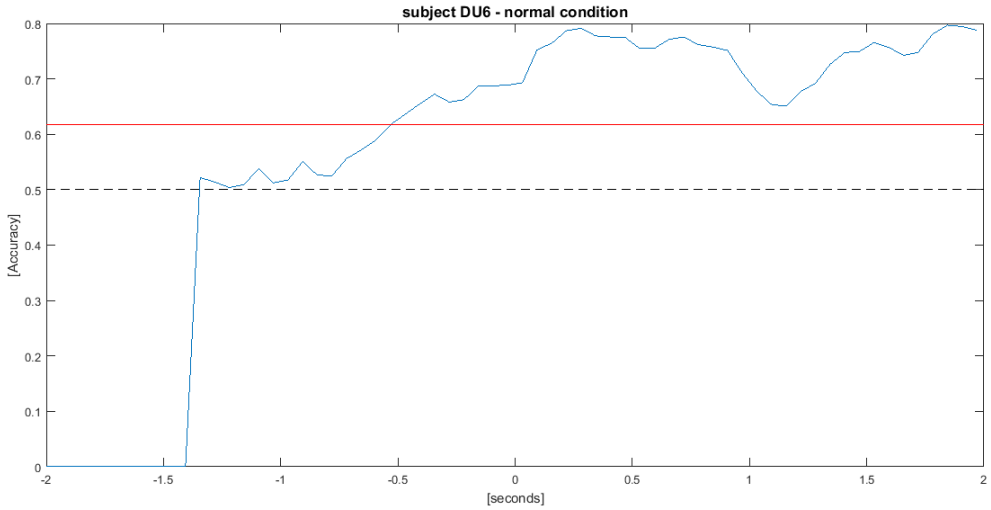

Figure 67

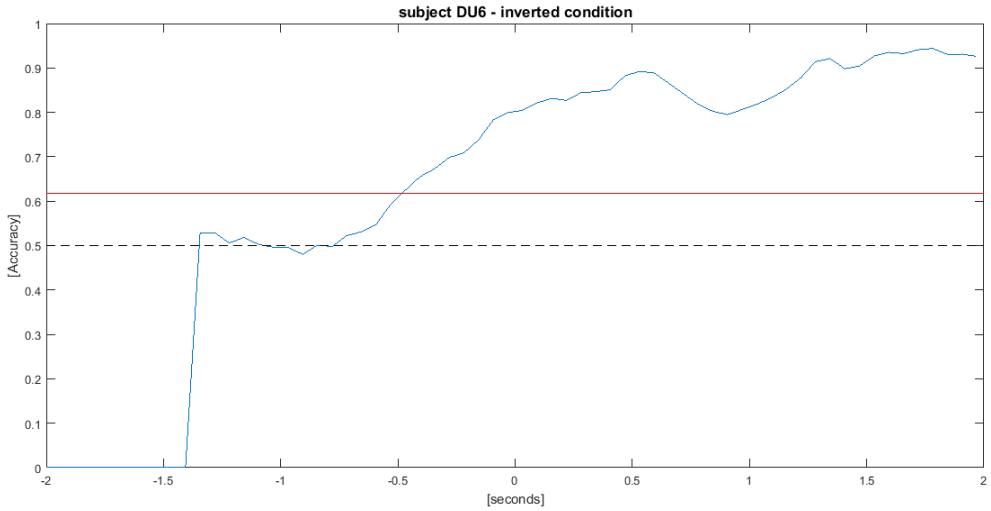

Figure 68

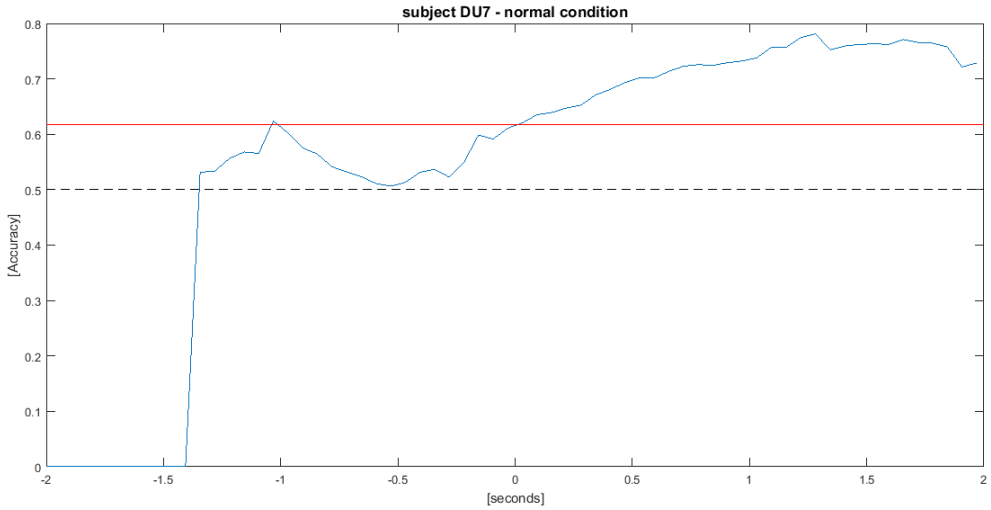

Figure 69

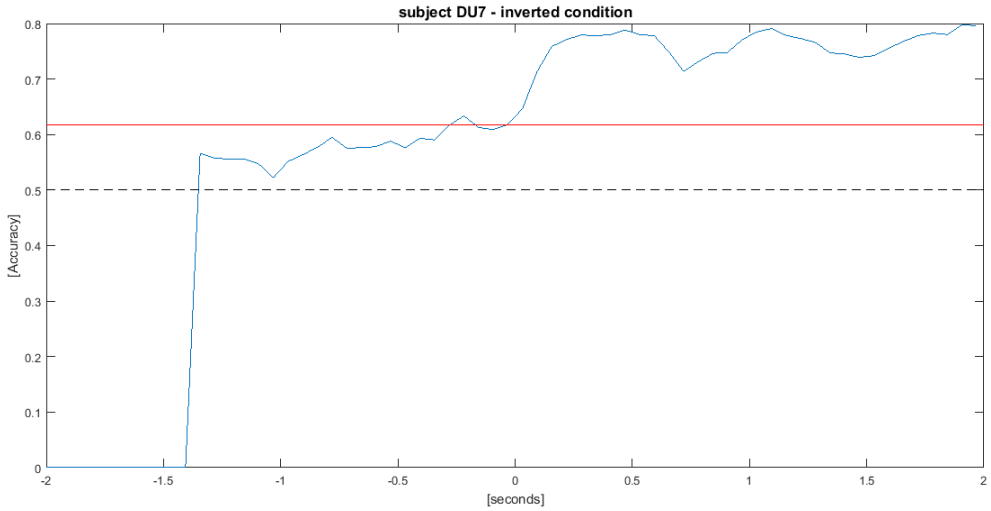

Figure 70

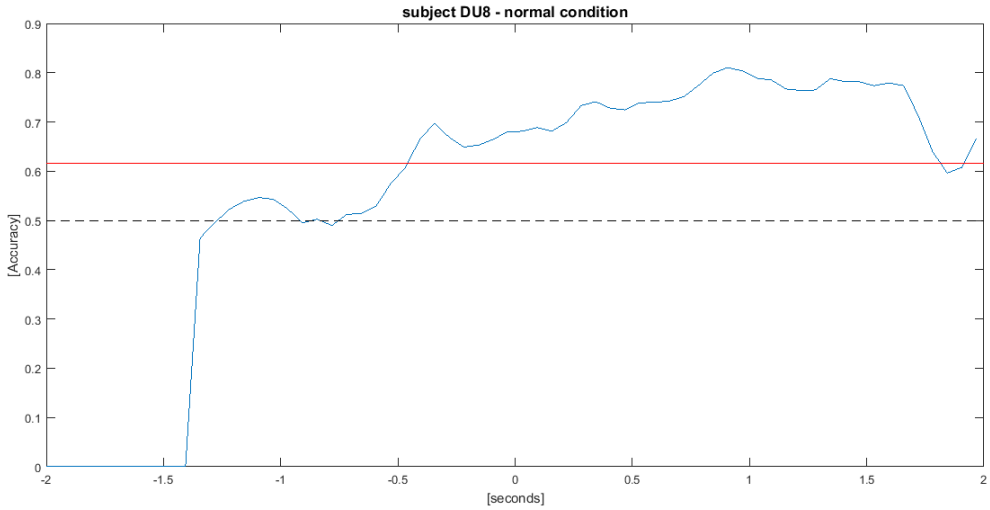

Figure 71

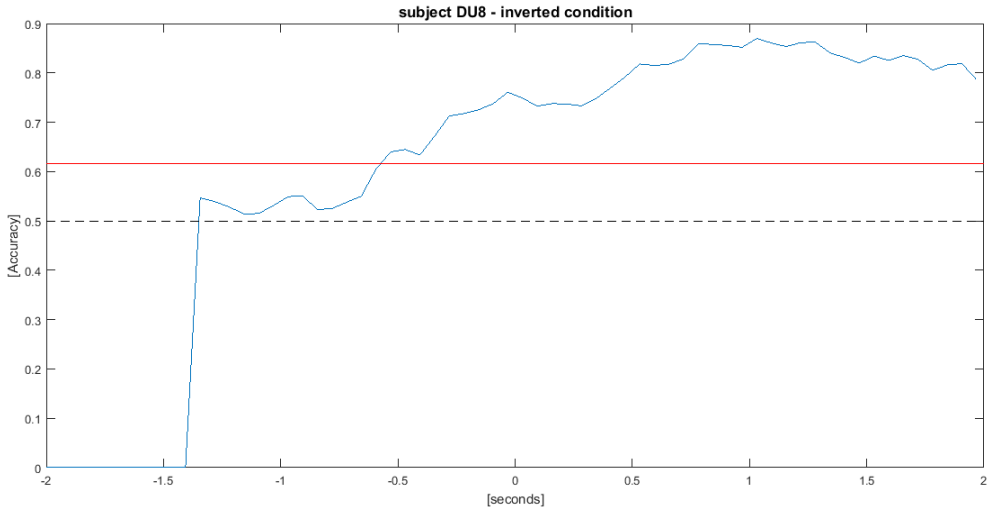

Figure 72

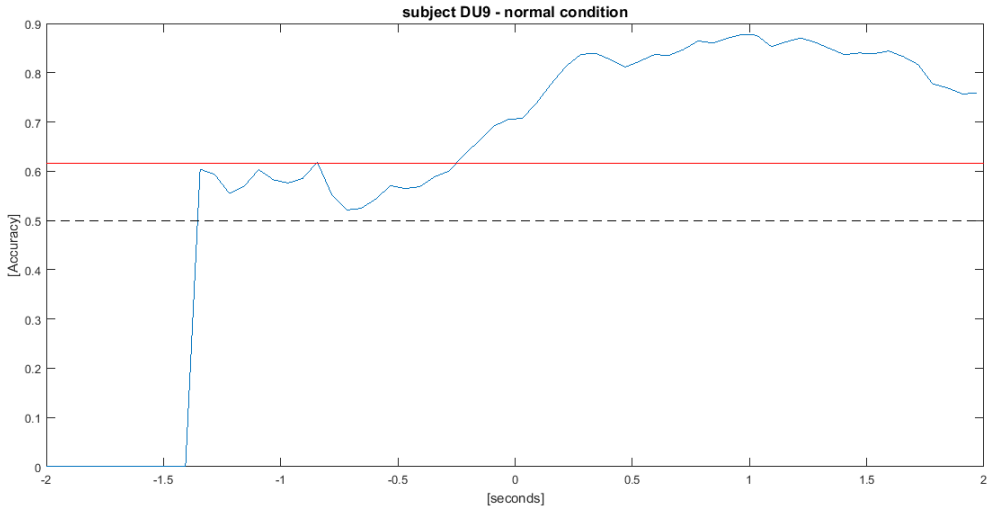

Figure 73

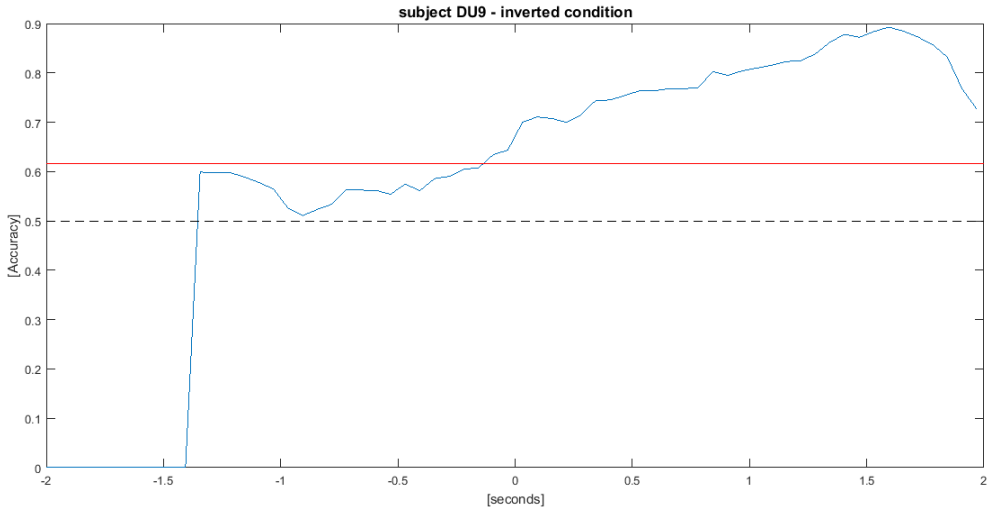

Figure 74

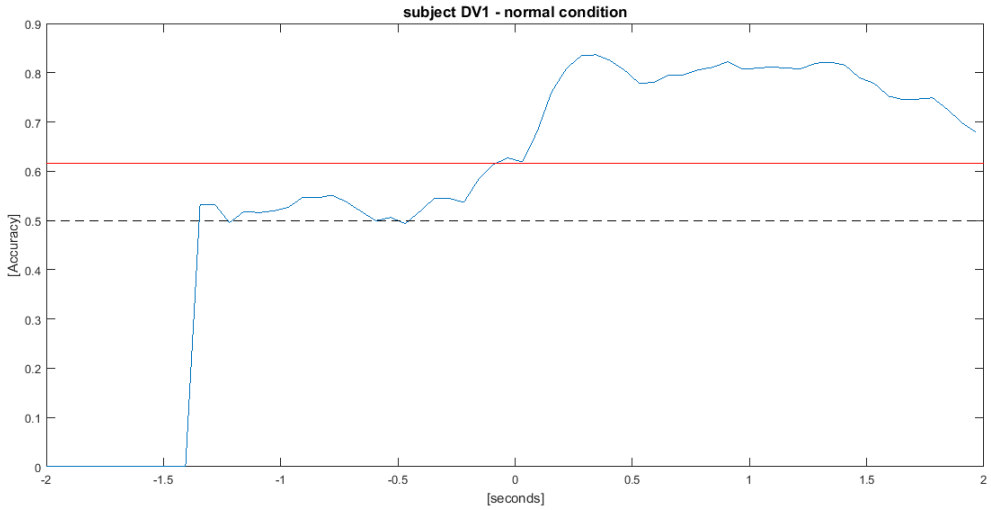

Figure 75

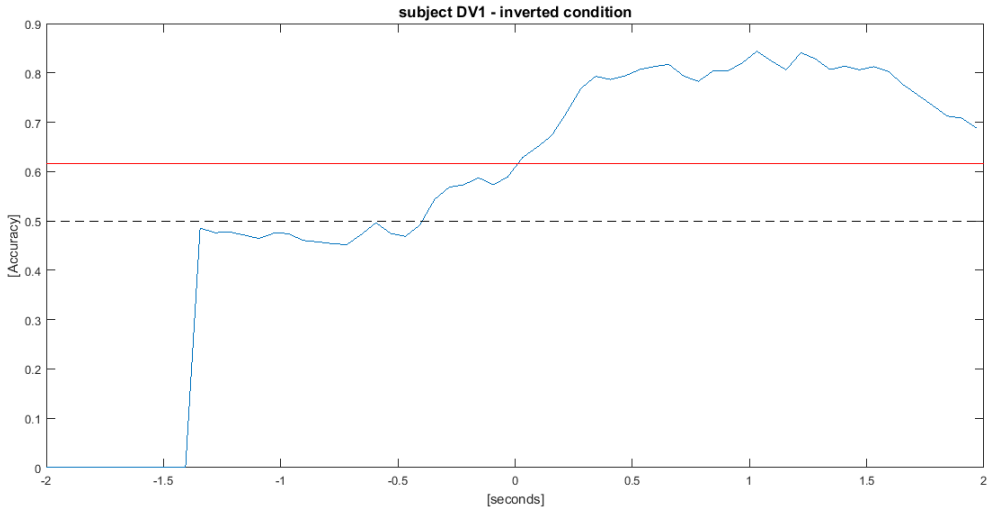

Figure 76

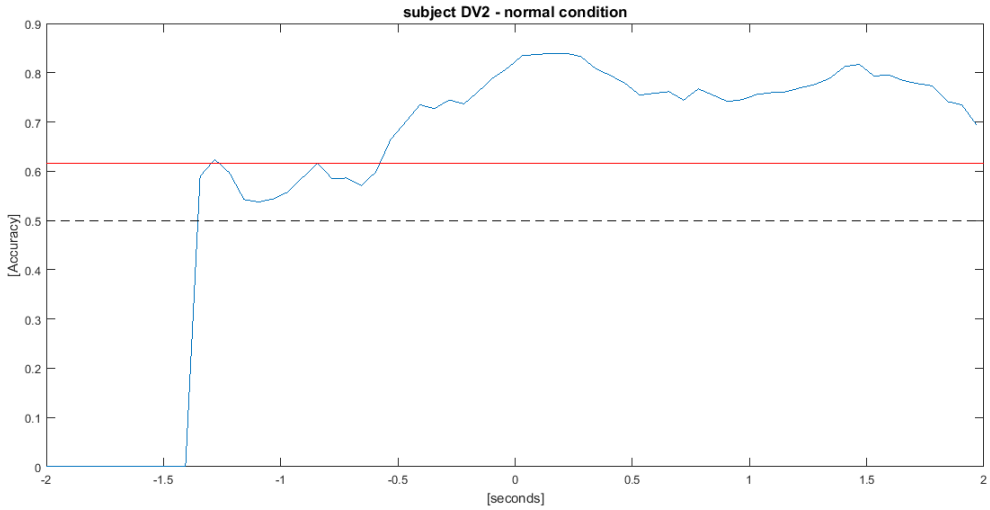

Figure 77

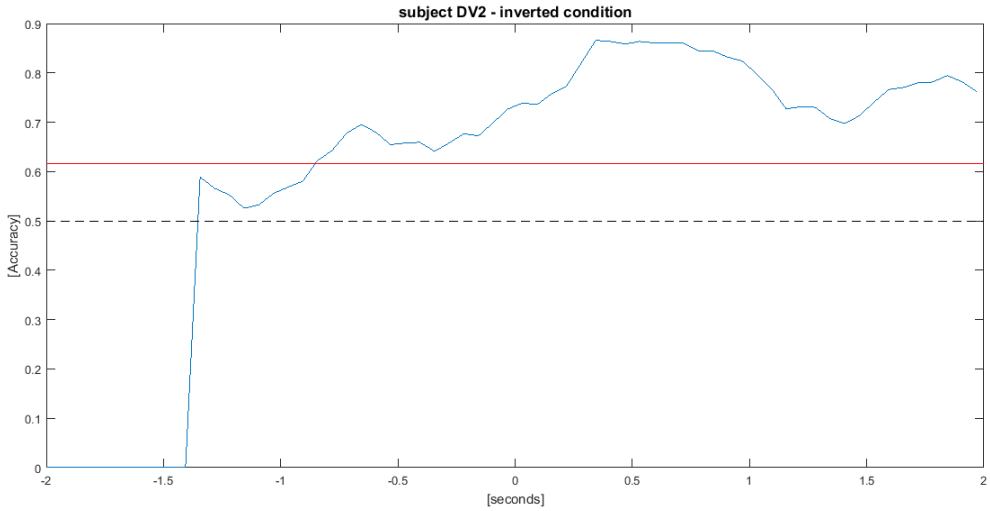

Figure 78

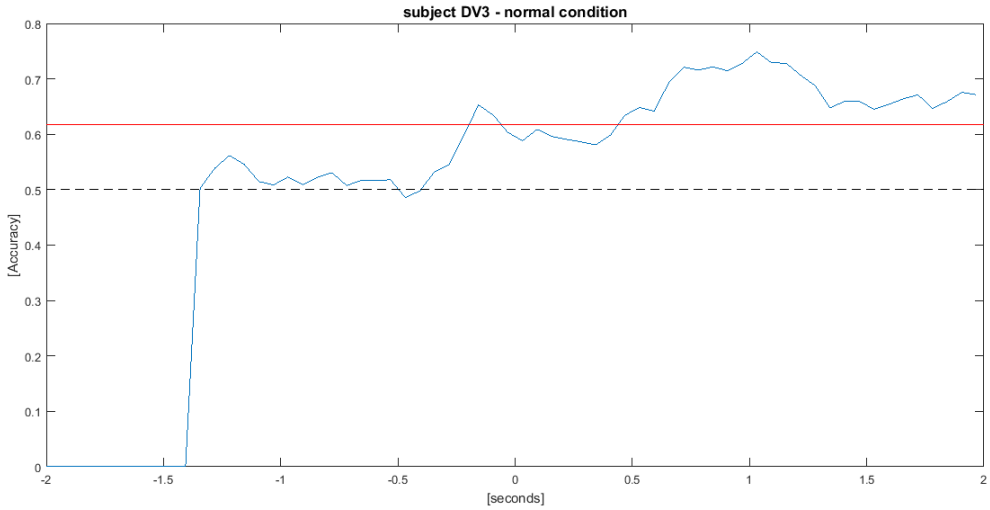

Figure 79

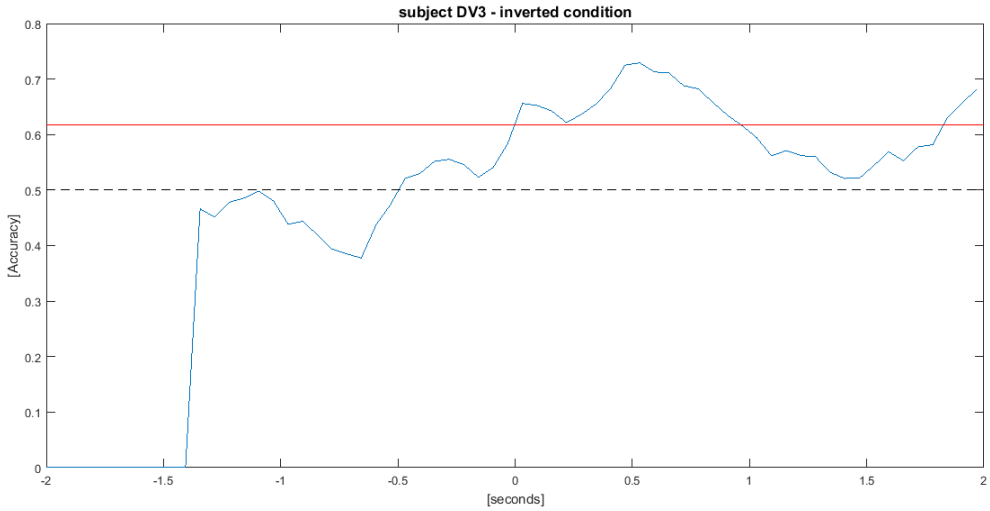

Figure 80

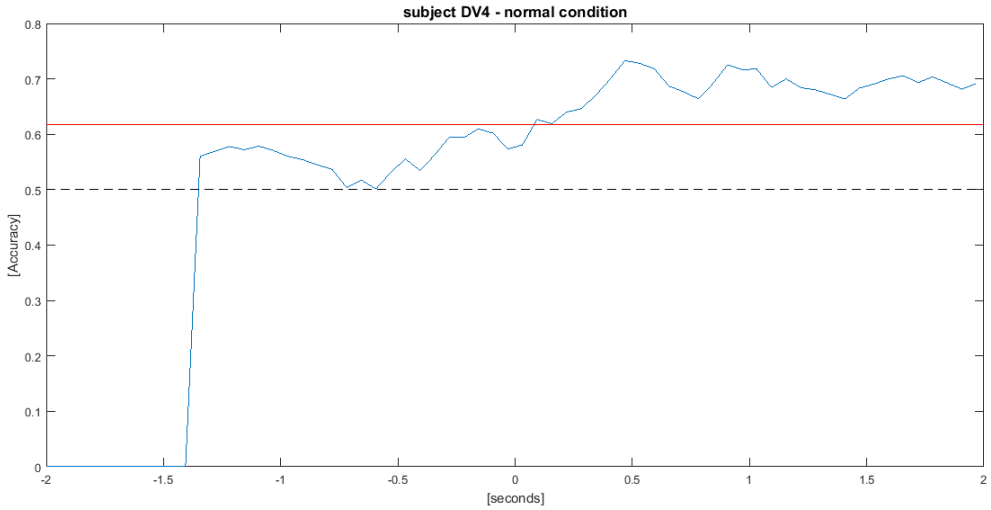

Figure 81

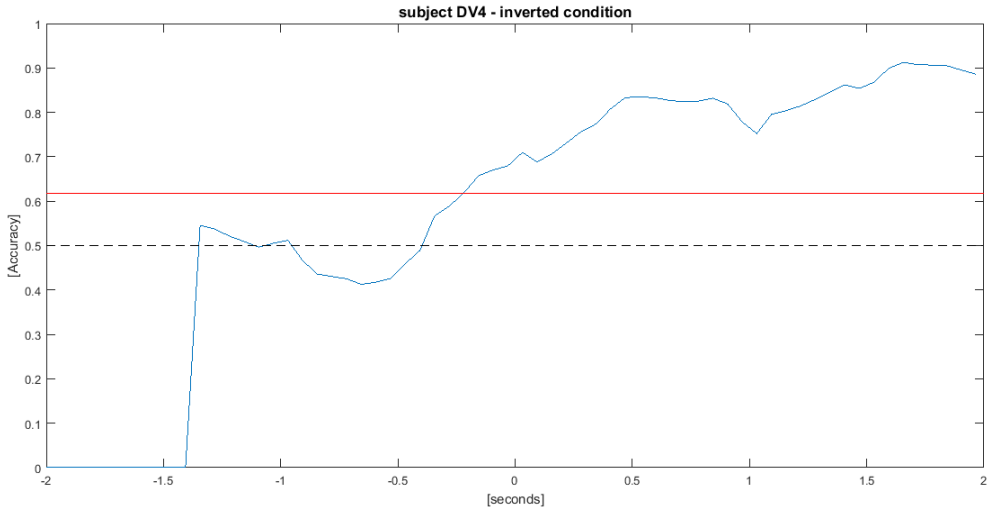

Figure 82

Classification (testing with inverted condition)

Figures 83 - 92 display the classification accuracies for every single subject that resulted from training with normal condition data and testing with inverted condition data. Time frame was chosen to be -1 s to 2 s relativ to movement onset. Dotted horizontal line marks chance level, red horizontal line marks significance level of 61.35 %

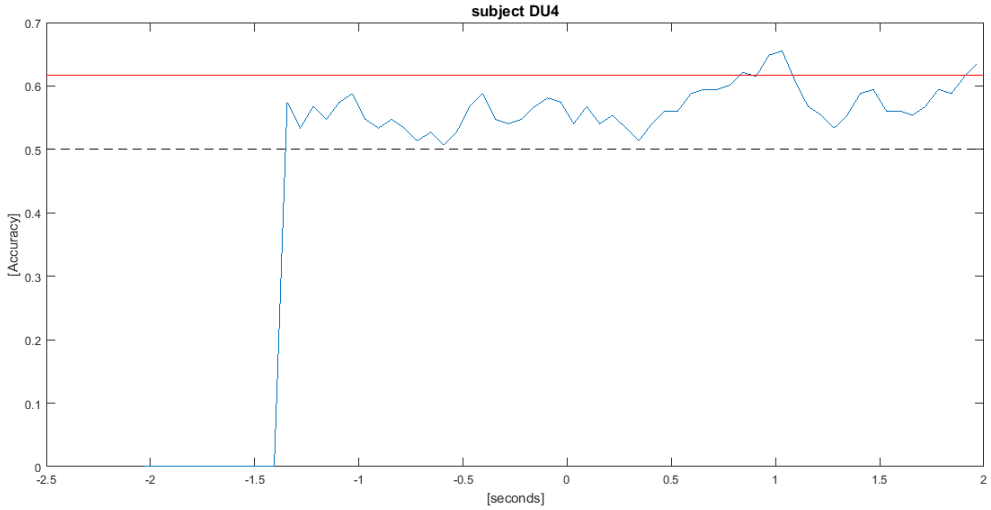

Figure 83

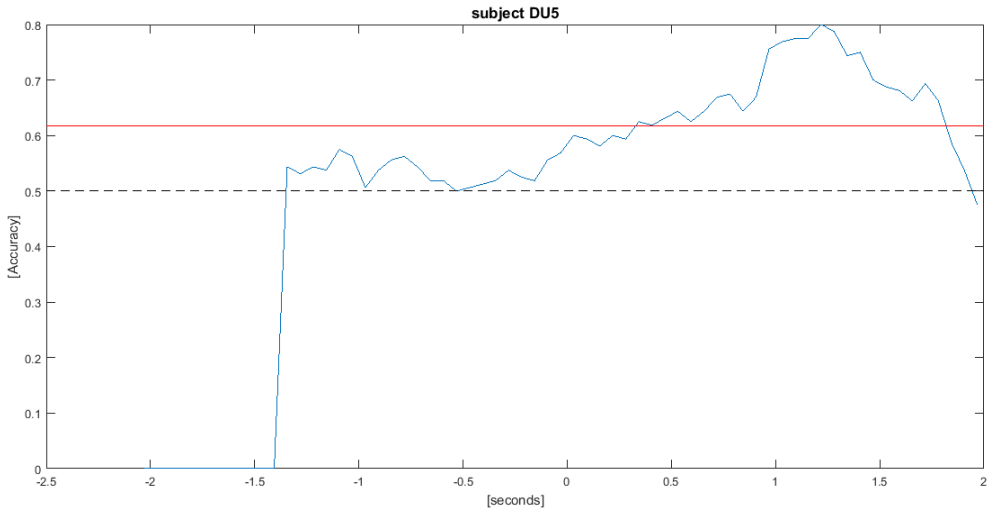

Figure 84

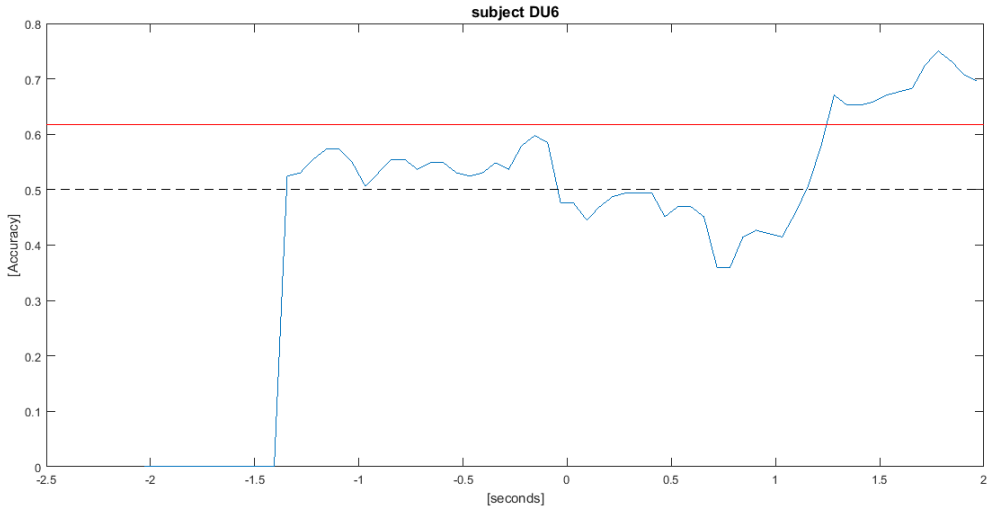

Figure 85

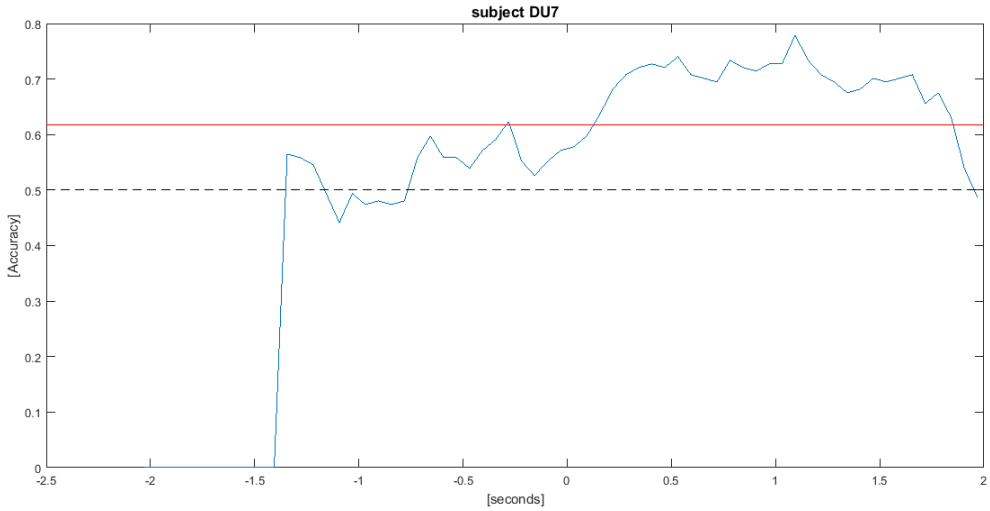

Figure 86

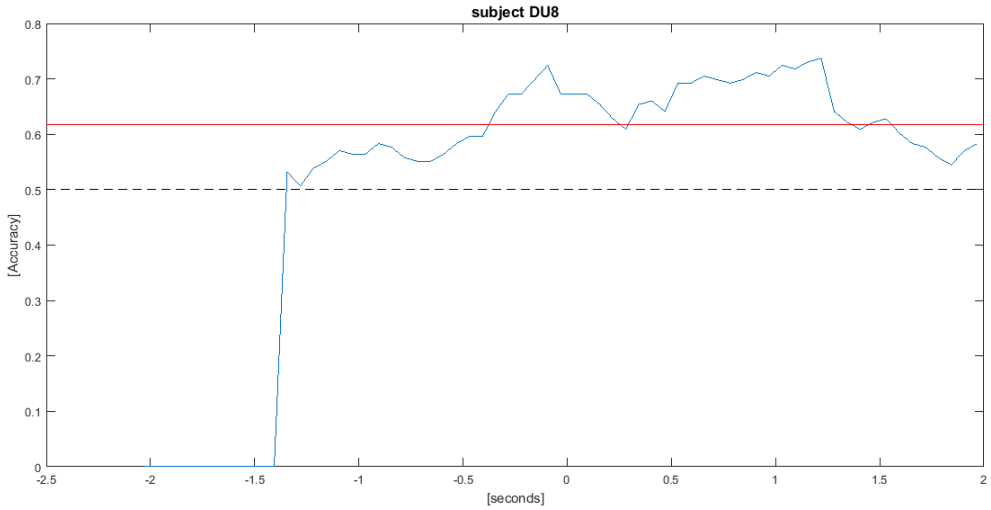

Figure 87

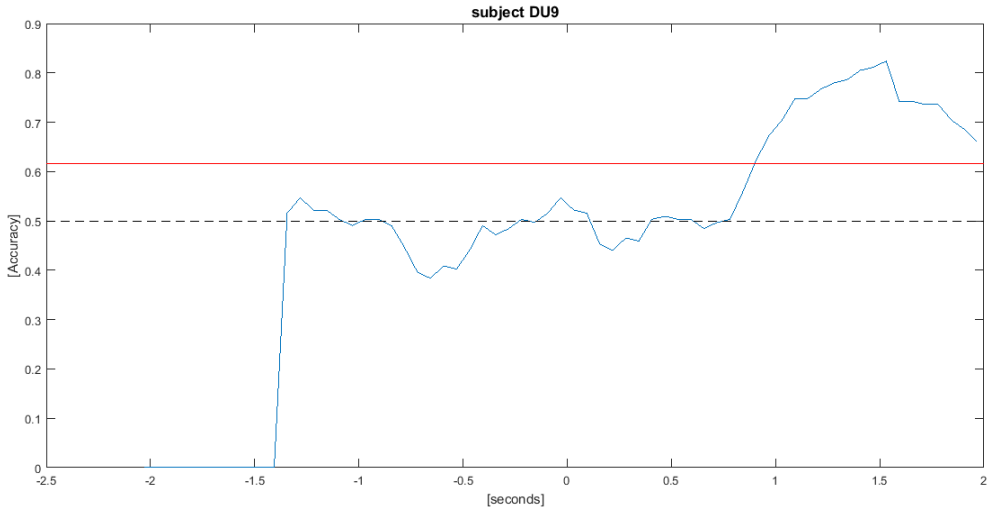

Figure 88

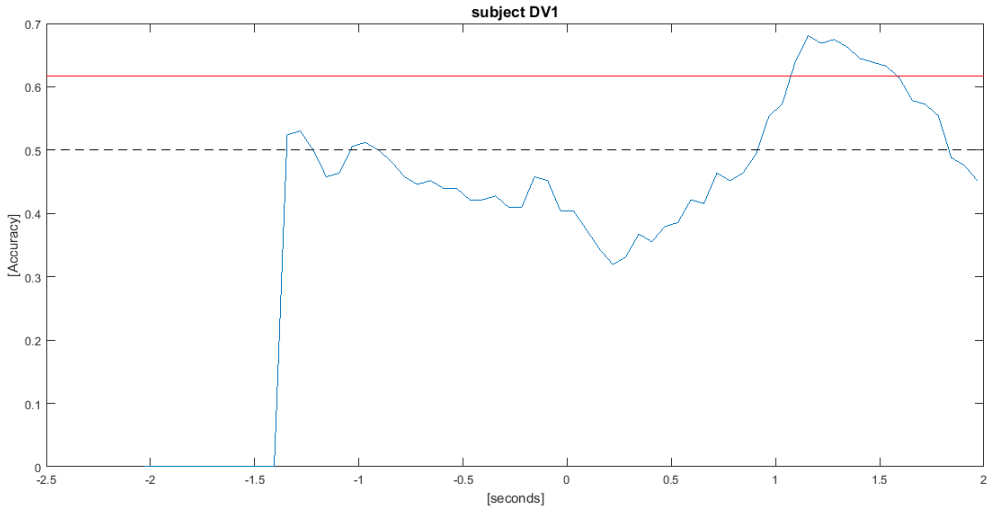

Figure 89

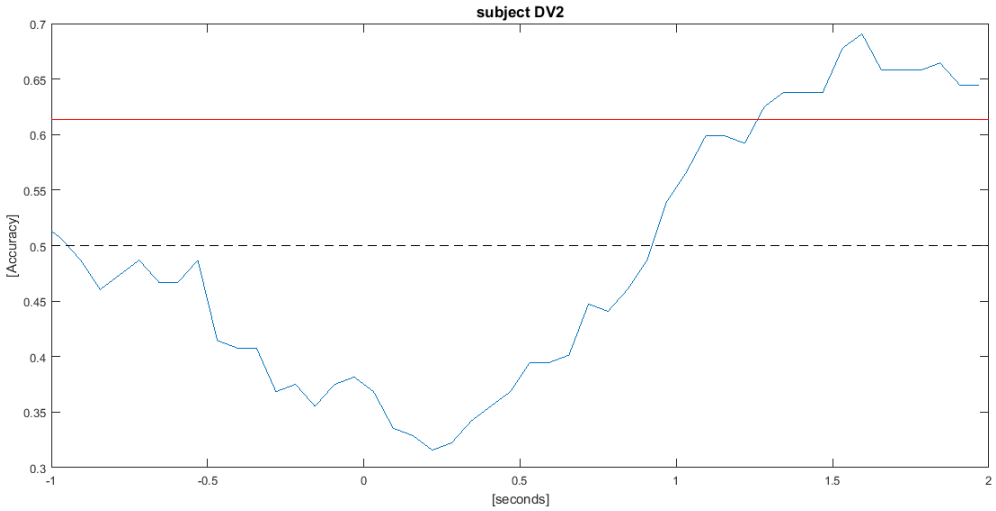

Figure 90

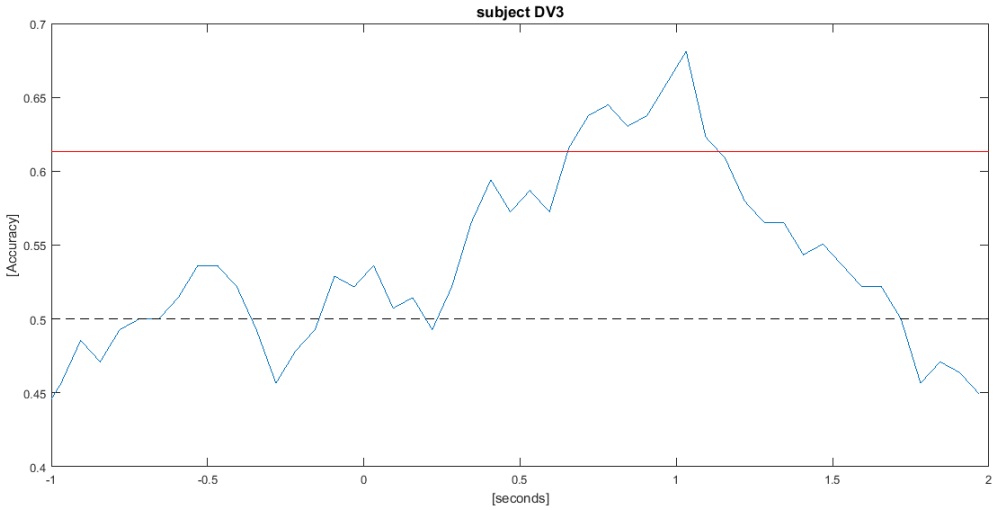

Figure 91

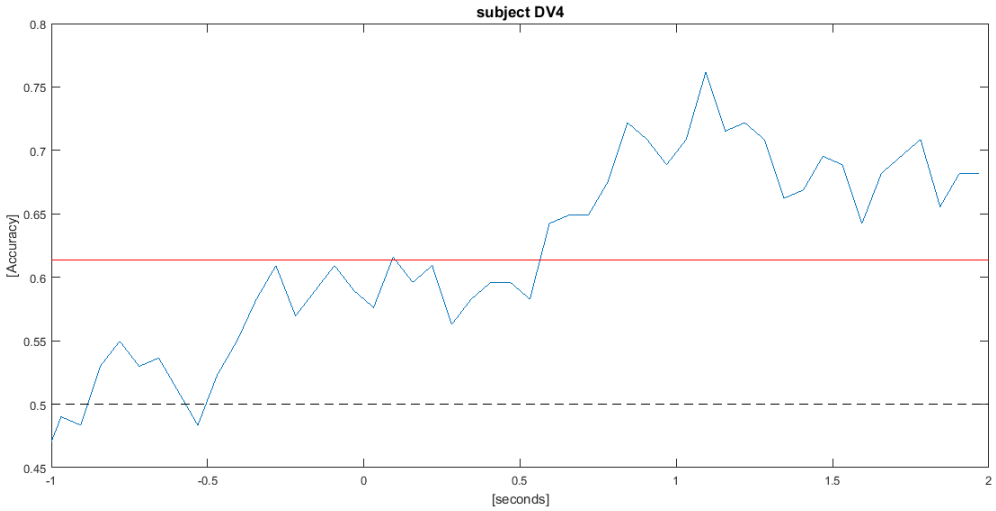

Figure 92